Photovoltaic potential of the Dutch shipping fleet

Experimentally validated method based on photovoltaic power calculations to simulate the energy yield of general cargo inland vessels

Dora de Jong

TU Delft

Photovoltaic potential of the Dutch shipping fleet

Experimentally validated method based on photovoltaic power calculations to simulate the energy yield of general cargo inland vessels

by

Dora de Jong

to obtain the degree of Master of Science in Sustainable Energy Technology
at the Delft University of Technology,
to be defended publicly on 17 December 2021

Student number:	4391144
Thesis committee:	Dr.ir. H. Ziar | TU Delft, ESE-PVMD Supervisor
	Prof.dr.ir. Olindo Isabella | TU Delft, Head of the ESE-PVMD group
	Prof.dr.ir. Mark van Koningsveld | TU Delft, CTIG Ports and Waterways
Institution:	Delft University of Technology
Place:	Faculty of Electrical Engineering, Mathematics Computer Science, Delft
Project Duration:	November, 2020 - December, 2021

An electronic version of this thesis is available at http://repository.tudelft.nl/
Cover Image: Harmonie enters Rotterdam, by Dora de Jong 2021

TU Delft

Abstract

Implementing renewable energy generation and more sustainable consumption behaviour in the future inland shipping industry is necessary. Electrification of the inland shipping fleet leads to an increase in electrical energy demand on the consumption side. The generation of decentralized photovoltaic (PV) energy systems on board of general cargo vessels can be one solution to these challenges. To estimate the potential of these decentralized energy systems, accurate simulation models are needed. The objective of this research is to **determine the photovoltaic potential of the Dutch general cargo inland shipping fleet.**

A method is developed to simulate the energy yield of moving general cargo vessels. The estimated energy yield is based on hourly power calculations. A difference is made between container and bulk vessels. This simulation model consists of a skyline, a vessel, an irradiance, a PV module temperature, and an energy model. In the skyline model, skyline profiles for 3036 waterway points are generated using LIDAR AHN3 height data. The waterways skylines are corrected for every vessel individually. In the vessel model, AIS (automatic identification system) data is used to simulate the sailing behaviour of 2746 vessels. In the irradiance model, the diffused, direct and ground reflection irradiance received by the PV panel is simulated. The diffused irradiance is calculated according to the Perez model. The PV module temperature is estimated according to the fluid-dynamic model. The additional air caused by the forward movement of the vessel and the water temperature is taken into account. Finally, the PV energy yield is calculated by the received irradiance, the suitable PV surface and the corrected PV module efficiency.

An experiment is performed to validate the developed model, where a PV panel is installed on the vessel Harmonie. Equipment is installed to monitor Harmonie during one docking week and two sailing weeks. A co-variance linear regression model describes the relationship between the measured and the estimated PV power. According to the co-variance linear regression model, the P-value for the simulated PV power is below 0.05 and, therefore statistically significant. The outcome of the linear regression model is overestimated by 4 % with a 95 % confidence interval between 0.87 and 1.05.

740,958 PV panels can be installed on the general cargo fleet. Together, these panels have an installed peak power of 267 [MW] and an annual estimated PV potential of 230 [GWh]. The annual PV energy per unit area of a container vessel is 171 [kWh/m^2] and for a bulk vessel 168 [kWh/m^2]. The annual PV energy per installed power for a container vessel is 864 [Wh/W_p] and for a bulk vessel 852 [Wh/W_p]. When the outliers are removed from the annual specific power [Wh/W_p] dataset, the complete fleet can be modelled by a Weibull distribution. A t location-scale distribution is suggested when the outliers are not removed from the dataset. The average annual energy demand of a container vessel is 1440 [MWh], 7.17 % of this demand can be supplied by the PV panels installed on the vessel. Bulk vessels have an energy demand of 1350 [MWh] on average, of which the installed PV panels can cover 5.82 %.

Acknowledgment

This research is carried out to obtain the degree of Master of Science in Sustainable Energy Technology at the Delft University of Technology. I am very fortunate to complete my learning path at university with such a great, exciting and personal research subject.

I would like to express my appreciation to my supervisor, Dr. Hesan Ziar, for taking the time to guide and educate me during this project. Not only did he help by bringing this research to a higher level, but he also inspired me to become a research engineer and to keep on working in this field of research.

Using received AIS data, this research has gained added value. I would like to thank Solange van der Werff for helping to retrieve this data. In addition, I would like to thank Sarah Arntz from Wattlab for providing helpful information about the implementation of solar panels in inland shipping.

Advice and help given by Maarten Verkou and Yilong Zhou about various Matlab models have been a great help in simulation the energy yield of the general cargo shipping fleet. Assistance provided by Andres Calcabrini and Yilong Shou during the module test in the PV lab is appreciated. I would like to thank Alba Alcañiz Moya for verifying the AHN4 and AHN3 skyline profiles from the surrounding of the docking harbour of Harmonie. I would like to express my appreciation to Stefaan Heirman, who made the discharge unit and to Daragh O'Connor, who has ordered the GPS data logger to conduct the experiment.

I am very grateful that Prof.dr.ir. Olindo Isabella, Head of the ESE-PVMD group, and Prof.dr.ir. Mark van Koningsveld, from the department CTIG Ports and Waterways, want to participate in my thesis committee.

Finally, I would like to express my gratitude to Susanne Verstegen for guiding me in writing this research report. Special thanks should be given to Florine Sreeram and Nadine Haagmans for 3D printing and modelling two miniature general cargo vessels.

Dora de Jong
Rotterdam, December 2021

Contents

List of Figures

List of Tables


LA PRIMAVERA
B.J. Spoelstra

1 Introduction

The motivation of the research is given in this chapter. In addition, the research objective and research questions are introduced as well.

Section 1.1 explains the motivation of this research. Then, the research objective and questions are given in section 1.2. And at last, the report outline is overviewed in section 1.3.

1.1 Motivation of the research

The demand for energy and resources increases as the human population grows. Fossil fuels are becoming scarce and polluted. Implementing renewable energy generation, such as Photovoltaic power plants, and more sustainable consumption behaviour, such as the electrification of inland shipping vessels, can be a solution. However, these solutions come with challenges as well. Renewable energy generation is volatile and causing problems to the electric energy network. Electrification is increasing the electrical energy demand at the source of consumption. The generation of off-grid decentralised sustainable energy systems can be one of the solutions to these challenges, see figure 1.1.

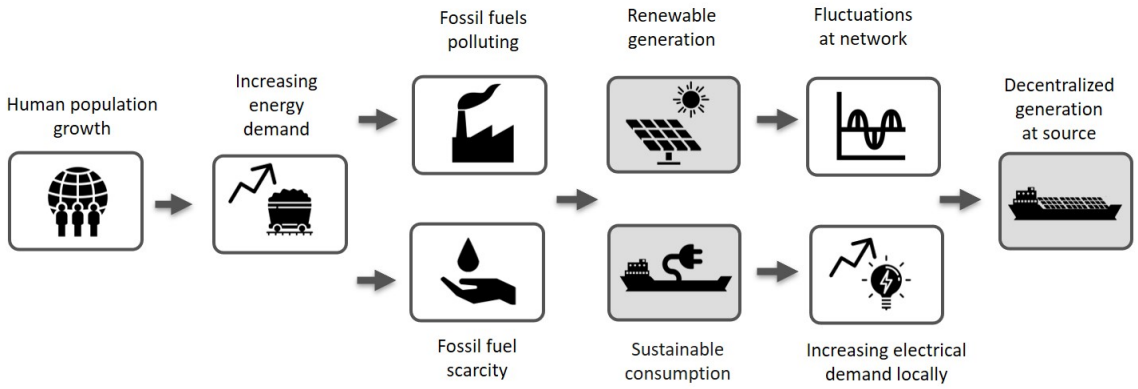

Figure 1.1: Decentralised generation of at the source of consumption

The research aims to estimate the potential of the implementation of photovoltaic energy on an inland shipping vessel. At the source of high energy demand, this implementation of decentralised energy generation can contribute to the mentioned challenges. To tackle those challenges, accurate calculation models are needed to gain accurate insights to innovate the future industry as optimal and sustainable as possible. The outcome of this research will be a mathematical model that can calculate this photovoltaic potential. This research contains an analysis of the results gained by the model. An experiment will verify the model. This research contributes towards both social and shipping industries future challenges.

Social challenges

Planet Earth is experiencing a sizeable human population growth, which leads to an increasing demand for energy and resources. As a result, fossil fuels, such as oil, gas, and coal are becoming scarce and negatively affect the earth. Implementing renewable energy systems, such as photovoltaic energy systems, can attend to this increasing demand while preserving the planet.

The installed PV capacity in the Netherlands, see subsection 2.1.1 is increasing, the share of renewable energy in the Dutch total primary energy supply remains small, 11.1 percentage (CBS, 2021). The Netherlands produces less energy than needed. To fill this gap, energy is also imported (Elgouacem & Jourmeay-Kaler, 2020). Especially for a relatively small and densely populated country like the Netherlands, it is essential to use the surface area effectively. Therefore, it is crucial to find more creative ways to integrate renewable energy into the current society. As this thesis proposes, implementing photovoltaic panels on vessels will also contribute to a more efficient surface utilisation.

The increasing share of renewable energy generation will also bring more complexity to the energy network. Renewable energy generation is very volatile. The energy generated by onboard photovoltaic energy systems will be generated in a decentralised and off-grid way and can be used directly, for example for propulsion, auxiliary energies or appliances. The energy can also be stored, for example, in battery packs and used on board later or delivered the energy to the grid when a vessel is docked. The battery pack can be used to stabilise the grid. When the energy demand is low, and there is an oversupply, the battery can be charged at a low cost. Decentralised energy production will also lower the power losses due to transmission.

The predicted size of the Dutch population will be 18.8 million inhabitants in 2035 and 19.3 million inhabitants in 2050. This is a growth of 1.4 million and 1.9 million inhabitants respectively with respect to 2020. In the largest cities in the Netherlands, the population is growing faster than in the rest of the country. Until 2030, the largest (ten) cities will increase by an average of ten percent. The growing population leads to an increasing demand for housing. Not only do more houses have to be built, but the height of the buildings must also increase (Gopal, Groenemeijera, van Leeuwen, Omtzigt, & Faessen, 2020). Over the past and coming years, the changing skyline will continue to impact on the sun's irradiance received by the urban area's surfaces. Therefore, it is essential to include the effects of skylines in photovoltaic energy calculations. This research will generate and consider over 3000 skylines throughout the Netherlands. These skylines can additionally be used for other research.

Shippings industry challenges

Figure 1.2 shows the percentage of the national inland shipping fleet with respect to the total European inland shipping fleet. The Netherlands has the largest fleet in Europe, making up 38.4% of the European shipping fleet (CCR, 2019). The entire Dutch inland shipping fleet consists of around 8000 vessels (IVR, 2018).

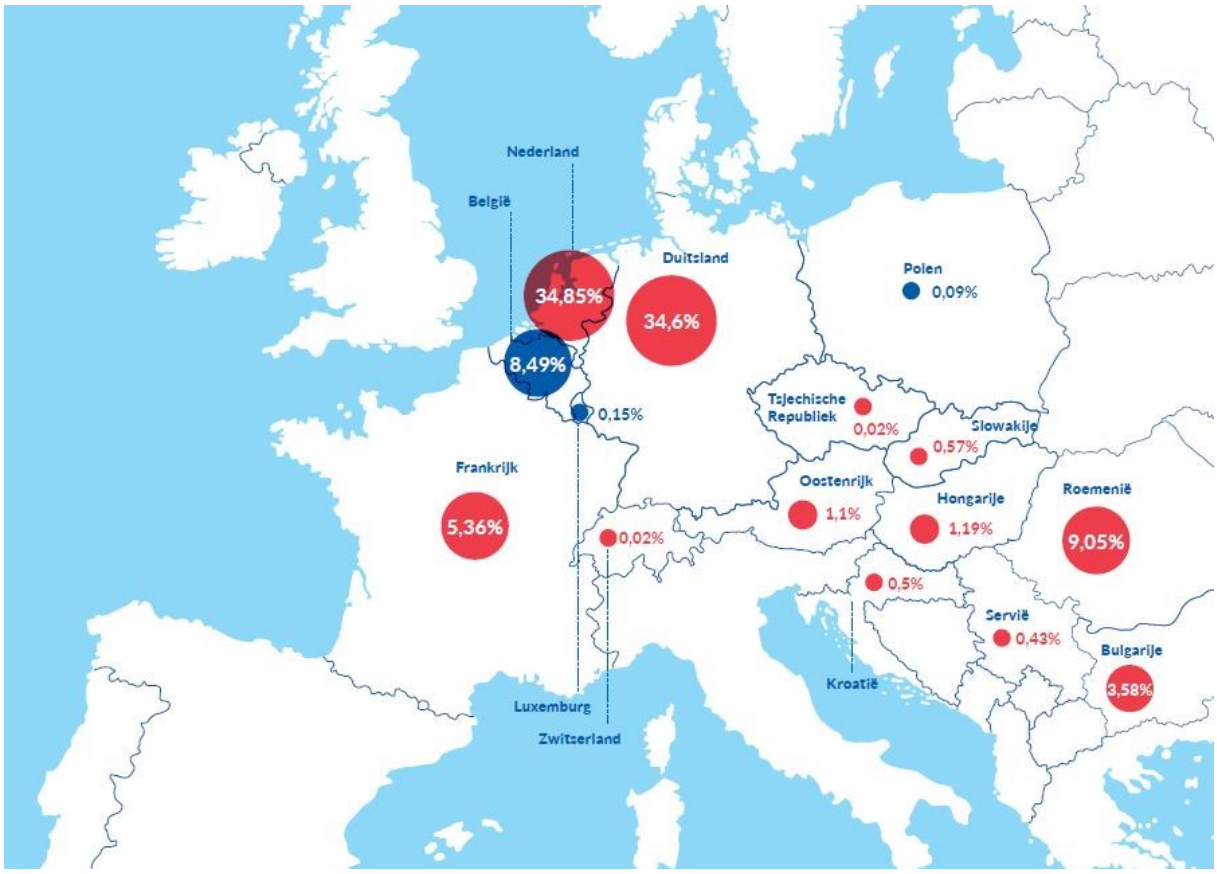

Figure 1.2: National percentage of inland waterway transport in Europe (CCR, 2019)

Goods and raw materials can be transported in containers or as bulk cargo. Bulk cargo is cargo transported in large quantities without packing, such as coal and sand. A standard size container vessel pollutes 38 and a bulk vessel pollutes 52 gram CO_2 (carbon dioxide) for every tonnes of cargo per kilometre. The emissions for various sizes of container and bulk vessels are given in the appendix A. This appendix also compares transport by road, track, and air transport. The CO_2 pollution from transport over water is smaller than the CO_2 pollution over road and air, but more significant for the transportation over a track by train (Klein et al., 2021).

The inland shipping industry aims to be climate neutral and emission-free by 2050. To achieve this, various goals have been set. According to the Green Deal COBALD GD208, from 2025 onwards, ships with propulsion that do not meet the phase 2 requirements of the guidelines 97/68/EG [1], are not allowed to enter the Rotterdam harbor area. This regulation concerns engines with a minimum CCR (Centrale Comissie voor de Rijnvaart) II standard (van Norel, 2018). The goal for year 2030 is to reduce CO_2 emissions from 2.1 megatons to 1.7 megatons per year. This takes into account the growth of the inland shipping industry. The total NO_x (oxides of nitrogen) emissions reduction in 2030 must be 3.8 $[kton]$ (Cuelenaere et al., 2021). To meet these goals, the propulsion of the inland shipping vessels need to change from diesel-powered to diesel-electric (short term), battery-electric (medium term) and hydrogen-fuel cell (long term). These changes in propulsion demand an enormous increase of on board energy (van de Geest & Menist, 2019).

[1] 'Reglement Onderzoek Schepen op de Rijn van de Centrale Commissie voor de Rijnvaart'

The energy generated by photovoltaic energy systems might be used on board of these future inland shipping vessels.

Off-grid photovoltaic energy systems can be a solution for the energy demand of moving vehicles, such as inland shipping vessels. Placing photovoltaic energy systems on vessels is advantageous because these systems do not compete with land intakes, such as residential land and agriculture. As a result, these vessels can now fulfil multiple purposes, transporting goods and generating sustainable energy. Inland shipping vessels are relatively large in comparison to trucks. The largest inland shipping vessel of the type VI 'Zesbaksduwstel' has a length of 193 meters and is 22.89 meters in width. This vessel can transport as much as 660 trucks. The class I 'Spits', is the smallest inland shipping vessel and is 38.6 by 5.05 meters. The Spits can transport as many containers as 14 trucks (Bureau voorlichting binnenvaart, 2018). These large surfaces are ideal for installing photovoltaic energy systems.

Placing photovoltaic energy systems on vessels has the advantage that these panels are additionally cooled by the forward speed of the ship itself. The energy efficiency of solar panels decreases when the temperature increases above the standard test conditions of 25 degrees Celsius, as the temperature coefficient of the solar panels power output is negative. The temperature coefficients used in this research can be found in Appendix B.

1.2 Research objectives

The aim of the research is to develop a method that estimates the photovoltaic potential of the Dutch general cargo fleet. The general research objective is as follows:

Determine the photovoltaic potential of the Dutch general cargo inland shipping fleet.

This research consists of different studies that will achieve the general objective. Eight research questions are formulated which contribute to achieving a particular objective.

Feasibility of the concept

The first two research questions introduce the implementation of photovoltaic energy systems on vessels and lead to an understanding of the feasibility of the concept.

1 Which methods exist to integrate photovoltaic energy systems on general cargo inland vessels?
2 What is the potential surface area of general cargo inland vessels that can be used to integrate photovoltaic systems?

Simulation modeling

This research will develop a simulation model that estimates the energy generated when installing PV panels on a general cargo vessel. Answering research questions three and four will contribute to the simulation of an energy system on a moving vessel.

3 How can the surroundings of the waterways be integrated in simulating the photovoltaic potential of a general cargo inland shipping vessel?
4 What is the sailing behaviour of general cargo inland vessels?

Model validation
The accuracy of the developed simulation model will be validated through an experiment. Research question five is related to this validation.

5 How accurate is the developed simulation model which calculated the photovoltaic potential of the general cargo inland fleet?

Photovoltaic potential
The last research objectives will give an insight into the photovoltaic potential of the general cargo inland fleet.

6 What is the photovoltaic energy yield of the general cargo inland fleet?
7 What is the photovoltaic potential of an individual general cargo inland vessel?
8 How much of the energy demand of inland general cargo vessels can be covered by photovoltaic energy? tge

1.3 Report outline

Chapter 2 introduces photovoltaic energy and the inland shipping industry. The methodology of the developed model to estimate the photovoltaic potential of the general cargo fleet and the executive experiment is given in chapter 3. The results of this experiment and the simulated general cargo vessels are featured in chapter 4. Chapter 6 concludes this research and offers answers to the formulated research questions. Chapter 5discusses the results and possible implications of the study. The last chapter 7 recommendation gives suggestions for further research


MAERSK
CMA CGM
RIDES
EPLEBND
H.J. RIBACHT

2 Literature review

This chapter provides a literature review, with the aim of better understanding this research. To develop a method that simulates the photovoltaic potential of the Dutch shipping fleet, knowledge of both photovoltaic energy and the inland shipping industry is required.

In the first section, background information about photovoltaic energy is given. Section 2.2 reviews the inland shipping industry.

2.1 Photovoltaic energy

In this section, the installed photovoltaic (PV) capacity worldwide and in the Netherlands will be displayed. Second, different PV applications will be discussed, together with an example. Two frameworks to simulate the PV systems are explained and compared. Finally, this section will take a closer look into PV modules and PV cells.

2.1.1 Photovoltaic energy market

In the last couple of years the photovoltaic market has increased worldwide. Figure 2.1 shows the cumulative PV installation from 2001 until 2020. The globally installed capacity in 2020 is at least 758.9 [GW_p]. With an installed capacity of 253.4 [GW_p] China is the world leader, followed by the European Union and the United states. In 2020 China has installed around 48.2 [GW_p] and the European Union has installed 19.6 [GW_p], as indicated in table 2.1 (PVPS, 2021). The decrease in the installation cost of PV modules lead to an increase in global installed PV systems.

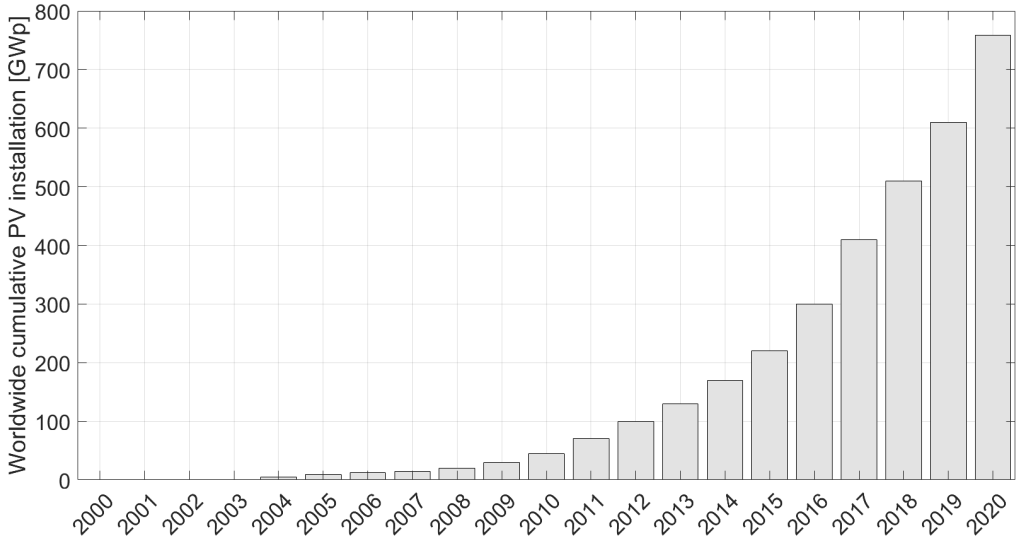

Figure 2.1: Worldwide cumulative PV installation (PVPS, 2021)

Table 2.1: Top 10 counties for cumulative and annual PV capacity in 2020 (PVPS, 2021)

	Annual installed capacity	**[GW_p]**	**Cumulative capacity**	**[GW_p]**
1	China	48.2	China	253.4
2	United States	19.2	United State	93.2
3	Vietnam	11.1	Japan	71.4
4	Japan	8.2	Germany	53.9
5	Germany	4.9	India	47.4
6	India	4.4	Italy	21.7
7	Australia	4.1	Australia	20.2
8	Korea	4.1	Vietnam	16.4
9	Brazil	3.1	Korea	15.9
10	Netherlands	3.0	UK	13.5

In Europe, Germany has installed the most PV energy, followed by Italy, Spain, France and the Netherlands. If we focus on the Netherlands, the cumulative PV installation follows almost the same trend as the total installed PV energy worldwide and is 10.2 [GW_p] (PVPS, 2021) (CBS, 2020).

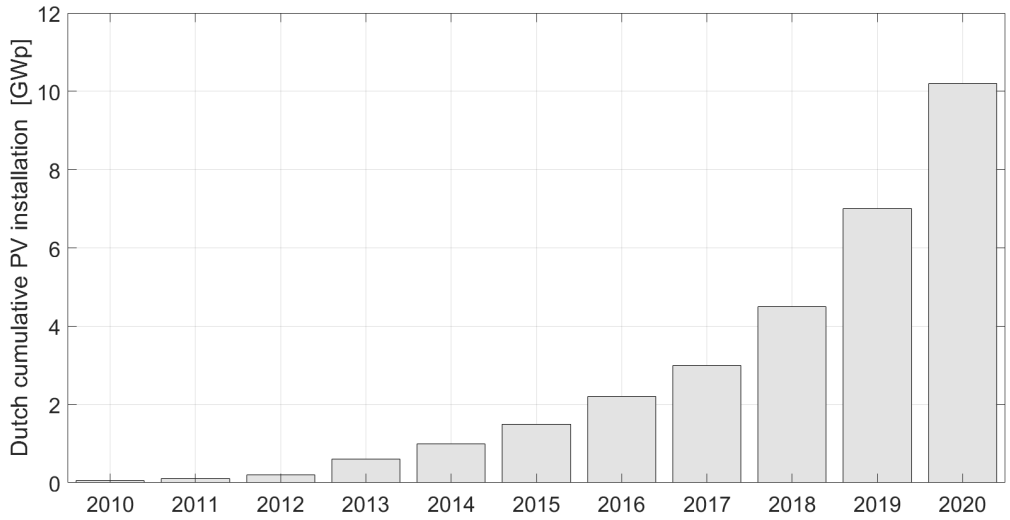

Figure 2.2: Dutch cumulative PV installation (CBS, 2020) (PVPS, 2021)

The PV market is still rising despite the COVID pandemic. According to IEA Photovoltaic Power Systems Programme (PVPS) the pandemic did not affect the PV market significantly, the delays in the lockdown in the first quarter in 2020 are almost caught up during the rest of the year (PVPS, 2021). The fact that the market has hardly been affected by the economic uncertainties caused by the pandemic shows the flexibility and potential of this sector.

2.1.2 Photovoltaic applications

PV energy can be used for different PV applications, see table 2.2. This research focuses on Vehicle-Integrated PV applications; PV integration on ships. An example in the Netherlands of a Vehicle-Integrated PV applications is given in subsection 2.2.3.

Table 2.2: Photovoltaic applications

Integrated PV	**Abbreviation**	**Examples**
Building applied PV	BAPV	PV modules on facades, PV module on rooftops
Building-integrated PV	BIPV	PV roof tiles, PV glass windows, PV facades
Urban-Integrated PV	UIPV	Information stations, telephone booths, atm stations, rural electrification, water pumping, bus Shelters, EV(electrical vehicles) charging stations
Environment-Integrated PV	EIPV	Grid connected floating PV systems(FPV), grid connected PV farms, solar roads
Vehicle-Integrated PV	VIPV	Space applications, PV on cars, trucks, ships and trains, EV charging stations
-	Product-Integrated PV	Phone charging, traffic lighting, navigational lighting systems, calculators, flashlights

An example of an Environment-Integrated PV is the INNOZOWA project. This project was an inspiration as well as the source of information, see section 3.15, for this research. In 2017, the Delft University of Technology in collaboration with partners[1] realized a floating PV energy system in Weurt, the Netherlands. The aim of the project is to model, design and monitor floating PV systems for inland water areas (Ziar et al., 2020).

Figure 2.3: INNOZOWA project (Blue 21, 2019)

[1]Waterschap Rivierenland, Hakkers BV and Blue 21

Regarding Vehicle-Integrated PV a research has been carried out to simulated the a PV energy system on board of a vessel (Lan, Wen, Hong, Yu, & Zhang, 2015). The vessel simulated is not an inland shipping vessel but sails in the open sea, therefore they are not shaded by the urban areas on land. In another research a cost-benefit analysis is executed for sea marine vessels where the PV systems are calculated with one fixed solar irradiance per zone, in this simulation the world is divided in 6 zones (Glykas, Papaioannou, & Perissakis, 2010). In both simulations, the surrounding, wind, cloud coverage and water temperature are not taken into account when simulation this energy yield.

2.1.3 Photovoltaic cells

This research is at photovoltaic energy system level, see figure 2.4. PV systems consist of several PV modules and PV modules consist of PV cells. It is important to have knowledge of the lower and more zoomed-in levels to make informed decisions for the simulation model.

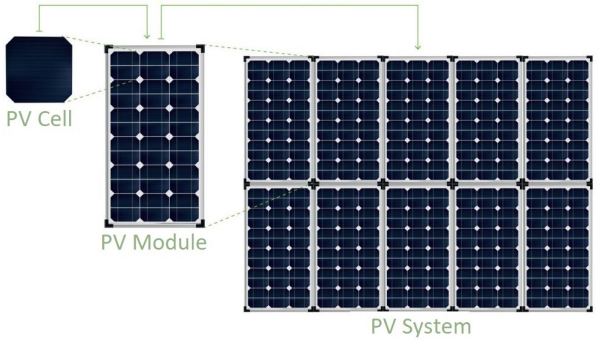

Figure 2.4: PV cell to PV systems (Scholz Solar, 2020)

PV Cells are the building blocks for PV modules. Figure 2.5 shows the working principle of a PV cell and explains how energy carried by light can be converted to direct electrical energy. This principle is based on the photovoltaic effect: the generation difference at the junction of two different materials in response to electromagnetic radiation. (Smets, Jager, Isabella, van Swaaij, & Zeman, 2016)

- Light in the form of photons entries the solar cell. Photons are absorbed in the absorber layer, the p-type semiconductor. For mono-crystalline silicon PV cells, silicon is used as semiconductor. Upon adsorption of the photons, an electron-hole pair is generated, in the absorber wafer. The electron is excited from its initial energy level to a higher energy level.
- The charge carriers - the electron and holes - need to be separated. Otherwise, the electron and hole will recombine; the electron will fall back to its initial energy level. The holes are positively charged and will move through the p-layer to the metal back contact. The electrons are negatively charged and will move through an n-type semipermeable membrane to the front metal contact.
- The electrons will flow through the electrical circuit, generating electricity. After the electrons moved through the electrical circuit, they will recombine with the holes at the metal back contact.

Figure 2.5 is a schematic representation of a PV cell, the dimensions of the different layers are not in proportion to real-life PV cells. For example, the n-type layer is many times thinner than the p-type semiconductor layer.

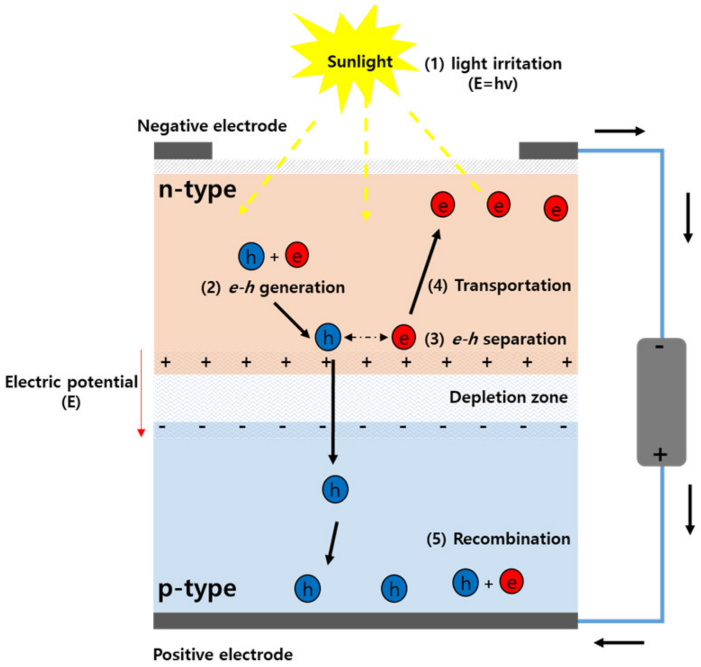

Figure 2.5: Working principle of a PV cell (Kim et al., 2021)

For crystalline silicon PV cells there are some technologies to achieve higher efficiencies. One of the most commercially used concepts is the PERC concept. PERC stand for Passivated Emitter Rear Cell or Rear contact, which adds a passivation layer to the rear of the cell. This passivation layer led to the increase of the cell efficiency (Tegio, 2018). The global production capacity of PERC cells rises rapidly. In 2014 the PERC cells had an efficiency of around 19% and an installed capacity of 1 GW. Comparing that to a capacity above 60 GW in 2019 and a cell efficiency of 21.7-22.2% (Balaji et al., 2021).

- The passivisation layer enables the reflection of unabsorbed photons to return into the absorber layer for a second absorption.
- This layer reflects photons with a specific wavelength, instead of absorbing these photons in the rear of the cell which leads to accumulating heat. As discussed in section 1.1 an increase in temperature will decrease the cell efficiency.
- This layer makes the movement of electrons easier and therefore generates an extra electric current.

2.1.4 Photovoltaic modules

PV systems consist of several PV modules. PV modules can be made up of different materials and technologies. Fourteen different types of PV technologies, along with their efficiency and some general information, are listed in table 2.3. The table has been compiled for this report based on three different sources (Sharma, Mehra, & Raj, 2021) (Smets et al., 2016) (Amin et al., 2017).

Table 2.3: Different PV technologies

Technologies	Efficiency	General information
Crystalline PV modules		
Polycrystalline silicon (poly c-Si)	±17-20%	Low cost, small crystalline grains, with random orientations causing lattice mismatches.
Monocrystalline silicon (mono c-Si)	±18-25%	Low cost, continuous lattice with no grain boundaries, commercially the most dominant PV technology.
Thin film PV modules		
Cadmium telluride (CdTe)	±18-22%	Lowest cost for thin-film, cadmium material is toxic, telluride is a rare element.
Copper indium gallium selenide (CIGS)	±20-22%	High efficiencies, challenging to perform large-area deposition, gallium is rare.
Microcrystalline silicon (a-Si:H or nc-Si:H)	±13%	Abundant material and not toxic, low processing temperature, not sensitive for high solar irradiation.
Gallium arsenide (GaAs)	±29%	High efficiencies, arsenide is highly toxic, expensive material as gallium is rare, used for space applications or concentrated PV.
Organic PV modules		
Organic (OSC)	±10-18%	Can be cheap but expensive encapsulation is needed, absorber materials are organic polymers or molecules, low stability and performance, low lifetime as these are degradable, commercialization is still difficult.
Hybrid organic-inorganic PV modules		
Perovskite (PSC)	±25%	Very strong absorption with low recombination, most cells contain lead which is toxic, cell degrades because of ultraviolet radiation and moisture.
Dye-sensitized		Low production cost, the electrolyte is unstable under various weather conditions, not commercially available.
Other concept PV modules		
Copper zinc tin sulfide (CZTS)	±12%	Low efficiencies, abundant, cheap and non-toxic elements.
Quantum dot (QD PV)	±16%	Easy fabrication process, consists of semiconductor nanoparticles
Concentrated (CPV)	±39%	Large mirrors and lenses concentrate the sunlight to a small solar cell, low operating cost.
Transparent (TSC)	±8%	Transparency of 80% can be achieved, used on the glass of buildings and vehicles,
Multijunction	±46%	More than one bandgap is used, very expensive, used for space applications and concentrated PV.

Monocrystalline silicon PV modules are worldwide the most dominantly used PV modules. Because of the low production cost and relatively high efficiencies, these modules are well suited for large integration into the inland shipping industry.

2.1.5 Photovoltaic systems

In this section, two approaches are explained to simulate PV systems. Photovoltaic systems are simulated with the aim to estimate the performance of the systems as accurately as possible. There are different methods to simulate the DC energy yield of a PV system. Two simulation frameworks are explained.

Simulation framework 1: Irradiance model based on power calculations

Figure 2.6 shows the diagram of the first simulation framework.

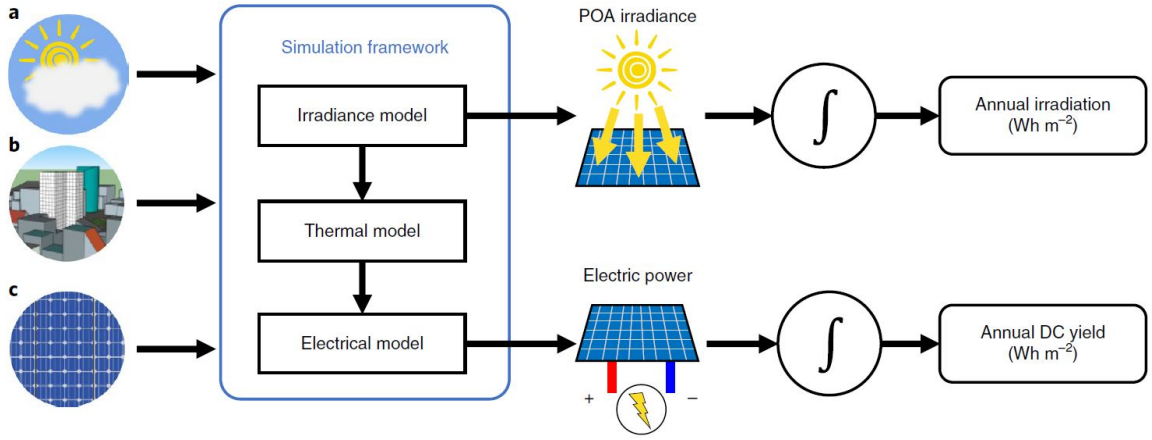

Figure 2.6: Irradiance-based model (Calacabrini et al., 2019)

The **inputs** needed for this framework are indicated with cluster circles a, b and c. There are three important components that affect the DC energy yield of a PV system.

- Meteorological data (a) can be obtained from various weather stations throughout the Netherlands. Examples of useful meteorological data are irradiance measurements, ambient and ground temperature, wind speed and cloud cover.
- A second input cluster which affects the DC energy yield are the location specifications (b). The landscape and objects around the PV system generate a skyline at a specific location. This skyline affects the sun energy, in the form of irradiance, received by the PV modules.
- The last cluster includes the PV module data (c). Mechanical, dimensional, electrical, optical and thermal parameters of the modules are needed to calculate the DC energy yield.

Three different **models** are needed to calculate the performance of the PV system, see again figure 2.6.

- The irradiance model uses the meteorological data (a) and the location specification (b) to calculate the POA irradiance received by the PV system.
  Most irradiance models use a decomposition model to obtain the direct normal irradiance (DNI) and the diffused horizontal irradiance (DHI) from the global horizontal irradiance (GHI). The GHI can be obtained from meteorological data (a).
  These three irradiance components can be used in transposition models to determine the plane of angle (POA) irradiance. The Hay's model is a robust

model, which gives a good estimation when the diffused irradiance is exactly known (HAY, 1993). The diffused component is split into two separate components. The Perez model is a sophisticated model, in where a third diffused component is used (Perez, Stewart, Seals, & Guertin, 1988). This model estimates when the measured globally horizontal irradiance on an hourly basis is known.

- The thermal model calculates the PV module temperature with the inputs of all the three clusters, which affects the efficiency of the PV modules as discussed in section 1.1. There are various thermal models to calculate the module temperature. The simplified steady state model, calculates the module temperature when taking into account only the ambient temperature. The Duffie-Beckman (DB) model also takes into account wind speed (Smets et al., 2016). The fluid-dynamic model is based on detailed parameters from the module itself and is surroundings, such as cloud covers (Smets et al., 2016).
- The electrical model uses the PV module data, the irradiance and the PV module temperature to calculate the electric power.

The **outputs** of this simulation framework are the annual irradiation and the annual DC yield.

- The annual irradiation is obtained by the POA irradiance. POA stands for plane of array. The POA irradiance is the irradiance received on the PV module by the sun when considering the orientation of the module relative to the sun. The unit of the POA irradiance is watts per square meter [W/m^2]. When the POA irradiance is integrated over time, the annual irradiation is calculated. The annual irradiation is given in watts-hours per square meters [Wh/m^2].
- The annual DC yield is obtained by the electric power output. The electric power, also known as electric power density, is given in watts per square meter [W/m^2]. This power output can be calculated for every moment in time. When the power output is integrated over time, the DC yield in [Wh/m^2] of the PV systems is calculated. The DC energy yield is the output of the PV system over a time frame, for example a year. The DC energy yield for one year is referred to as the annual DC energy yield. The DC energy yield is the energy converted by a PV system before other energy conversions, such as by power converters.

This simulation framework has the disadvantage that the simulation computational time is relatively large, as the energy yield calculations are based on time-dependent hour calculations.

Simulation framework 2: Simplified irradiation model

The second framework aims to accurately estimate the annual irradiation and DC yield with a significant lower computational time. This simulation framework is based on the fact that weather conditions are usually similar over a couple of years. Average weather data of several years is analysed to generate climate data. As explained in simulation framework 1, the annual irradiation is calculated according to meteorological data (a), weather data, and locations specifications (b). As the meteorological data is now fixed, the irradiation is dependent on its location specifications.

The **annual irradiation** can be calculated according to the following expression (Calacabrini et al., 2019).

$$I = (c_4 + c_5\alpha_{gnd})SVF + \sum_{k=1}^{3} c_k(1 - SCF^k) \tag{2.1}$$

- The correlation coefficients c_1,...,c_5 in $[Wh/yr]$ are coefficients for a specific location and orientation of the PV module.
- The SVF (sky view factor) indicates the proportion of the sky that is visible from the centre of the PV module.
- The SCF (sun coverage factor) is the ratio between the time that the sun is blocked (the sun is behind the module or blocked by the skyline) and the annual sunshine duration at that location (taking into account a clear horizon). The SCF is not an irradiance weighted parameter.

The **annual DC yield** can be calculated with the annual irradiation given by equation 2.1 and the efficiency of the PV module. This efficiency is, amongst others, dependent on the module temperature and the irradiance level. The solar irradiance levels and the module temperature, which is dependent on the ambient temperature, vary from month to month. Therefore the performance of the PV systems varies as well. As this variation is less than 10%, the annual DC yield can be calculated similarly(Calacabrini et al., 2019).

$$E = (d_4 + d_5\alpha_{gnd})SVF + \sum_{k=1}^{3} d_k(1 - SCF^k) \tag{2.2}$$

When comparing the two frameworks, the simplified irradiation model has a lower computational time. But this framework has the disadvantage that the annual irradiation and DC yield are calculated on a yearly dependence and can therefore be less accurate. An other disadvantage of the second framework is that the solar incidence angle on the PV panel and the air mass coefficient are not taken into account in this model.

2.2 Inland shipping

In this section the Dutch shipping fleet is reviewed. Secondly, the general cargo vessels that are suitable for the integration of PV panels are identified. The inland waterway traffic, with important waterways is discussed in section 2.2.2. Finally, several innovations concerning the inland shipping industry are included.

2.2.1 General cargo inland fleet

The inland shipping fleet of the Netherlands is the biggest in Europe as discussed in section 2.7. The inland fleet consists of 5060 vessels, with various types, indicated in figure 2.7. Each type of ship has its own purpose, which leads to a different ship design. The vessel types, in figure 2.7 are named by their Dutch vessel type name, as translation to English is not always possible. (IVR, 2020) The columns indicated in figure 2.7 in green are from the general cargo type.

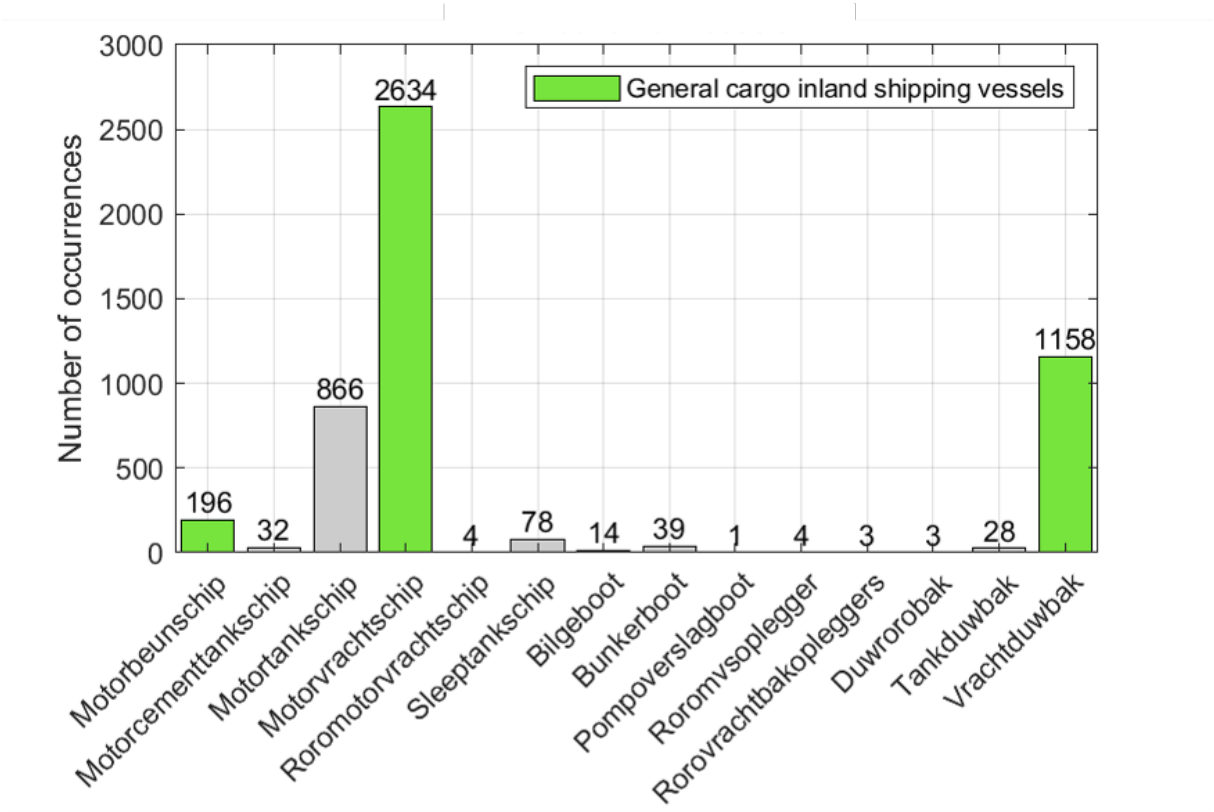

Figure 2.7: Distribution of vessels

Advantages general cargo vessels

General cargo vessels seem to be suitable for the implementation of PV panels. There are a couple of advantages of these vessel types that make them suitable for the implementation of PV panels. These ships have little equipment installed on top of their deck. Most vessel types have a lot of equipment installed on the top of their decks, which limits the implementation of PV panels on these vessels. General cargo ships have a relatively large surface area that is only used to store goods, the hold. Above this hold, PV panels can be installed by means of a construction. All ships of this type look similar. The ship is designed as square as possible, in order to be able to transport as many goods as possible onboard. The wheelhouse is at the back, before that there is the hold. After the hold is a small part that contains the necessary equipment, such as anchors and cranes. From the complete inland shipping fleet, 79% of the vessels are general cargo inland vessels (IVR, 2020). These ships are organised in 6 different classes. Every class has guidelines for the dimensions of the ships. These guidelines are based on the dimensions of the canals, sluices and bridges. These fixed dimensions make systematically deploying PV panels easy. These classes (CEMT-class) and corresponding ship dimensions are indicated in table 2.8.

CEMT-klasse	breed-te (m)	lengte (m)	diepgang (m)		strijkhoogte (m)	laadverm. (ton)	motorverm. (kW)	boegschroef (kW)
			geladen	leeg				
I	5,05	38,5	2,5	1,2	4,25	365	175	100
II	6,6	50 - 55	2,6	1,4	5,25	535 - 615	240 - 300	130
III	8,2	67 - 85	2,7	1,5	5,35	910 - 1250	490 - 640	160 - 210
IV	9,5	80 - 105	3,0	1,6	5,55	1370 - 2040	750 - 1070	250
Va	11,4	110 - 135	3,5	1,8	6,40	2900 - 3735	1375 - 1750	435 - 705
VIa	17,0	135	4,0	2,0	8,75	6000	2400	1135

Figure 2.8: Characteristics general cargo vessels (Rijkswaterstaat, 2020)

Bulk and container vessels

Under general cargo vessel, a distinction is made between two types: container vessels and bulk vessels, indicated in figure 2.9 en 2.10 respectively. The container vessels and bulk vessels can each be classified into the different CEMT-classes (Bureau voorlichting binnenvaart, 2018). Container vessels transport containers and bulk vessels transport bulk goods such as sand, coal and grains. On the hold of the bulk vessels hatches are installed.

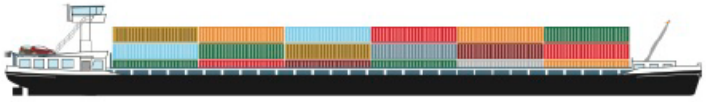

Figure 2.9: Container vessel (Bureau voorlichting binnenvaart, 2018)

Figure 2.10: Bulk vessel (Bureau voorlichting binnenvaart, 2018)

Even though there is a distinction between container and bulk ships, these ships are often the same and can transport both types of goods. It is therefore difficult to know exactly what the ratio between these ships is within the general cargo fleet. Centraal Bureau voor de Statistiek (CBS) estimated that 78% of the general cargo vessels carry bulk and 22% transport containers. (CBS, 2019a)

Prospect inland shipping industry

Because of the energy transition and the nitrogen crisis, the inland shipping industry is decreasing. Due to the COVID pandemic, the industry is declining even more. In general, the amount of goods transported by the inland shipping sector is declining from 12.9% to 10.2% with respect to 2019 (Panteia, 2020).

Due to the COVID pandemic, the container fleet decreased by 3% in 2020 with respect to 2019. It is expected that the container fleet will increase again after 2025 by a percentage of 19% to 25% (Panteia, 2020). This increase in container transport has various reasons. Looking to the future there will be a shift in bulk to container transport. A great deal of cargo, both liquid and dry bulk, which used to

be shipped in bulk ships, is going to be 'packaged' in containers and transported with container ships. This way, the goods can be grouped for smaller shipments to multiple receivers. As a result, the useful space of the ship will be fully utilized. Loading and unloading are also faster and easier. It is estimated that half of the transportation costs are caused during the loading and unloading of goods (Panteia, 2020).

Due to the COVID pandemic and the rising energy transition is the demand for bulk transport is declined. The demand for coal and other oil products is decreasing. In the long term, it is expected that the transport of livestock feed will also decrease. At the moment, the corona crisis is already leading to reduced demand for the transport of construction materials which will be even more due to the nitrogen crisis (Panteia, 2020). Therefore, bulk transport is declining more sharply and probably will not have the opportunity to bounce back.

2.2.2 Inland shipping traffic

Inland vessels have different sailing patterns, even within the same classification and size. Likewise, for general cargo ships, each ship has its own sailing pattern, which can also change over time. There are ships that sail on the spot market, depending on supply and demand. These ships transport depending on where and when there is work. There are also ships that transport goods in regular services. These ships transport goods between container or bulk terminals on a continuous basis. The division between these two shipping profiles within the general cargo shipping fleet is unknown. Therefore distinguishing general trends within the transport pattern of the inland shipping industry is difficult. Simulating a representative trajectory of an inland shipping vessel is not possible as the sailing pattern varies for every vessel individual.

In order to find out the real trajectory of inland shipping vessels, location data of individual ships is needed. This vessel location data is collected in AIS data. AIS data stand for automatic identification systeem and every professional ship must send the aforementioned parameter to a central database (International Maritime Organization, 2019). The vessel traffic services (VTS) uses this data with as goal to avoid collisions and to increase safety on board ships. AIS used VHF(very high frequency) transceiver with Gloabl Posistioning system receiver combined with on-board installed sensors, see figure 2.11.

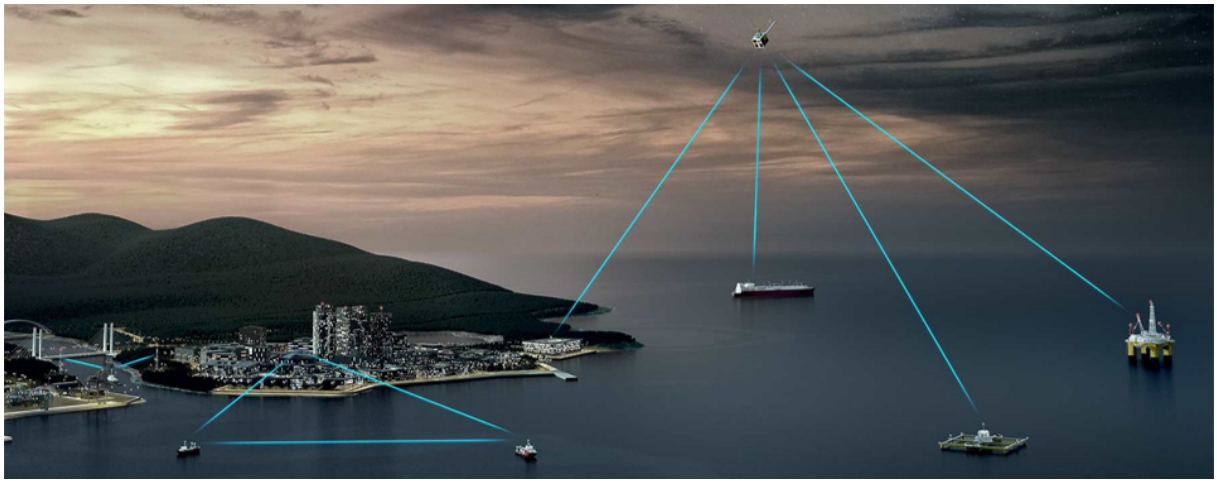

Figure 2.11: AIS (KONGSBERG MARITIME, 2021)

Figure 2.12 shows the main waterways in the Netherlands, which are used by general cargo inland shipping vessels. Goods are mainly imported from sea via the Noordzeekanaal, Nieuwe Waterweg, Hartelkanaal and Kanaal zuid-Beverland. These goods are redistributed in the seaports of Rotterdam, Amsterdam, Zeeland and Groningen, in order of size (CBS, 2019b). From there, the goods can be shipped further into the Netherlands or exported to other countries. The goods are mainly transported to the east via the Waal and the Rijn. Towards Belgium, the goods are transported over the Schelde, Kanaal Ghent-Terneuzen and the Maas.

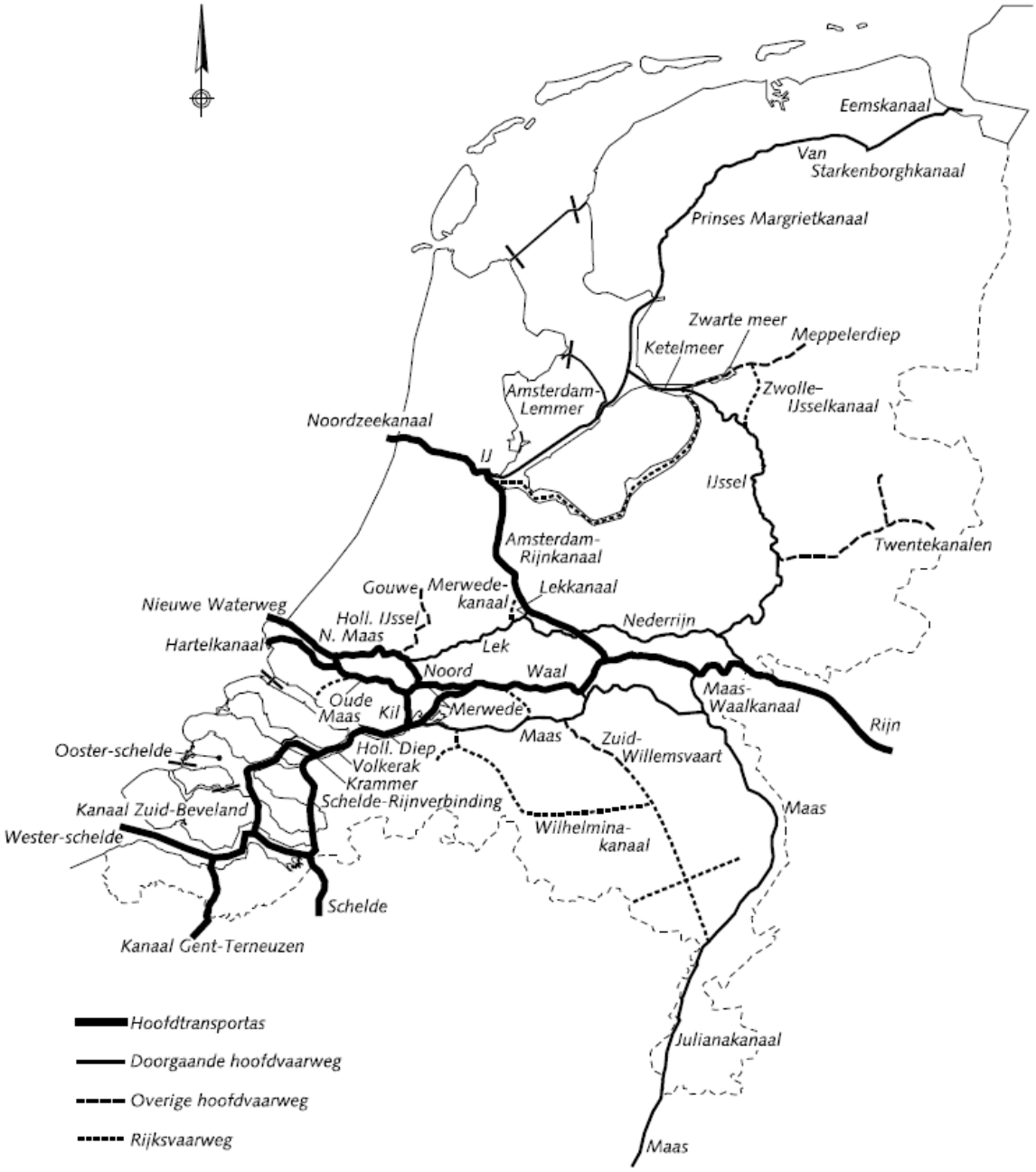

Figure 2.12: Main waterways in the Netherlands (Bureau voorlichting binnenvaart, 2018)

2.2.3 Sustainable inland shipping innovation

In the Dutch inland shipping industry, different innovations regarding sustainable shipping are developing. Figure 2.13 shows the first Dutch inland vessel propelled by an electrical engine with the electrical energy demand delivered by interchangeable energy containers (ZES, 2021).

Figure 2.13: Alphenaar (ZES, 2021)

The Alphenaar uses a lithium-ion interchangeable energy container developed by ZES (Zero Emission Services) to meet the electrical demand onboard. These 20ft container batteries can be easily changed during loading and unloading the other containers. The battery containers can have a grid-stabilizing effect and can be charged in case of energy oversupply. The ZES containers are charged at the first charging station at the container terminal in Alphen aan den Rijn (ZES, 2021). The Dutch government and the European Union have given millions for subsidies for the shore power facilities, to be able to realize the aforementioned projects and to reduce generator consumption on board of ships (Schuttevaer, 2020) (Maritiem Nederland, 2021) (Nieuwsblad Transport, 2021).

Figure 2.14: ZES interchangeable energy containers (ZES, 2021)

The Dutch company Port Liner has developed a new generation general cargo inland shipping vessels. These ships have not yet been built, but the goal is to have 15 ships in service on short term (when exactly unknown). Five of these ships will be EC52 type. The EC52 vessels are Port Liners zero emission 52 metres ”Kempenaar”-sized multi-purpose vessel. The other ten is from the type Port Liner EC110. The EC110 is a standard 110x11.45 meters vessel, with an action radius of 30 hours, see figure 2.15. Both the EC52 and the EC110 vessels have a wheelhouse that can move vertically and can transport bulk and containers. The Port Liner vessels are battery-electric propelled, with vanadium Redox flow batteries (Port Liner, 2020).

Figure 2.15: Computer graphic of the Port Liner EC110 (Port Liner, 2020)

The consortium Wattlab, Damen Shipyards and Blommaert Aluminium are integrating PV panels on the hatches of the bulk vessel Ms Oleander, see figure 2.16. The Ms Oleander is currently sailing with a second test set-up of solar panels, in order to find out the ease of use, the energy yield and the robustness of the system. The PV panel provided by Watllab are foil to foil-based. Wattlab expects that every hatch will have an annual energy yield of 2900 kWh (Solar magazine, 2021). The Ms Oleander can hold 22 hatches and is 110 meters in length. Wattlab claims that the payback period of their solar hatches is 5 to 8 years (Solar magazine, 2021).

Figure 2.16: Ms Oleander (Solar magazine, 2020)

2.3 Implementation of photovoltaic panels

In this chapter literature on photovoltaic energy and the inland shipping industry. This is a foundation of decisions that are made in the simulation model and for execution the experiment. It also provides an answer of the first research questions. Implementing photovoltaic panels on general cargo vessel can reduce there emissions. Additionally, the travel range of a electrical vessel, such as the Alphenaar, can be extend when installation a photovoltaic system onboard.

PERC monocrystallinge PV panels are low in production cost and the relative high efficiency made them well suited for large scale integration of PV systems. PV systems can be simulated by two different frameworks: Irradiance model based on power calculations and Simplified yearly irradiation model. The Irradiance model based on power calculations can calculate the PV energy yield for a specific period of time, with every specified time step size. The Simplified yearly irradiation model is a yearly depended model and has a faster simulation time.

Reviewing the Dutch inland shipping fleet the implementation of PV panels on general cargo shipping vessels is founded the most favorable, because of the following reasons:

- The general cargo fleet takes up 78% of the complete inland shipping fleet.
- General cargo vessels various in size, but a large number of these vessel are relatively large.
- Little equipment is installed on top of the decks of general cargo vessels.
- These vessels are as rectangular as possible, to transport maximum amount of goods.
- General cargo vessels look all similar and have standardized dimensions, making systematically deploying PV panels convenient.
- A large surface area of the vessels, the hold, can be used to integrate PV panels can be stored.

The PV panels can be placed on the holds of the general cargo vessels. The other surfaces are not suitable as there is equipment installed or there is a wheelhouse located. Between general cargo inland vessels two type of ships can be distinguished: container vessels and bulk vessels. The PV panel installed on the hatches of the Ms Oleanders is an example of how the PV panels can be implemented for the bulk type of vessels, see figure 2.17. For container vessels there is not yet an example of the implementation of PV panels, but the PV panels can be placed on top of the containers itself as done in figure 2.18. As containers have standard sizes and made to stack on top of each other, PV panel can be easily connected and systematised placed on containers.

Figure 2.17: Hatch implementation (Delta TU Delft, 2020)

Figure 2.18: Container implementation (Fence4Events, 2021)

3 Methodology

In this chapter the methodology of this research is described. The design decisions of the simulation model are described, to calculate the photovoltaic energy yield of a vessel. The input parameters, for both simulating the general cargo inland fleet as well as Harmonie, are discussed. In this research an experiment is conducted, to estimate the accuracy of the developed simulation model. The chapter gives an overview of the monitoring plan and equipment of this experiment

The first section, section 3.1 of this chapter describes the simulation model. The experiment is discussed in section 3.2.

3.1 Simulation model

The simulation model which is developed in this research is designed to simulate the energy yield of general cargo inland vessels. An experiment is conducted, in which a test vessel Harmonie, will validate this developed model. To simulate Harmonie in the model, some input parameters are different. The differences between the simulation of the general cargo vessel and Harmonie are explained in this section.

3.1.1 Simulation framework

While designing this simulation model, various choices are made. These choices have impacts on the output and inputs of the model. The design choices and their importance are discussed in this subsection.

Time dependency

In the simulation model, the energy yield of a moving vessel is simulated. As indicated in figure 3.1, a vessel follows a path over time. The location of the vessel is changing over time, and so are the parameters depending on the location around the vessel. As discussed is section 2.1.5 the simulation framework has three input components: meteorological parameters, surrounding parameters and PV module parameters. The meteorological and surrounding parameters are changing for every location. Since the location is changing over time, the simulation needs to be time-dependent.

Section 2.1.5, discussed and compared three different types of simulation frameworks. The developed simulation model is based on the first simulation framework: an irradiance model based on power calculations, as this framework allows the energy yield to be time-dependently.

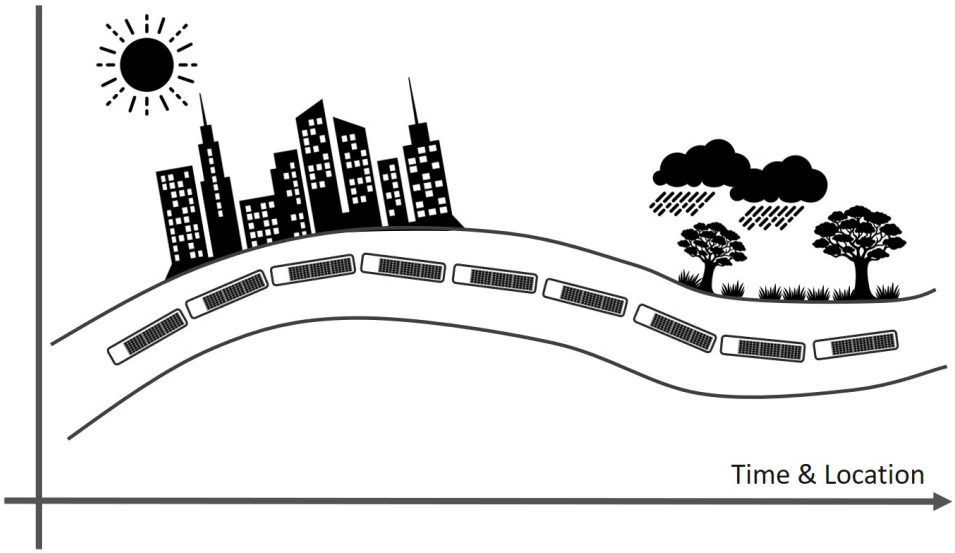

Figure 3.1: Path of a moving vessel

A simplified overview of the developed model is provided in figure 3.2, and contains the different components of simulation framework 1. An extended version of the simulation model is given by figure 3.3.

With this design decision, the simulation is able to simulate a vessel that follows a path over time, with a changing location and is able to calculate the energy yield based on the time and location.

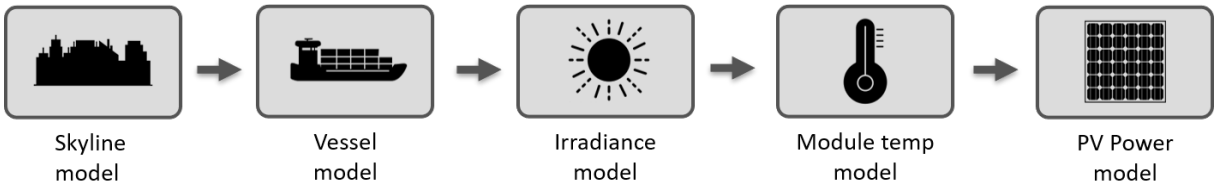

Figure 3.2: Simulation model overview

Large simulation framework

When a PV system at a fixed location is simulated, for example installed on a roof, the simulation of the PV system is relatively small and straightforward. One PV system on one location needs to be simulated. In the developed model in this research, 2147 PV systems on vessels are simulated. Every of those 2147 PV systems has changed location over time throughout the Netherlands.

As this simulation is relatively large, the computational time will be a limiting factor in simulating the energy yield. Therefore, the time step of the power calculations is set to be one hour. On yearly basis, the simulation size is 8760 time steps of one vessel. By the law of large number (LLN) the average energy yield will come close to reality the larger the size of the simulated points. With an hourly time step the simulation size of one vessel is 8760. As there are 2747 vessels with hourly time step, the complete simulation size of the complete fleet consists out of 24,054,960 time steps.

With this design decision of one-hourly time steps, the computational time will be feasible, while preserving the accuracy of the simulation.

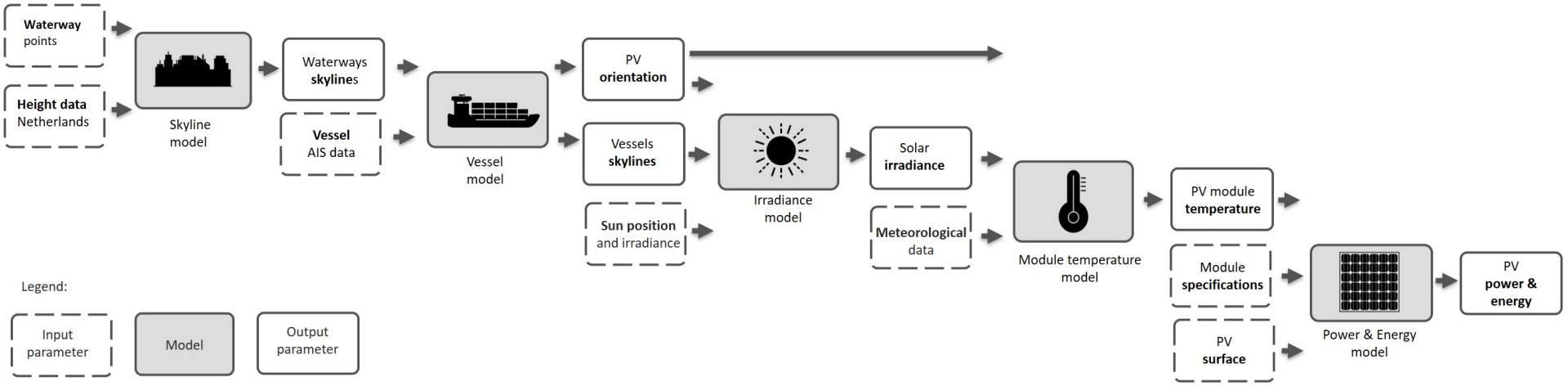

Figure 3.3: Simulation model overview extended version

3.1.2 Skyline model

As discussed the surrounding for a simulated vessel is changing over time. Therefore. for every hour the surrounding is needed to be simulated. When simulating the surrounding of 2147 vessels for every hour over one year, 24,054,960 skylines of the surroundings are needed to be simulated, see figure 3.4. Generating a skyline is a time consuming process, the computational time is relatively larger.

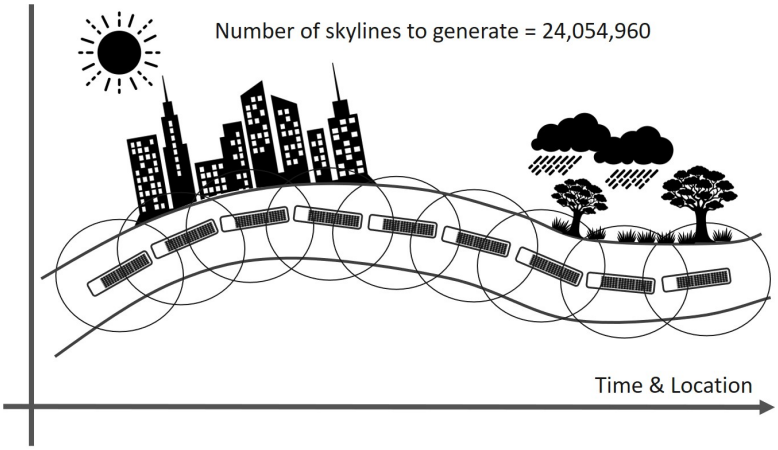

Figure 3.4: Skyline simulation for every vessel individually

Therefore this skyline model is designed differently. The skyline model generates skylines of the surroundings of the waterways in the Netherlands which are used by general cargo vessels, see figure 3.5. The general cargo vessels sailing over the waterways, the location of the vessels will correspond to the surrounding of the waterways. The surrounding of the waterways are simulated by 3036 skylines, this is 6193 times smaller and faster than the above-explained simulation.

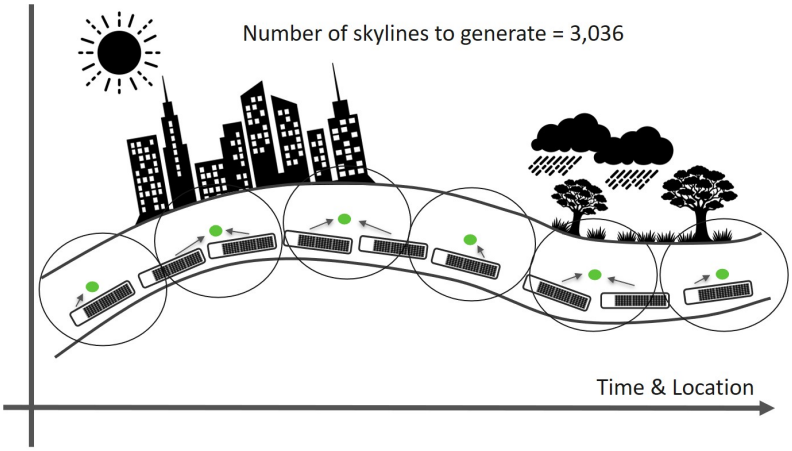

Figure 3.5: Skyline simulation method for the waterway points

The skyline model is developed to simulate the surroundings of the Dutch inland shipping waterways. The model uses geo-referenced waterway points and Height data of the Netherlands as input parameters and gives as output 3036 skyline profiles around the waterways.

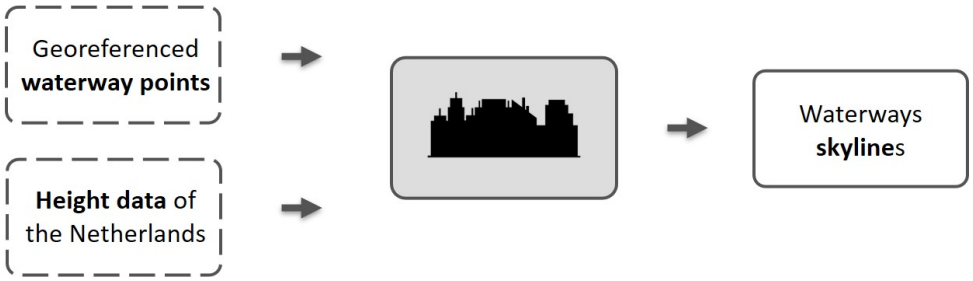

Figure 3.6: Skyline model

Input: Geo-referenced waterway points

The waterways points provide a representation of the locations of the waterways used by inland shipping vessels. For every waterways datapoint, a skyline is generated to simulate the surroundings of that location. The waterways point of the Netherlands is provided by the Dutch government, Rijkswaterstaat (Rijkswaterstaat, 2020). The points can be uploaded in various geographical visualize programs. In this research, the program QGIS is used to visualize these points and save them to a shapefile, so they can be uploaded in the Matlab simulation model. The distance between the points is on average 1000 meters. Rijkswaterstaat only provides waterway data points for the canals, not for the open waters such as Ijsselmeer. Figure 3.7 shows the waterway datapoints provided by Rijkswaterstaat in QGIS.

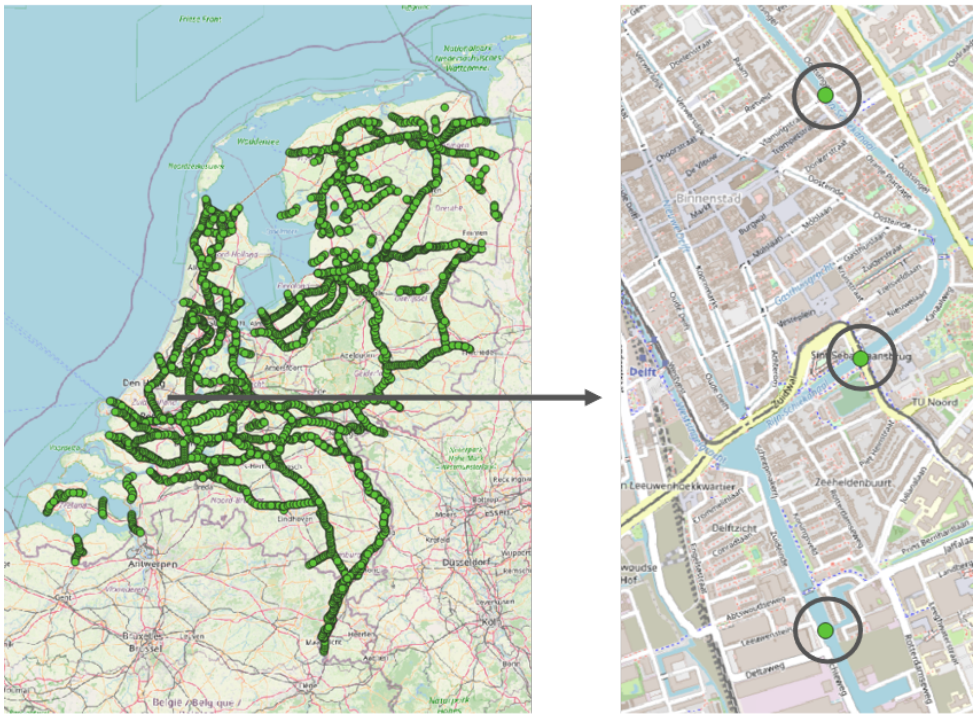

Figure 3.7: Waterways datapoints, left: the whole Netherlands, right: port of Delft

Input: Height data of the Netherlands

Height data of the Netherlands is used to generate a skyline of a specific waterway point. The government of the Netherlands provides various height data set as open source. The two main available data sets are Digital Terrain System (DTS) and Digital Surface Model(DSM). The DTS model represents height data of the surface

of the earth. The DSM model also includes the height of vegetation and building on the surface of the earth. A skyline of the surroundings of the waterway points can be generated with the use of a digital surface model (DSM). Light detecting and ranging technologies (LIDAR) are used to generate this DSM dataset. The most accurate dataset that the government provides is the AHN3 (Actueel Hoogtebestand Nederland 3) with a resolution of 0.5x0.5 $[m^2]$ (Rijkswaterstaat, 2021). The government is currently creating a new dataset: AHN4. To generate skylines as accurate as possible, the skyline model is developed in such a way that the new dataset AHN4 can be used as well by the time it is published.

The waterway points are scattered throughout the whole of the Netherlands, so the AHN3 DSM dataset of the complete Netherlands is needed to simulate the skylines of the points. The AHN3 DSM dataset of the complete Netherlands is divided into 1374 tiles. Each tile represents a Tiff image with a size of around 500MB, which leads to a complete AHN3 DSM dataset of 656GB. To process this amount of size of data, the model is developed in a way that for each waterway point location it can identify in which of the 1374 tiles it is located. To generate a skyline for this point, it only has to process that specific tile.

Output: Waterways skylines

The skyline model scans the horizon to generate a skyline such as figure 3.8. For the 360 degrees view of a specific waterway datapoint, the altitude elevation of the vegetation and buildings is calculated.

The scan radius which will be used to generate a skyline at a specific point is 1000 meters. To generate a skyline as accurate as possible a width range of the area around the waterway point is needed to scan the horizon. If a radius around the waterway data point is used to generate the skyline, it is possible that the elevation of the building and vegetation that will be influencing the skyline profile, are not taken into account. A radius of 1000 meters is selected to ensure that the above problem will not occur. The chosen radius in this model is very large, which means that this radius sometimes falls outside the range of the processed tile. To ensure an accurate skyline, the model will upload adjacent tiles and merge them into one big tile.

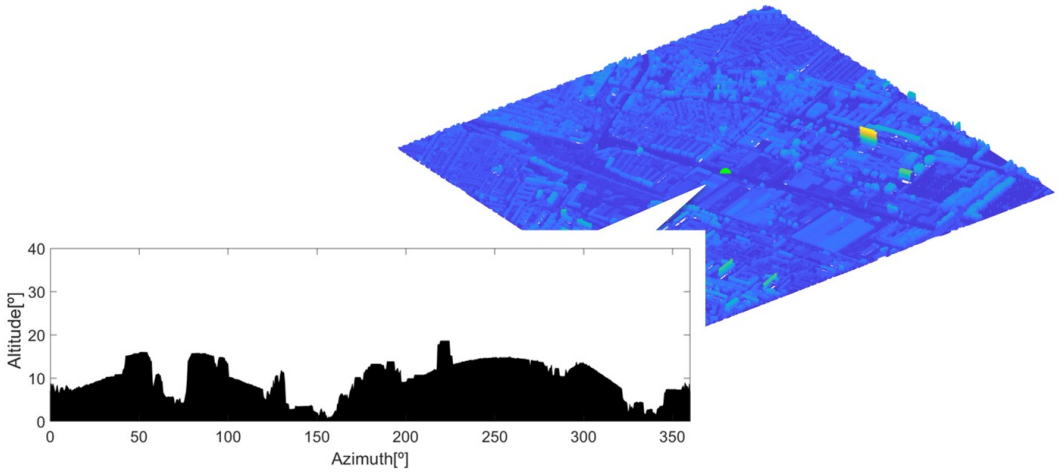

Figure 3.8: Skyline of a waterway point in Delft

The solid angle of the sun is an indication of how large the sun appears to an observer who is located on earth. The sun covers the sky on average with an angular diameter of 0.53 degrees (Swinburne University of Technology, 2021). Because of the size of the sun's solid angle, the step size in which the skyline model dived the sky is 0.5 degrees, for both the altitude and the azimuth.

The skyline is generated from the waterline up. A waterline height of -0.745 is used, this is the average drainage level of the Netherlands. A drainage level is the water level of the canals with respect to Normaal Amsterdams Peil (NAP). Water is pumped trough the Netherlands to make sure there are no floods, leading to a variation in the drainage level. The drainage level is set as a target level and kept fixed if possible. There are different drainage levels trough the Netherlands, they variate between -0.4 NAP and -1.28 m NAP (Hoogheemraadschap, 2020).

The location of a waterways datapoint in a 3D grid can be considered by x_{ww} and y_{ww} and with a height of h_{ww}, which is defined as -0.745 meters. The LIDAR height data of the Netherlands gives us information about every point in the skydome. When considering one point from this height dataset, this location can be defined as x_p and y_p in a 2D map and h_p is the height of the location point. The raised altitude and azimuth of this specified point p, with respect to the waterways point, can be calculated by equations 3.1, 3.2 and 3.3 (Keijzer, 2019). For every azimuth from 0 to 360 degrees, with a step size of 0.5 degrees, the highest raised altitude, observed from the waterway point, is visualized in the skyline profile. The altitude will be scanned within a radius of 1000 meters, $r_{ww-p,max} = 1000[m]$.

$$r_{ww-p} = \sqrt{(x_p - x_{ww})^2 + (y_p - y_{ww})^2} \tag{3.1}$$

$$\theta_{ww-p} = \arctan\left(\frac{x_p - x_{ww}}{y_p - y_{ww}}\right) \tag{3.2}$$

$$\alpha_{ww-p} = \arctan\left(\frac{h_p - h_{ww}}{r_{ww-p}}\right) \tag{3.3}$$

3.1.3 Vessel model

The Vessel model is developed to simulate the different vessels for which the energy yield is calculated. The model uses the skylines of the waterways generated in the skyline model, described in section 3.1.2. As second input, the Vessel model uses various parameters of the vessels to simulate them. Figure 3.9 gives an overview of the inputs and outputs of the Vessel model.

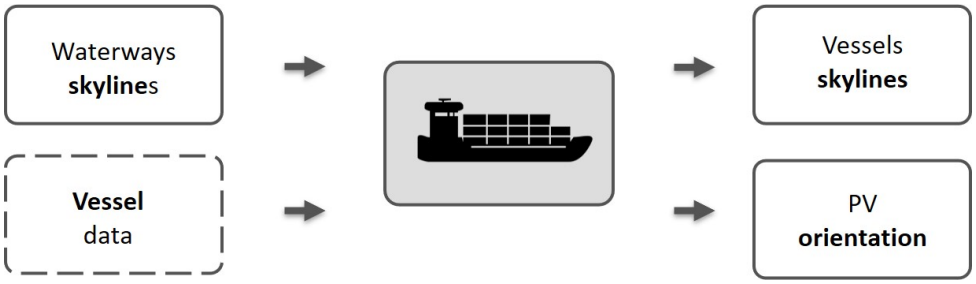

Figure 3.9: Vessel model

Input: Vessel data

To simulate vessels in the Vessel model the location, heading, speed, length and width of all the individual vessels are needed. These parameters are combined from the vessel data set. These parameters are obtained differently for the General cargo fleet and Harmonie, see table 3.1.

Table 3.1: Source of the parameters needed for the vessel data set

Parameter	Unit	General cargo fleet	Harmonie
Vessel width and length	[m]	AIS data	Real life measurement
Vessel longitude and latitude	[°]	AIS data	On-board GPS data logger
Vessel speed	$[m/s]$	AIS data	On-board GPS data logger
Vessel heading	[°]	AIS data	On-board GPS data logger

General cargo fleet

The vessel dataset of the general cargo fleet can be obtained from AIS data, as discussed in section 2.2.2. AIS data is stored for every corporate vessel in the Netherlands for every second. The AIS dataset provided by the government is very large and disorganised. The AIS data set is anonymous, the name and cod of the vessels are removed.
The processed dataset for this research is uploaded to a workstation at the technical university of Delft. With the programmes Github, Sourcetree and Pyhton the comprehensive dataset is processed, so that the data can be uploaded into the Matlab simulation model. The Python script that is used to process the AIS data can be found in appendix C.
The data set provide contains AIS data from 2019 for the months: January, April, July and October. Data for the whole year was to large to be provided, several terabytes in size. The year 2019 is chosen as this is the most recent year, while COVID was not interfering with the inland shipping industry.

Harmonie

For the simulation of Harmonie, the vessel data is not obtained through AIS, but by executing the experiment, discussed in section 3.2.2. The data needed to create a vessel dataset of Harmonie is depicted in the first column of table 3.1. The dimensions of the Harmonie are measured and described in section 3.28. The vessels longitude, latitude, speed and heading are received from a GPS data logger onboard of Harmonie.

Output: Vessels skyline

The waterway skylines are used to generate skylines for every hour for every vessel. Figure 3.10 shows how the waterway points with corresponding skylines are used to generate hourly skylines of a vessel. For every hour the vessel location is known. The skyline of the waterway point closest to this location is be assumed to be the vessel skyline. The waterway points are scattered over the canals with a distance of 1500 meters. The open waters are not indicated with waterway point, by the government. When a vessel is located with a distance further than 1500 meters

from a waterway point, the vessel's location is assumed to be on open water and the skyline of the vessel is completely free, see figure 3.11. The assumption is also based on the radius of 1000 meters used in the skyline model to generate a skyline. With a distance of 1500 meters is can be stated that the surrounding of the vessel is not interfering with its skyline.

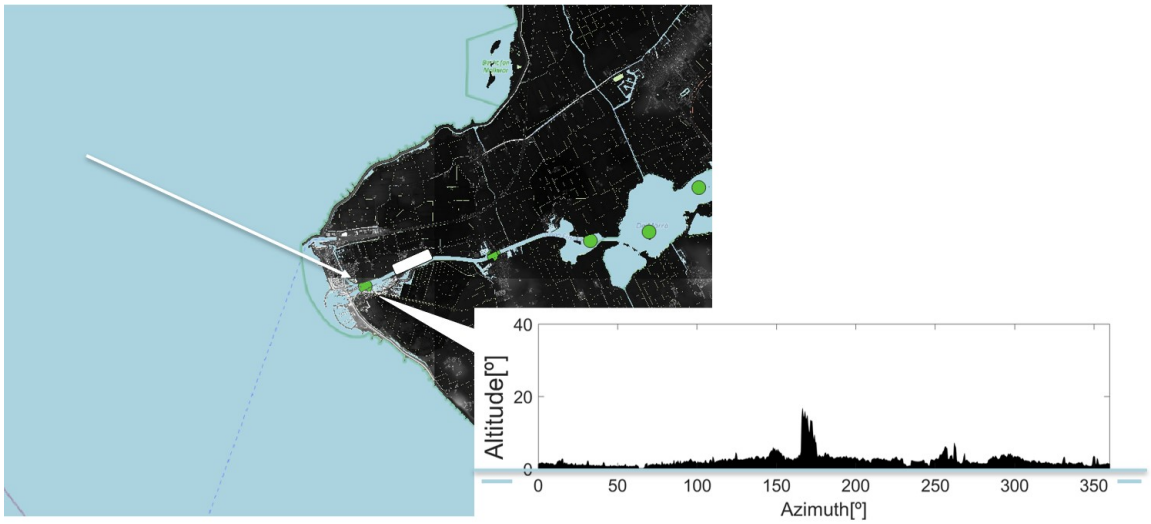

Figure 3.10: Vessels skyline at a canal

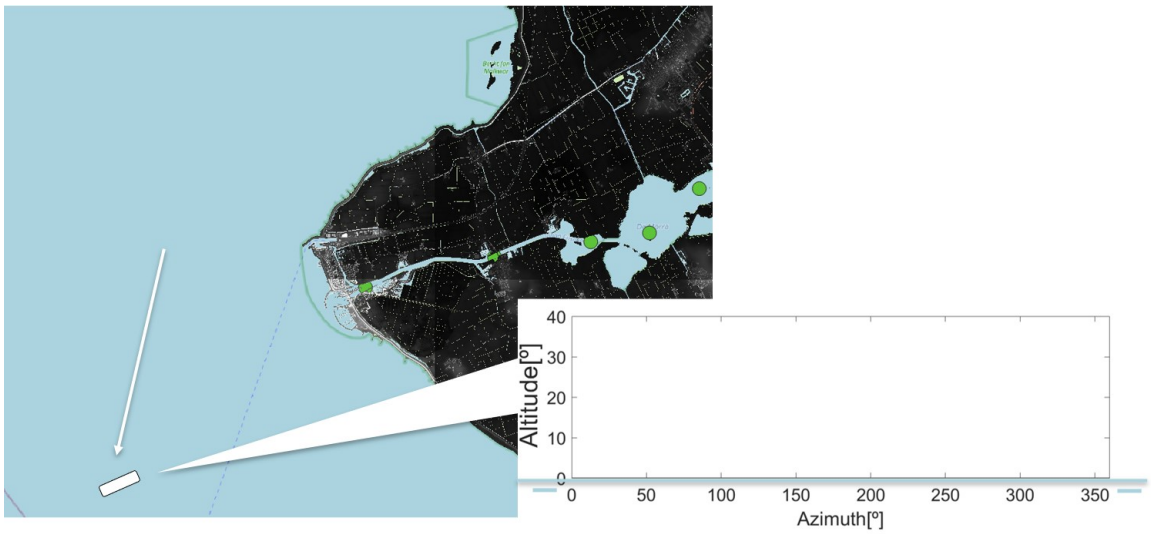

Figure 3.11: Vessels skyline at open waters

The skylines of the waterways are generated from the waterlines of the canals up. The PV panels are placed on the loads or holds of the inland shipping vessels, therefore the skyline is corrected. The height of the holds of the vessel depends on the load installed on the vessel. If the vessel is transporting cargo the draught of the vessel is higher, as the vessel sinks deeper. Therefore the height of the hold with respect to the waterline is smaller. This concept is visualised in figure 3.12. The draught of a vessel for a specific vessel length, when it is loaded or unloaded is provided by the governmental organisation Rijkswaterstaat (Rijkswaterstaat, 2020). The table of the different draughts and heights are displayed in appendix D.

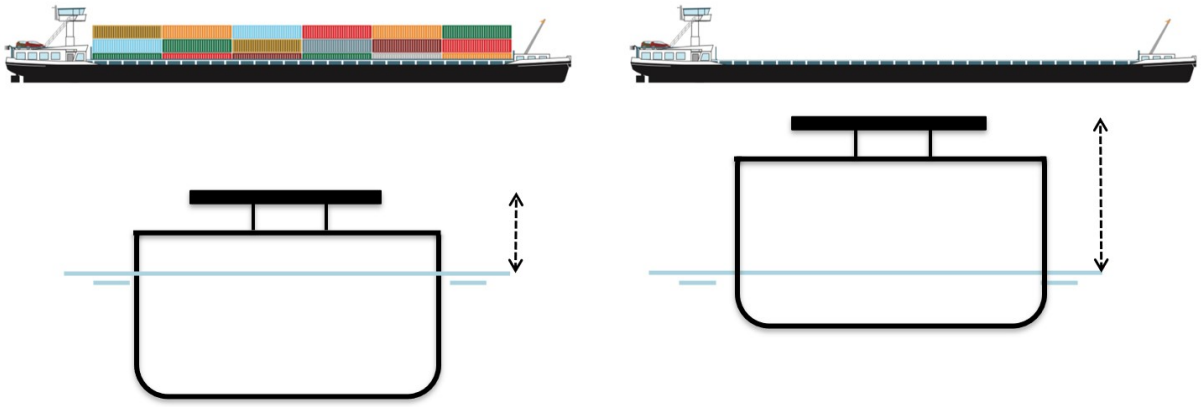

Figure 3.12: Draught dependent on the cargo transported

In this model, it is assumed that half of the time the vessel is transporting cargo. The average height of the PV panel when the vessel is loaded and unloaded is used as a height correction on the skyline. Figure 3.13 shows the height correction of the PV panel on the skylines of the waterways.

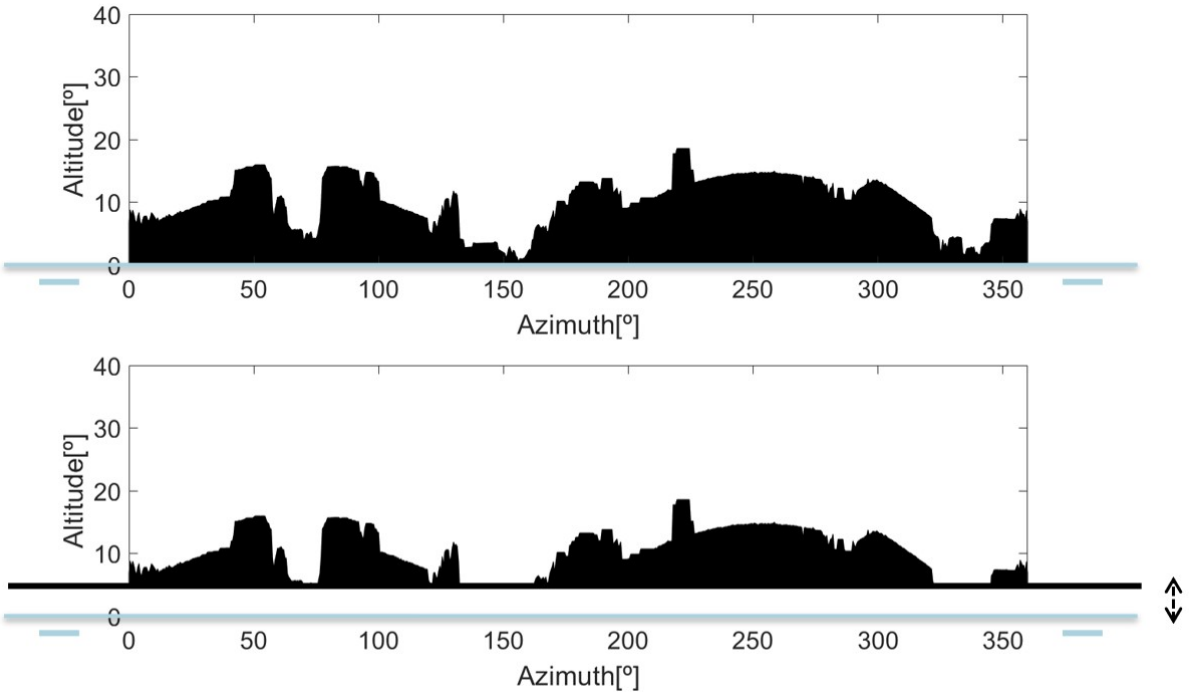

Figure 3.13: Height correction skylines

Output: PV orientation

The second output of the Vessel model is the PV orientation. The PV panels orientation is needed to calculate the irradiance received at the PV panel. There is a difference in simulating the PV orientation for the general cargo fleet and the Harmonie, see table 3.2.

Table 3.2: PV panel orientation for different types of vessels

	General cargo fleet		Harmonie	
Type	**PV tilt**	**PV azimuth**	**PV tilt**	**PV azimuth**
Container	0[°]	Heading vessel[°]	0[°]	Heading vessel[°]
Bulk	8[°] to port	Heading vessel -90[°]	8[°] to port	Heading vessel-90[°]
Bulk	8[°] to starboard	Heading vessel +90[°]	X	X

General cargo fleet

As discussed in section 2.2.1 there are two types of general cargo inland vessels: vessels that transport containers and which transport bulk. On a container vessel, the PV panels are installed flat. The vessel that transport bulk have hatches installed and therefore the PV panels installed are tilted on both side of the hatches, see figure 3.14.

The hatches have corridors that need to be free, for safety reasons. The dimensions of the PV surfaces are explained in section 3.1.6. The average tilt of the tilted part of the hatches is eight degrees, (Blommaert, 2021). Table 3.2 shows the PV orientation of the PV panel of the different inland shipping vessels. The orientation of the PV panels is the same as the heading of the Vessel. The orientation of the PV panels which are installed on the bulk vessels depends on the side on which they are installed. The heading of the panels installed on the starboard side has a heading of +90 degrees of the heading of the vessel itself. The heading of the panels installed on the port side has a heading of -90 degrees of the heading of the vessel itself, as indicated in figure 3.14.

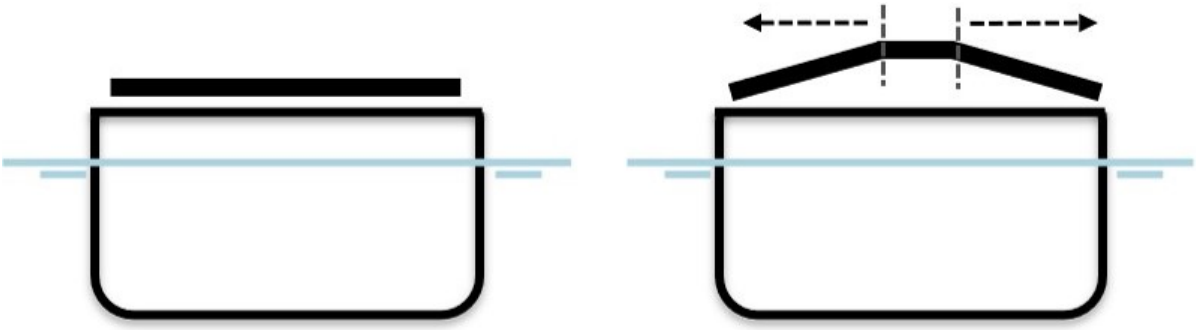

Figure 3.14: Cross section container (left) and bulk (right) vessel

Harmonie

During the experiment, the test vessel Harmonie simulates a bulk vessel with only one PV panel oriented 8 degrees to the port side, as there is one PV module available on board. Harmonie also simulates a container vessel with one horizontally placed PV panel.

3.1.4 Irradiance model

The third model needed to calculate the photovoltaic energy yield of a moving vessel is the irradiance model. This model uses the vessels skylines and the orientation of the PV panels, which are calculated in the Vessel model, section 3.1.3. This model

uses climate data as input to simulate the solar irradiance received by the PV panel, see figure 3.15.

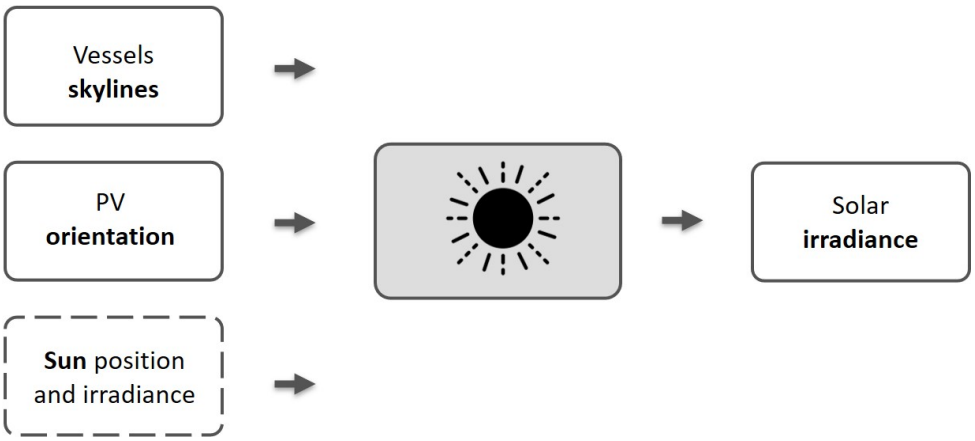

Figure 3.15: Irradiance model

Input Sun position and irradiance

The parameters for the suns position and irradiance is the following: DHI, Direct Normal Irradiance (DNI), Diffuse Horizontal Irradiance (DHI), suns altitude (a_s) and the suns Azimuth (A_s), see table 3.4.

Table 3.3: Source of the sun position and irradiance

Parameter	**Unit**	**General cargo fleet**	**Harmonie**
Time period		Average of 30 years	30/08/2021 12:00 until 21/09/2021 17:00
Suns a_s & A_s	[°]	Dutch PV portal	Mathematical equations for the book Solar Energy (Smets et al., 2016)
GHI	$[W/m^2]$	Dutch PV portal	Selected KNMI weather station
DHI	$[W/m^2]$	Dutch PV portal	Decomposition form GHI with BRL model
DNI	$[W/m^2]$	Dutch PV portal	Decomposition form GHI with BRL model

General cargo fleet

For the simulation of the general cargo fleet, the average annual energy yield over 30 years is simulated. Therefore the input parameters used are also average values over 30 years.

These four parameters are provided by the Dutch PV portal, a Meteorological data portal developed by the research team PVMD(Photovoltaic Materials and Devices). The Dutch PV portal obtained the DNI and the DHI by the irradiance decomposition model of BRL (Boland-Redley-Lauret) (Boland, Huang, & Ridley, 2013). In this model, the DNI and the DHI are decomposed from the GHI (Global Horizontal Irradiance) (Boland et al., 2013). The Global Horizontal Irradiance is obtained by averaged data of various KNMI weather stations through the Netherlands. The Dutch PV portal obtained the solar altitude and the azimuth according to mathe-

matical equations described in appendix E of the book Solar Energy (Smets et al., 2016). These four parameters are implemented province and hourly dependent.

Harmonie

When simulating the energy yield of Harmonie, the energy yield of a specified time period is simulated, from 30/08/2021 12:00 until 21/09/2021 17:00. Therefore using the averaged input for the general cargo fleet is not suitable. The suns position and the irradiance component are obtained also by mathematical equations and by the BRL decomposition model, but then for a specific time period.

The PV panel is installed on a moving vessel and not on a fixed location with one weather station close by. To make the dataset more accurate, the GHI is downloaded for the province through which the vessel sails, for each particular moment. Harmonie is moving through six different provinces: Zuid-Holland, Noord-Holland, Utrecht, Flevoland, Gelderland and Overijssel. For every province, a specific weather data station is selected, as indicated by the orange dots line in figure 3.16. The weather station in Overijssel is relatively far from the route because the weather station closer by did not have a complete dataset for the specific period. The longest distance between the weather station and Harmonie is 51.88 kilometres, according to google maps.

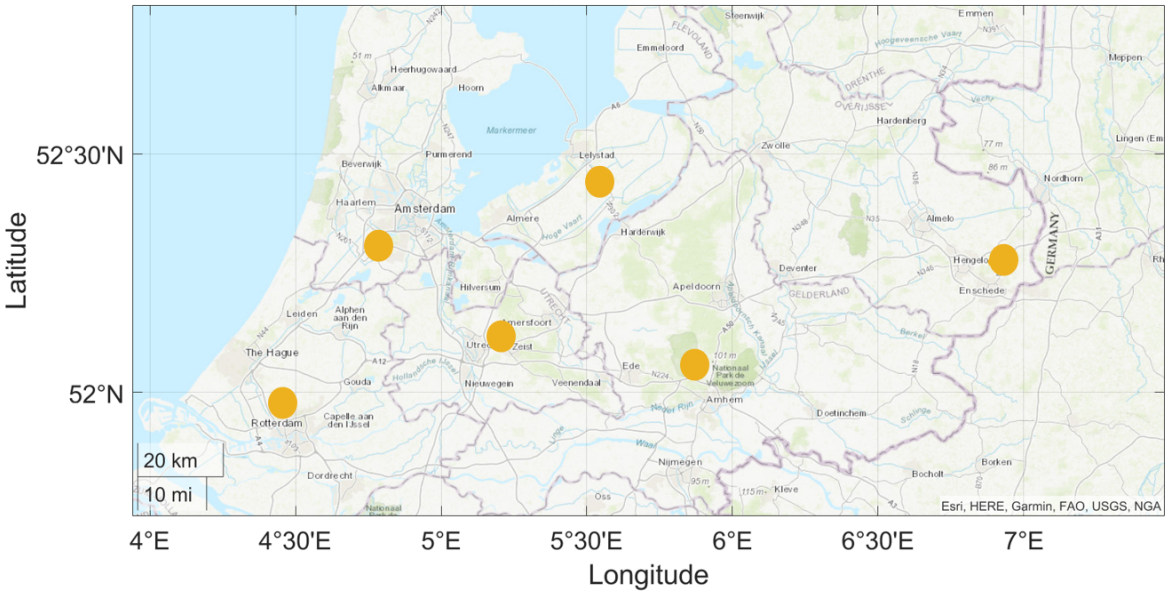

Figure 3.16: Selected weather stations

Output: Solar irradiance

The irradiance on the PV panel is divided into three different components, direct, diffused and reflected components, indicated in figure 3.17 and formula 3.4.

$$G = G_{dir} + G_{dif} + G_{ground} \tag{3.4}$$

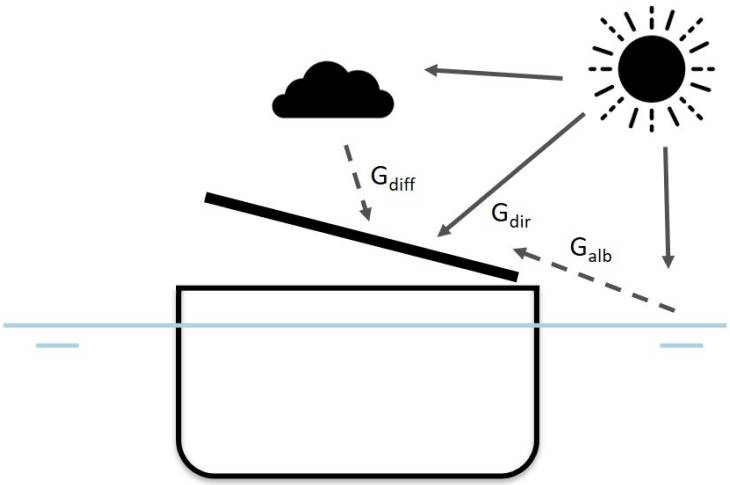

Figure 3.17: Irradiance components

The direct component of the irradiance is a proportion of the DNI, corrected with the angle of incidence (AOI), as indicated in formula 3.8. The angle of incidence is the angle between the normal of the PV panel and the incident direction of the sunlight. The mathematical expression is indicated in formula 3.6 (Smets et al., 2016) .

If the sun is blocked by its surrounding object, the PV panel will not receive direct irradiance. The skyline effect on the PV panel is integrated with the shading factor(SF), see figure 3.18. This component is one if the sun is not blocked by its surroundings and the component is zero if PV panel is blocked by the skyline. The subscripts s and m indicate the sun and panel respectively. θ_m is the PV panels azimuth and a_m is the PV panels altitude.

$$G_{dir} = DNI \cdot cos(AOI) \cdot SF \tag{3.5}$$

$$cos(AOI) = sin(\theta_m)cos(a_s) + cos(A_m - A_s) + cos(\theta_m)sin(a_s) \tag{3.6}$$

$$SF = \begin{cases} 1 & \text{when the sun is not blocked} \\ 0 & \text{when the sun is blocked} \end{cases} \tag{3.7}$$

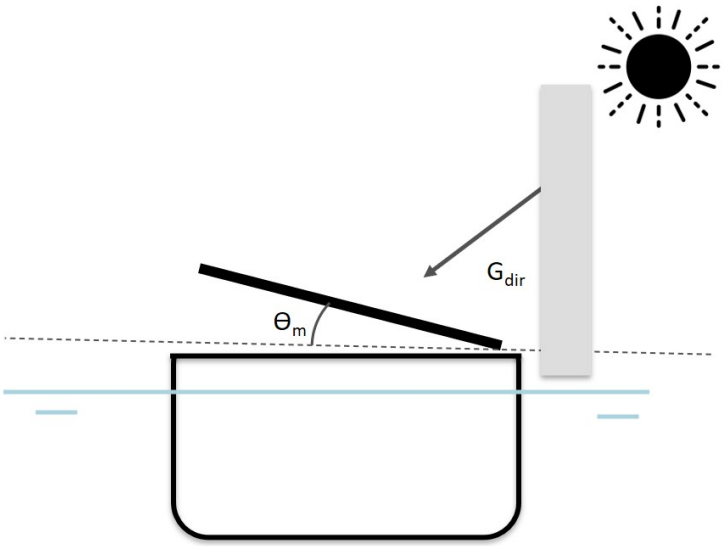

Figure 3.18: Direct irradiance component

Generally, there are two models to calculate the diffuse irradiance, the Liu and Jordan's (Liu & Jordan, 1960) correlation and the Perez model (Perez et al., 1988). In this research, the Perez model is used to calculate the diffused component, as this is a sophisticated model that takes hourly data into account. The diffused irradiance is composed of three components, indicated in figure 3.19 and formula 3.8 (PVPMC, 2018). The first component is the isotropic component, which indicates the overall irradiance from the skydome, formula 3.9. The circumsolar component represents the irradiance in an area around the sun. The parameters A and B are determined by formula 3.11. The last component is the horizon brightening component. This component indicates the horizontally diffused irradiance.

The Perez model calculates the circumsolar and horizon brightening component on complex empirical fitted functions F1 and F2. F1 and F2 can be calculated with from various coefficients (f11 ,f12 ,f13 ,f21 ,f22 ,ff23) for a specific bin of clearness (PVPMC, 2018). The equations of the F1 and F2 and the coefficients are depicted in appendix E.

The sky view factor (SVF) is a factor that indicates the proportion of the sky that is visible from which the PV panel can receive irradiance. The SVF is calculated from the skyline profiles. The sky is 3D dom, therefor the path sunlight travels can vary. The skyline profiles are corrected, with an air mass correction matrix, based on the work of D.G. Steyn (Steyn, 1980). The SVF is the summation of the normalized and corrected skyline profiles.

$$G_{diff} = G_{iso} + G_{cir} + G_{hor} \tag{3.8}$$
$$G_{iso} = DHI \cdot SVF \cdot (1 - F1) \tag{3.9}$$
$$G_{cir} = DHI \cdot F1 \cdot (A/B) \cdot SF \tag{3.10}$$
$$A/B = max(0, cos(AOI))/max(cos(85), sin(a_s)) \tag{3.11}$$
$$G_{hor} = DHI \cdot F2 \cdot sin(\theta_m) \tag{3.12}$$
$$\tag{3.13}$$

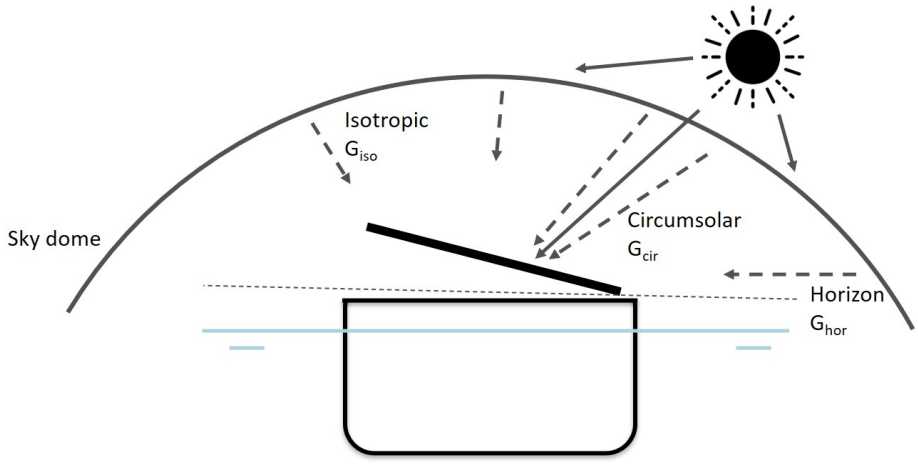

Figure 3.19: Diffused irradiance component

The ground reflected component is a function of G_h, see formula 3.14. G_h is an indication of the irradiance that is reflected by the surface of the earth. It contains

the components of irradiance which is received by the earth's surface; the vertically component of the direct irradiance, the circumsolar diffused irradiance and the isotropic diffused irradiance, see formula 3.15.

The albedo component, second indicator in formula 3.14, indicates the selectivity of the ground. In this research the albedo factor of water of 0.06 is taken (Ziar et al., 2020). The GVF is a factor that indicates the proportion of the ground from which the module can receive the reflected irradiance. (Smets et al., 2016) (PVPMC, 2018)

$$G_{alb} = G_h \cdot \alpha_{albedo} \cdot GVF \tag{3.14}$$
$$G_h = (DNI \cdot sin(a_s) \cdot SF) + G_{iso} + G_{cir} \tag{3.15}$$
$$\alpha_{albedo} = 0.06 \tag{3.16}$$
$$GVF = (1 - cos(\theta_m))/2 \tag{3.17}$$

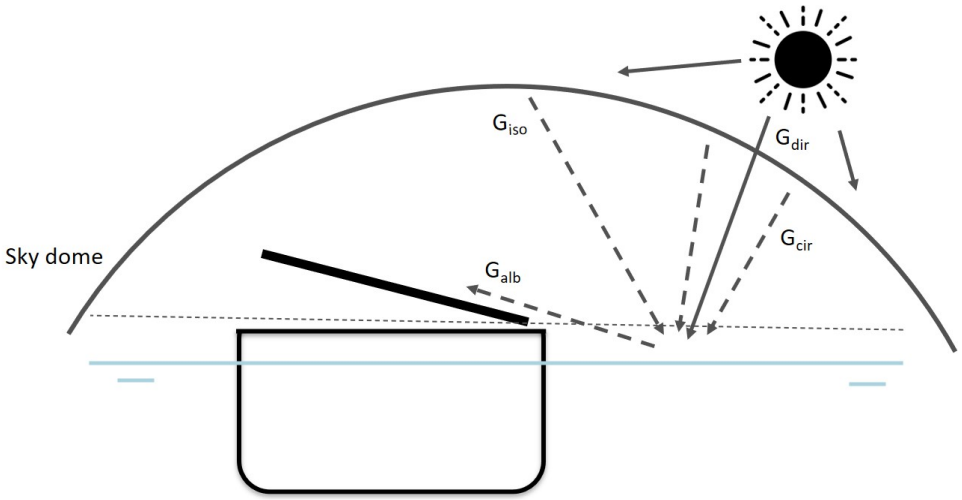

Figure 3.20: Ground reflected irradiance component

3.1.5 Module temperature model

The module temperature model is developed to simulate the temperature of the PV panel itself. The module temperature has a influence on the performance of the PV panel. The model uses the PV orientation and the solar irradiance calculated in the before mentioned model. As third input the Vessel model uses climate data. Figure3.21 gives an overview of the inputs and output of the temperature model.

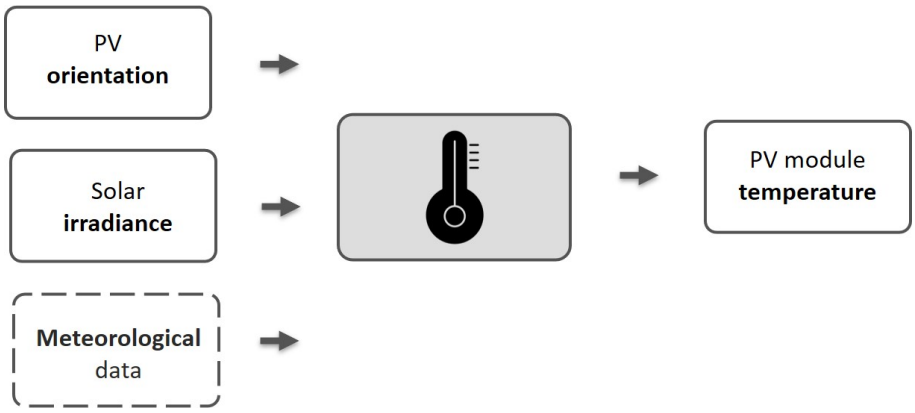

Figure 3.21: Temperature model

Input: Meteorological data

The meteorological parameters needed for this model are the wind speed and direcetion, ambient temperature, water temperature and cloud coverage.

Table 3.4: Source of the parameters needed for the meteorological data set

Parameter	**Unit**	**General cargo fleet**	**Harmonie**
Time period		Average of 30 years	30/08/2021 12:00 until 21/09/2021 17:00
Wind speed	$[m/s]$	Dutch PV portal	Data logger onboard
Ambient temperature	[°C]	Dutch PV portal	Data logger onboard
Cloud coverage	[Octa]	Dutch PV portal	Selected KNMI weather station
Water temperature	[°C]	Rijkswaterstaat	Rijkswaterstaat

General cargo fleet

As discussed in this irradiance model, the energy yield is estimated for a average year over a time period of 30 years. Therefore climate data is used as meteorological parameters, instead of weather data.

The wind speed, ambient temperature and cloud coverage are provided by the Dutch PV portal. The Dutch PV portal is explained in section 3.15. The water temperature is obtained by Rijkswaterstaat. A dataset with water temperature on daily basis for 12 locations in different province is obtained. Obtaining the water temperature on hourly basis was not possible, but as all the canal together can be assumed as one big heat sink the water temperature will not vary significantly over one day.

Harmonie

For the simulation of Harmonie, weather data instead of climate data is needed, as the energy yield is calculated for a specific time period. The weather can change by time and location, the closer the weather data can be measured to the measurement setup, the more accurate the simulation will be. Ideally, these parameters are therefore measured onboard of Harmonie.

The ambient temperature and the wind speed will be measured and stored with data loggers onboard of the Harmonie, this will be discussed in next section. The data from the data loggers are used in the weather dataset. The water temperature is obtained by the Rijkswaterstaat and the cloud coverage are downloaded from six different KNMI (Koninklijk Nederlands Meteorologisch Instituut) weather station.

Output: PV module temperature

As discussed in section 2.1.5 there are various thermal model that can calculate the model temperature. In this research the Fluid-dynamic model is used as thermal model (Smets et al., 2016). This model is able to take into account more meteorological parameters than the other models.

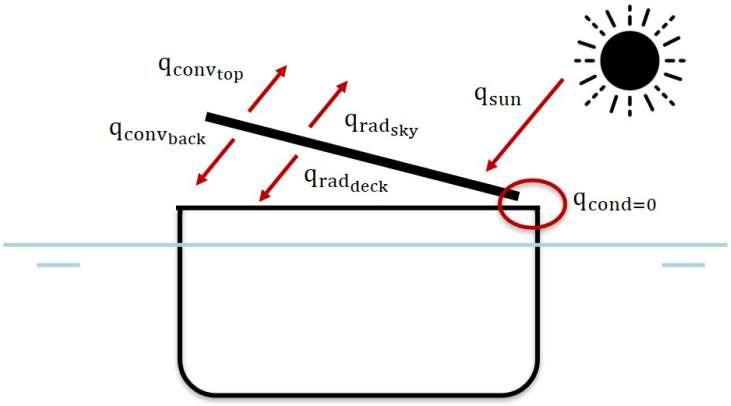

Figure 3.22: Heat transfer components

The PV panel receives heat in the form of irradiance. There are three different ways how the PV panel can deliver this heat back to its surrounding: radiation, convection and conduction, as indicated in figure 3.22. The conduction coefficient is neglected as very small area of the PV panel has contact to the mounting structure. The PV panel radiates heat towards the sky and towards the deck of the vessel. The PV panel will also convect heat to the air at the top and back of the PV panel. This is indicated in the heat transfer balance in formula 3.18. The four components in this formula can be calculated according to formula 3.19.

$$q_{sun} = q_{rad,deck} + q_{rad,sky} + q_{conv,top} + q_{conv,back} \tag{3.18}$$

$$\alpha G = h_{c,top}\,(T_m - T_a) + h_{c,back}\,(T_m - T_a) + h_{r,deck}\,(T_m - T_{\text{deck}}) + h_{\text{r,sky}}\;(T_m - T_{\text{sky}}) \tag{3.19}$$

The convection on the back side of the PV panel is lower than the convection on the top side of the PV panel, as the PV panel is mounted to a structure. The convection difference between the top and the back of the PV panel is calculate with the ratio factor R, where R is this ratio between the actual and the ideal heat loss from the back side. R, takes into account the effect of the mounting structure by correcting the nominal operating cell temperature (NOCT) (Smets et al., 2016). In this simulation model the NOCT is correction with + 10[ºC], Indicating the PV panel mounted of a distance of around 2.50 [cm] form the surface.

The module temperature can be calculates when rewriting equation 3.19, see equation 3.20. From this formula it can be seen how the irradiation G and the ambient temperature T_a are implemented in the calculation of the module temperature. The wind speed is implemented in the top convective heat transfer coefficients $h_{c,top}$.

The deck temperature T_{deck} is for simplicity reasons assumed to be the same as the water temperature. The water temperature is also taken into account in the radiative heat coefficients $h_{r,sky}$ and $h_{r,deck}$. The effect of cloud coverage implemented the temperature of the sky T_{sky}.

$$T_M = \frac{\alpha G + h_{c,top} T_a + h_{c,back} T_a + h_{r,\text{ sky}}\, T_{\text{sky}} + h_{r,\text{ deck}}\, T_{\text{deck}}}{h_{c,top} + h_{c,back} + h_{r,\text{ sky}} + h_{r,\text{ deck}}} \tag{3.20}$$

When a PV panel is installed on a moving body it is possible that the PV panel is cooled more when comparing it to a fixed PV panel. This is because the PV panel experiences more air flow, caused by the movement of the vessel. This additional cooling effect, will decrease the module temperature, which increases the performance of the module. The air speed of the PV panel is calculated according to equations 3.21. V_{vessel} indicated the air flow around the PV panel caused by the forward movement of the body itself. It is assumed that a body which is moving at a certain speed, encounters an air flow with the same speed as that of the moving body.

$$V_{air} = V_{vessel} + V_{wind\ corrected} \tag{3.21}$$

The PV panel additionally experiences an air flow around the PV panel caused by the wind. When a PV panel is installed on a moving body, this wind is relative to the movements. Therefore the wind speed needs to be corrected with the direction of the vessel, $V_{wind\ corrected}$. Wind is a vector quantity, it contains a magnitude and direction. The vessels speed is also a vector quantity. Both the magnitude and direction of the vessel speed and wind affect the correct wind component. The wind can be directed upwards the vessels heading and downward of the vessels heading, see figure 3.23.
When the wind direction is facing in the heading of the vessel the corrected wind velocity is the velocity of the wind and the velocity of the transposed vessel speed, $cos(x)V_{vessel}$, see equation 3.22.

$$V_{wind\ corrected} = V_{wind} + cos(x)V_{vessel} \tag{3.22}$$

When the wind direction is in the direction of the vessels heading the corrected wind velocity is the velocity of the wind minus the velocity of the transposed vessel speed, see equation 3.23.

$$V_{wind\ corrected} = V_{wind} - cos(x)V_{vessel} \tag{3.23}$$

V_{vessel} is the velocity with respect to the ground, SOG (speed over ground), as the wind is also in respect to the ground. The transposed vessel velocity, is calculated according to the angle, indicated with x, between the vessel heading and the wind direction, see figure 3.23.

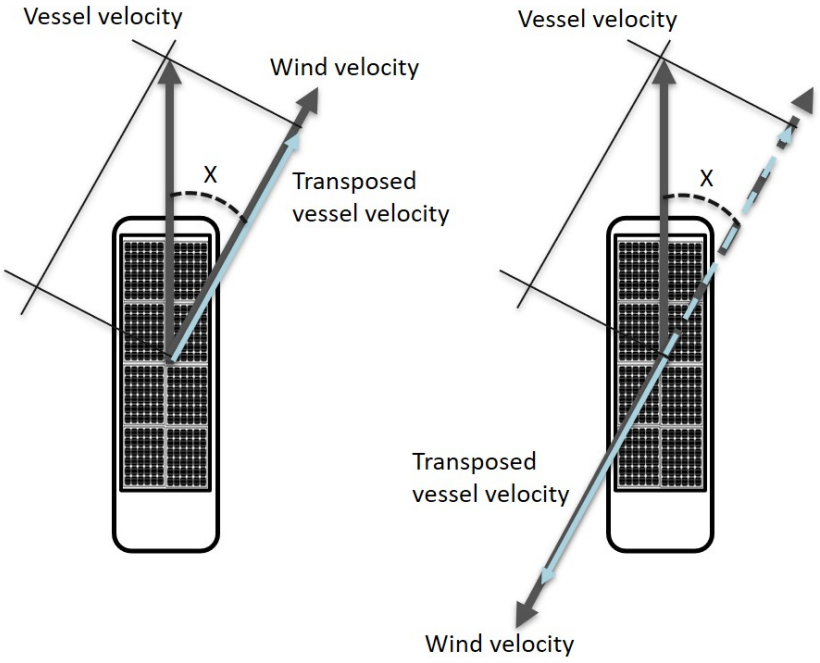

Figure 3.23: Transposed vessel velocity

3.1.6 Photovoltaic energy model

The power and energy model uses the PV module temperature and the solar irradiance, simulated in the Module temperature model and the Irradiance model respectively, as input parameters, indicated in figure 3.24. The model also includes PV module specifications, which can be found in appendix B, as input parameter. To calculated the PV power, the PV surface for every vessel is needed. How this surface is obtained is explained in this subsection.

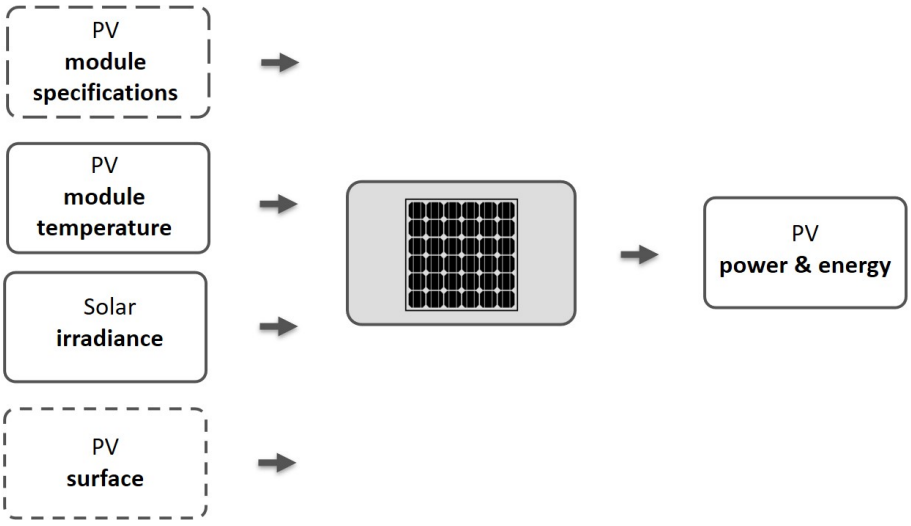

Figure 3.24: Power and energy model

Input: PV surface

The PV surface is calculated for every vessel individually. The PV surface is calculated differently for the general cargo vessels and the Harmonie, see table 3.5.

Table 3.5: PV surface

Parameter	Unit	General cargo fleet	Harmonie
PV surface	$[m^2]$	PV surface calculator	Pv panel data sheet

General cargo fleet

As discussed in section 2.2.1 and 3.1.3, the PV panels will be installed above the hold of the vessels. For the container vessels the PV panels will be placed flat, above the containers in the hold. The PV panels installed on the bulk vessels will be installed on both side of the hatches. The flat part of the hatches, will not be used as PV surface as this must fulfill the purpose of a corridor.
The dimensions of the hold for every vessels depends on the dimensions of the vessels. AIS data, discussed in section 3.1.3, will provide the length and width of the vessel, but will not proved the dimensions of the holds. The company Blommaert Aluminium Constructions develops the hatches for almost all general cargo ships in the Netherlands (Blommaert, 2021). The company has provided, for this research, the relationship between the dimensions of the ships themselves and the hold for four characteristic sizes. As discussed in section 2.2.1 and figure 2.8, general cargo ships have fixed sizes based on, for example, locks. As a result, four characteristic ships provide a good indication of the complete fleet, even if there are relatively few reference points. Figure 3.25 shows the data provided by Blommaert Aluminium Constructions and the linear fit from these data points. Besides the dimension ratio of the holds, Blommaert Aluminium Constructions also provides the ratio of the corridor width, see figure 3.25 and the average tilt angle of 8 degree of the hatches.

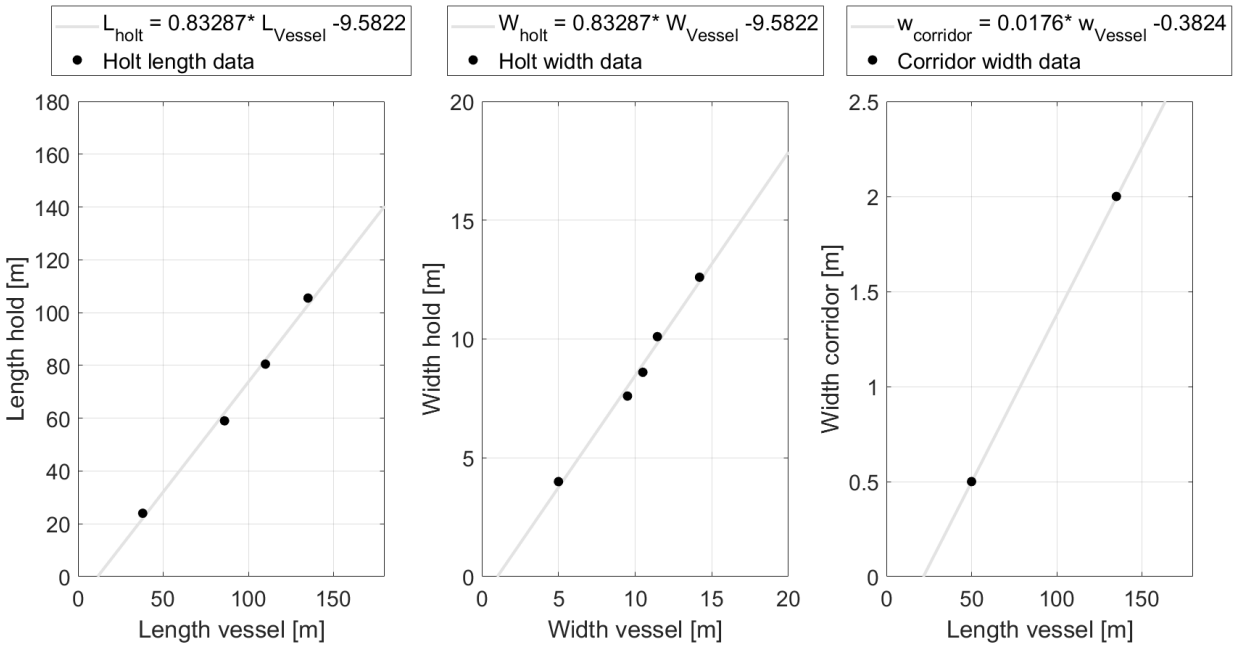

Figure 3.25: Hold and corridor dimensions

The PV surface will is calculate for every vessel individually. The PV surface will take into account a 0.1 meters mounting spacing on both sides of the hold. The spacing of 10 centimeters is decided after a field survey.

Figure 3.26: Field survey towards mounting spacing

In the PV surface calculation is a PV panel fitting calculator implemented. This PV panel fitting calculator will calculate the maximum number of installed PV panels for every vessel. The PV panel fitting calculator will run a simulation for both landscape and portrait PV panel orientation. Selected is the orientation where the best PV surface utilisation is indicated. Figure 3.27 gives a top view with cross section of how the PV panels will be placed on the container and bulk vessels.

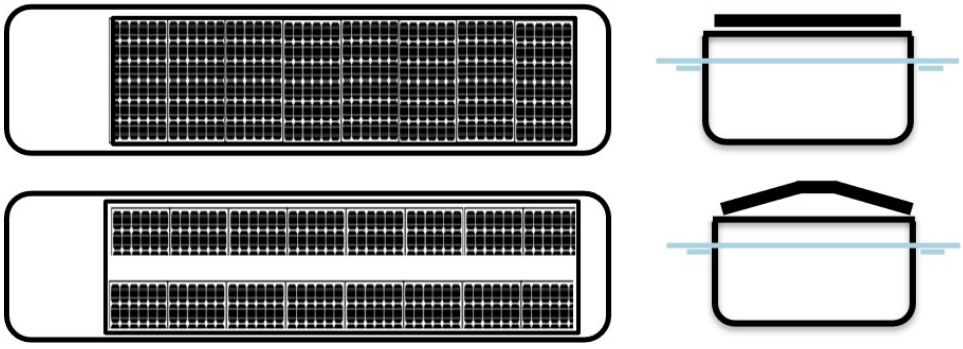

Figure 3.27: PV surface

Harmonie

Harmonie has one installed PV panel during the execution of the experiment. Therefor the PV surface is the same as the area of the PV panel that is used, see the data sheet of the PV panel in appendix B.

Output: Power

The PV panel performance is depending on the irradiance, the module temperature, PV surface and the PV module specifications. The input parameters as indicated in figure 3.24.

This model, that calculates the PV power, is based on efficiency calculations. The performance of the PV panel depends on how well the PV panel can convert, η, the received irradiance, G, into electrical power. 3.24. The efficiency provide by the manufacturers on the datasheet of a PV panel, indicated in appendix B, takes into account standard test conditions, STC, where a module temperature is 25 degrees and the irradiance is 1000 [W/m^2]. The calculated module temperature and irradiance, calculated in the Irradiance model and the Module temperature model, are different than the STC values. Therefore the STC efficiency, needs to be corrected with the simulated module temperature, T_m and the simulated irradiance, G. This corrected efficiency is indicated in formula 3.25 (Smets et al., 2016). There is A_m and n_m the PV surface are and the number of panels, respectively.

$$P(T_m, G) = \eta(T_m, G) \cdot G \cdot A_m \cdot n_m \tag{3.24}$$

The $\eta\left(T_M, G\right)$ is the efficiency of the PV panel when taking into account the module temperature and the module irradiance and is calculated by equation 3.25 (Smets et al., 2016). The component in the square brackets, gives a efficiency correction factor for the module temperature. This is done based on the by the manufacturer provided temperature correction values.

$$\eta\left(T_M, G\right) = \eta\left(25^{\circ}\mathrm{C}, G\right)\left[1 + \left(\frac{1}{\eta(\mathrm{STC})}\frac{\partial \eta}{\partial T}\right)\left(T_M - 25^{\circ}\mathrm{C}\right)\right] \tag{3.25}$$

The manufacturer doesn't often provide correction values for the irradiance. Therefore the irradiance corrected efficiency is calculated by the irradiance corrected open circuit voltage and short circuit current, see the equations 3.26, 3.27, 3.28 and 3.29 (Smets et al., 2016). There is. n is a ideality factor of 1.2, k_B is the Boltzmann's constant, T is the STC temperature of 25 degrees celcius, q is the electron charge and FF is the fill factor.

$$\eta\left(25^{\circ}\mathrm{C}, G\right) = \frac{FF \cdot V_{\mathrm{oC}}\left(25^{\circ}\mathrm{C}, G\right) I_{\mathrm{sc}}\left(25^{\circ}\mathrm{C}, G\right)}{G * A_M} \tag{3.26}$$

$$V_{\mathrm{oc}}\left(25^{\circ}\mathrm{C}, G\right) = V_{\mathrm{oc}}(\mathrm{STC}) + \frac{n k_{\mathrm{B}} T}{q} \ln\left(\frac{G}{1000}\right) \tag{3.27}$$

$$I_{\mathrm{sc}}\left(25^{\circ}\mathrm{C}, G\right) = I_{\mathrm{sc}}(\mathrm{STC})\frac{G}{1000} \tag{3.28}$$

$$FF = \frac{P_{mpp}}{Voc_{stc} \cdot Isc_{stc}} \tag{3.29}$$

Output: Energy yield

The PV power in the simulation is calculated for every hour for every vessel individually. This PV power can be integrated over time, to calculate the PV energy.

Complete general cargo fleet

For the complete general cargo fleet the energy yield for a whole year is simulated and the PV power is integrated over 8760 hours, see equation 3.30. du indicated a time step of one hour. The simulations are based on yearly climate data, which are assumed not to vary for 30 years. Therefore this energy yield is an averaged energy yield for a time period of 30 years, which is also the estimated lifetime of a PV panel, see the data sheet of the PV panel in appendix B.

$$E(Tm, G) = \int_0^{8760} P(Tm, G, u)\, du \tag{3.30}$$

Harmonie

The power of Harmonie will also be simulated on a hourly basis. The experiment will not take place for over a year, but for three weeks. As these three weeks are specified and not an representative year for longer period of time, the calculations and the integration of the PV power, is also specified, see equation 3.31.

$$E(Tm, G) = \int_{30/08/202112:00}^{21/09/202117:00} P(Tm, G, u)\, du \tag{3.31}$$

3.2 Experiment

The developed simulation model, discussed in the previous section is validated by an experiment. A PV panel is installed on a vessel, which sails a route through the Netherlands. This vessel is called Harmonie, and some background information about the vessel is given in section 3.2.1. The PV panel and the ship are monitored, so that the PV energy yield can be measured. The same panel and vessel are simulated in the developed model to estimate the PV energy yield. The simulated and measured energy yields are compared. This validation provides valuable information about the accuracy of the simulation model.

Besides being able to compare the measured and estimated energy yield, conducting this experiment will also be useful for better understanding possible unsimulated effects. It may give an insight into the different situations that an inland vessel experiences, which may not have been taken into account when designing the model. To get a better overview of this, photographic documentation will be carried out while sailing, to record unexpected situations. So a better understanding of the sailing pattern of inland vessels can be carried out.

3.2.1 Harmonie

The vessel Harmonie is a motor yacht built in 1979 in the Netherlands. Figure 3.28 shows a schematic illustration. The hull is made of steel, and the ship weighs 10 tons. The ship's dimensions are as follows: 10 meters in length, 2.85 meters in width, and the draught is 0.9 meters. The ship was previously used for recreational fishing at sea. The mast on the ship is used for lighting and can lift various goods on board. Harmonie is electrical-battery based propelled, see figure 3.29.

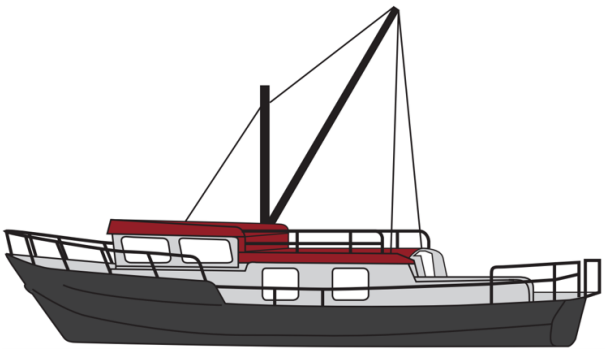

Figure 3.28: Illustration of Harmonie

On board of the vessel, there is an energy system installed as displayed in figure 3.30. This system provides energy to the electrical engine and delivers energy to the household appliances.

Figure 3.29: Harmonie electrical engine and batteries

- In a 48V battery system, energy is stored. The battery system consists of 24 2V OPzV gel cells with a capacity of 800Ah.
- The stored energy in the batteries is delivered by shore energy. The Victron Multiplus battery charger can charge the batteries with a current of 70A.
- The Multiplus can also invert energy stored in the batteries to a continuous power of 5000VA (4000W) and supply energy demanded by the household appliances while sailing or in off-grid mode.
- A 22 kW 3-Phase AC asynchronous electrical motor is used for the propulsion of the vessel.
- The motor controller converts the energy stored in the batteries to an AC-3phase current and adjusts the engine's speed by frequency control.

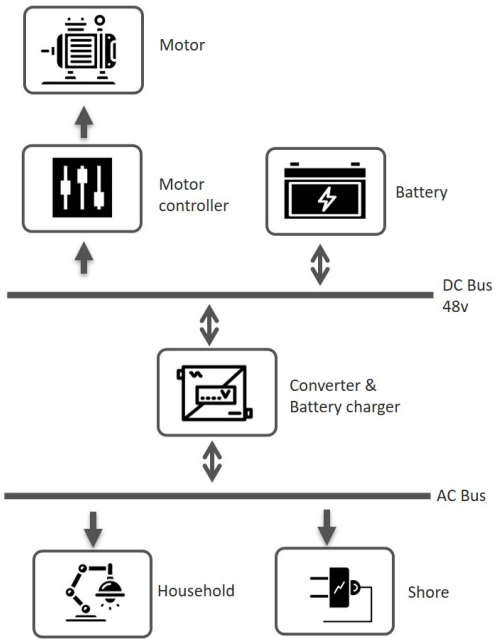

Figure 3.30: Energy system on-board

3.2.2 Travel plan

Harmonie sails two weeks through the Netherlands. During these sailing weeks, Harmonie will imitate the sailing behaviour of inland vessels as much as possible. Inland vessels are sometimes moored for a longer period of time, for example during loading and unloading or for maintenance. Harmonie has also imitated this by spending a week in an urban environment in Rotterdam. A harbor in Rotterdam was chosen as the port of Rotterdam is the largest and busiest port in the Netherlands (CBS, 2019b).

As discussed in section 3.1.3, container vessels have a simulated PV tilt of zero and bulk vessels are simulated with a PV tilt of 8 degrees to port and starboard. Therefore during the first sailing week Harmonie's PV panel tilt will be zero, imitating a container vessel, and during the second sailing week the Harmonie's PV tilt will be 8 degrees towards the port, imitating a bulk vessel, see figure 3.31. In the harbor the Harmonie's PV panel tilt is 8 degrees.

Figure 3.31: Harmonie's panel tilt: zero degrees(left) and eight degrees to port side(right)

During two sailing weeks on average per day, Harmonie has sailed 4 to 5 hours. Each experiment week consist of 5 days sailing and 2 days of rest. The mast of Harmonie has been lowered during the entire experiment, to prevent shadows on the panel. The travel route of Harmonie is indicated in figure 3.32. This sailing route has been mapped out in such a way that Harmonie sails in different directions and sails different types of waters. Harmonie follows four main and busy canals. Harmonie has also crossed the largest open water of the Netherlands, the IJsselmeer and Markermeer. Navigating these different waters provides insight into how the simulated model responds to different surroundings and waters.

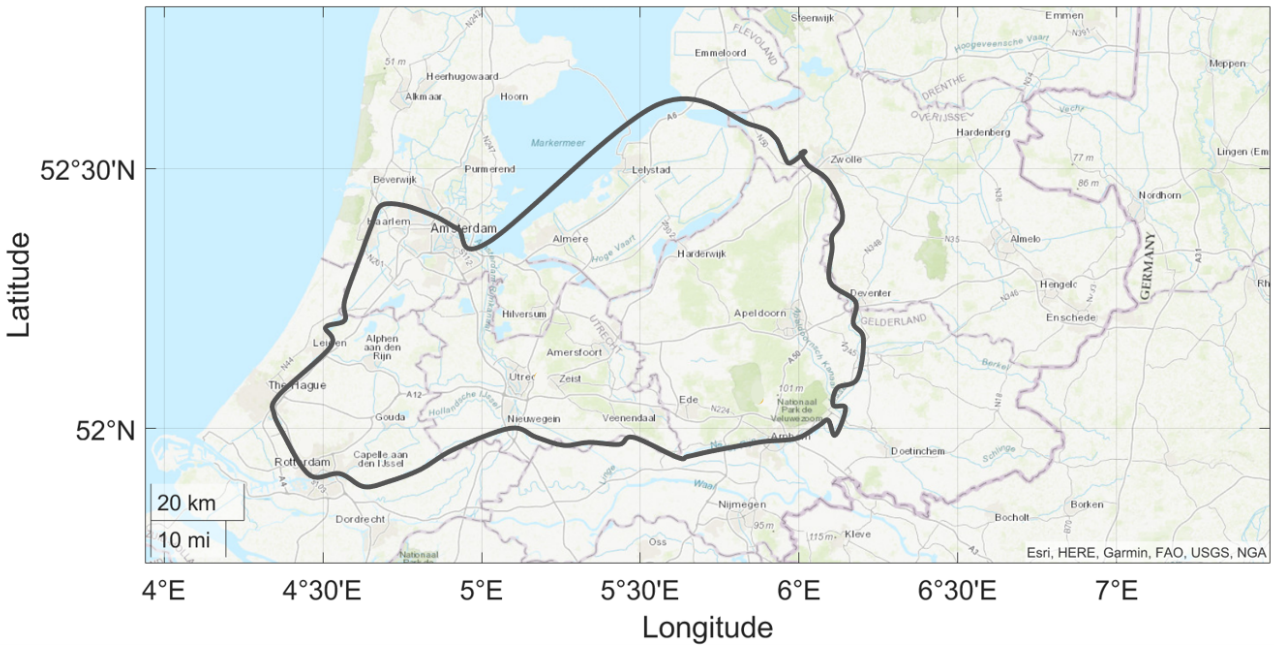

Figure 3.32: Travel route

3.2.3 Equipment

To perform the experiment, an energy system with PV panel, is installed. This energy system and Harmonie itself are monitored with various data loggers, combined with the monitoring system.

Energy system

The energy system displayed in figure 3.30 is installed for the experiment. The bullet point below explains the different components of this energy system.

- On the vessel's top deck, a LR4-60HPB Longi 360 watt peak PV panel is installed. The PV panel uses low LID mono PERC and half-cut technology and is installed on a construction that enables various panel tilts. The panel specifications are discussed in the next paragraph.
- The PV panel is connected to a EPsolar Tracer 415BN 12/24V 40A charger controller, which uses maximum power point tracking (MPPT).
- The energy that is generated is stored in two lead-acid batteries. The batteries are connected in series, with a voltage of 12V and a capacity of 240Ah.
- When the batteries are fully charged, the charge controller cuts off the PV panel to prevent overcharging. To maintain valid measurements, a discharge unit is connected to the battery bank. The discharge unit will discharge the batteries when they reach a voltage which indicates that the battery is almost full. In this way, the batteries are never fully charged, and the PV power can be monitored continuously. Figure3.34 shows a picture including this discharge unit. This unit is made by Stefaan Hairman.

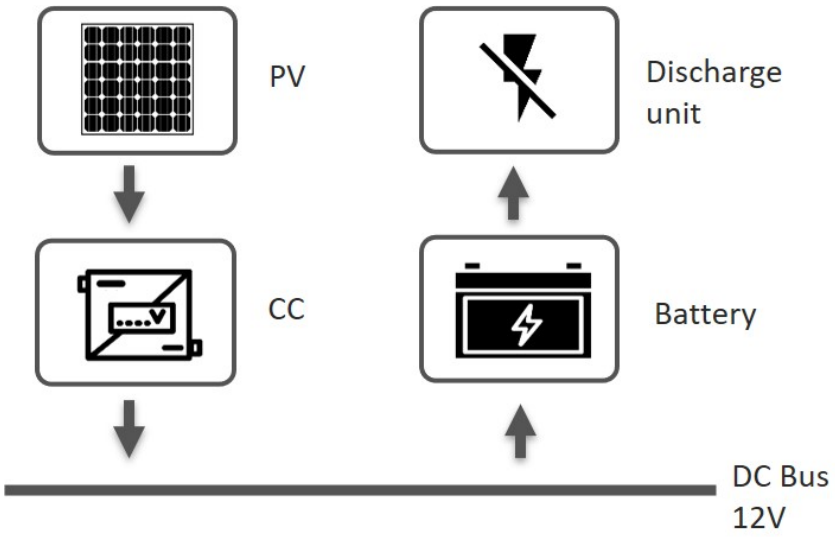

Figure 3.33: Energy system installed at Harmonie

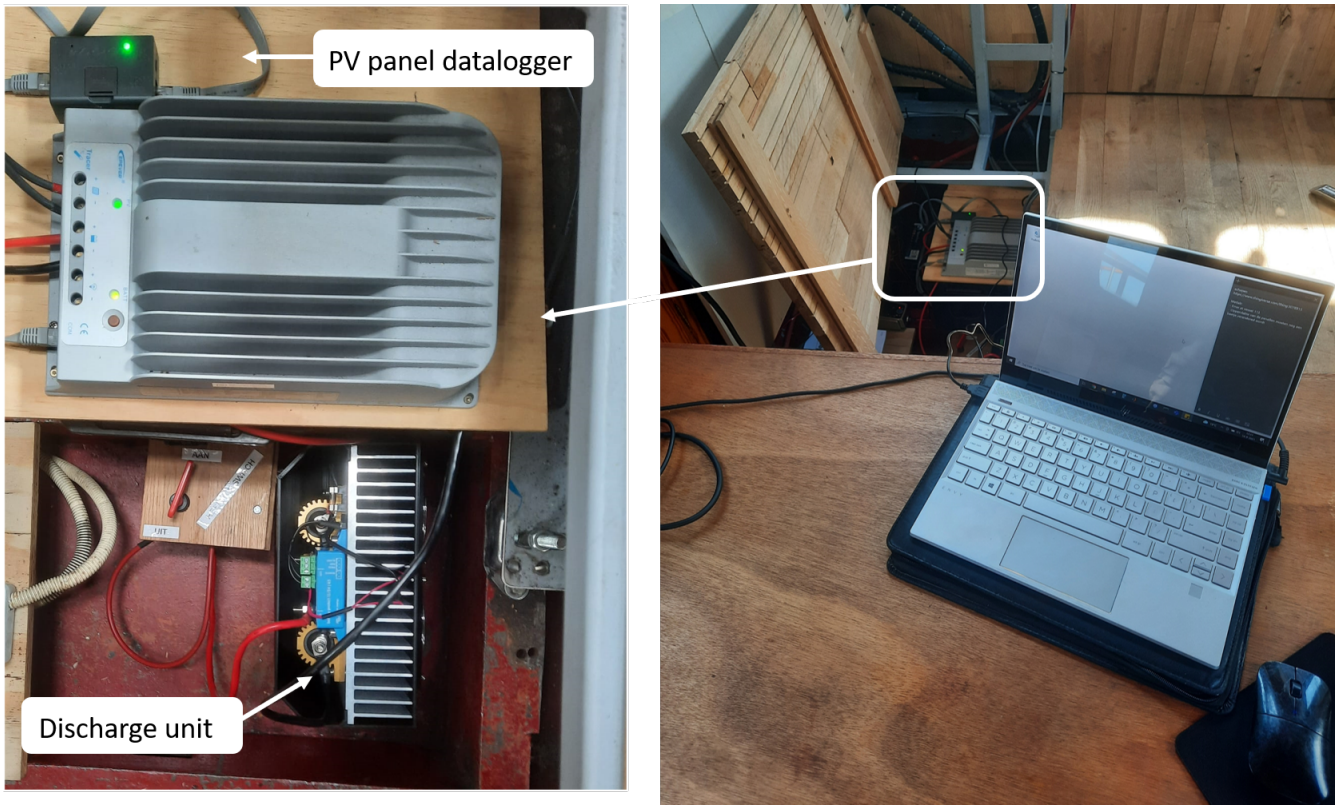

Figure 3.34: Discharge unit and PV panel datalogger

PV panel

The **PV panel specifications** are presented in table 3.6, the complete data sheet is provided in appendix B.

Table 3.6: PV panel specifications

Electrical Characteristics	**Unit**	**STC**
Maximum Power	[W]	360
Open circuit voltage	[V]	40.6
Short circuit current	[A]	11.33
Voltage at maximum power	[V]	34.8
Current at maximum power	[A]	10.35
Mechanical parameters	**Unit**	
Cell orientation	[-]	120 (6x20)
Junction box	[-]	IP68 three diodes
Dimension	[mm]	1755X1038X35
Operating parameters	**Unit**	
Nominal Operating cell temperature	[°]	45±2
Temperature rating	**Unit**	**STC**
Temperature coefficient Isc	$[\%/C]$	+0.048
Temperature coefficient Voc	$[\%/C]$	-0.270
Temperature coefficient Pmax	$[\%/C]$	-0.350

The performance of the **PV module is tested** in the PV lab at the faculty of Elektrotechniek, Wiskunde en Informatica. This test has been carried out to check whether the data from the data sheet is correct or whether the PV panel has already been degraded. The first test was carried out to confirm the performance of the PV panel under standard test conditions, as given in the data sheet of the PV panel. On the PV panel, five Directtemp probes are installed, one in every corner and one in the middle. The PV panel is placed under the solar simulator with an illumination between 950 and 1050 $[W/m2]$, see figure 3.35. The power of the PV panel is calculated according to the PV panel measured current. The power-voltage curve of the PV panels during this test is given in figure 3.36. When comparing the power-voltage curve to the power-voltage curve on the data sheet they are similar. The temperature increase as the PV panel is illuminated by the solar simulator. Measuring the module temperature, with the Directtemp probes, gives an estimation of the temperature coefficient of the PV model. Figure 3.36 shows the performance of the PV panel when the temperature is rising due to the illumination. The calculated temperature coefficient is -0.275 $[\%/C]$. The second test provides information about the uniformity of the area of the PV panel. By the use of electroluminescence (EL) a picture of the PV panel is made, which gives information about possible cracks and defects in the PV cells. Figure 3.36 shows the electroluminescence image of the PV panel. There are no cracks present on the panel. After performing two different tests in the PV lab, it can be concluded that the PV panel is not degraded. The PV panel does not show cracks and the power voltage curve is similar to the one on the data sheet, the I_{sc}, V_{oc} and the P_{max} from the data sheet are assumed to be valid. The temperature coefficient is somewhat different. However measuring the temperature coefficient is very sensitive and it is concluded that the PV panel is not degraded, therefore in this simulation, we assume the temperature coefficient of the panel.

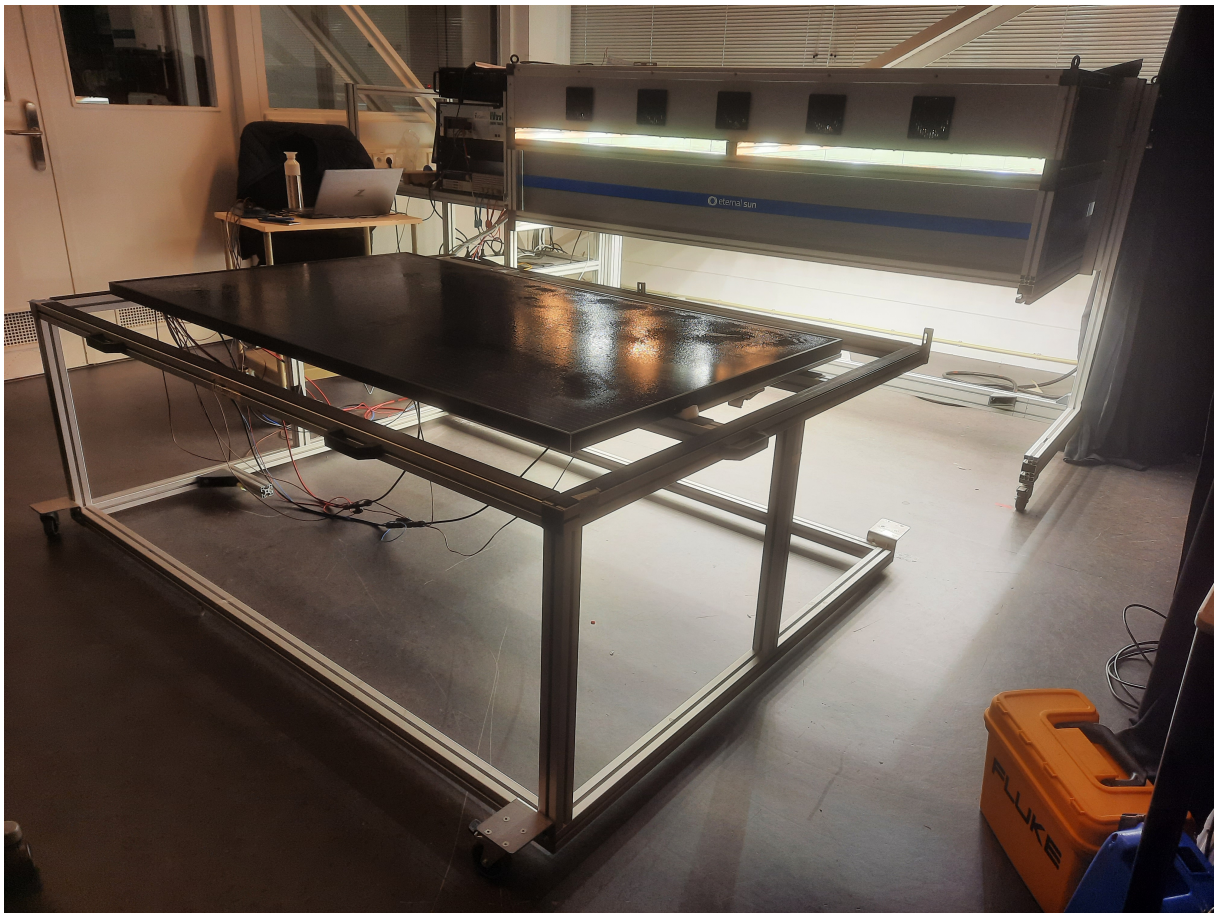

Figure 3.35: PV panel test at the PV lab

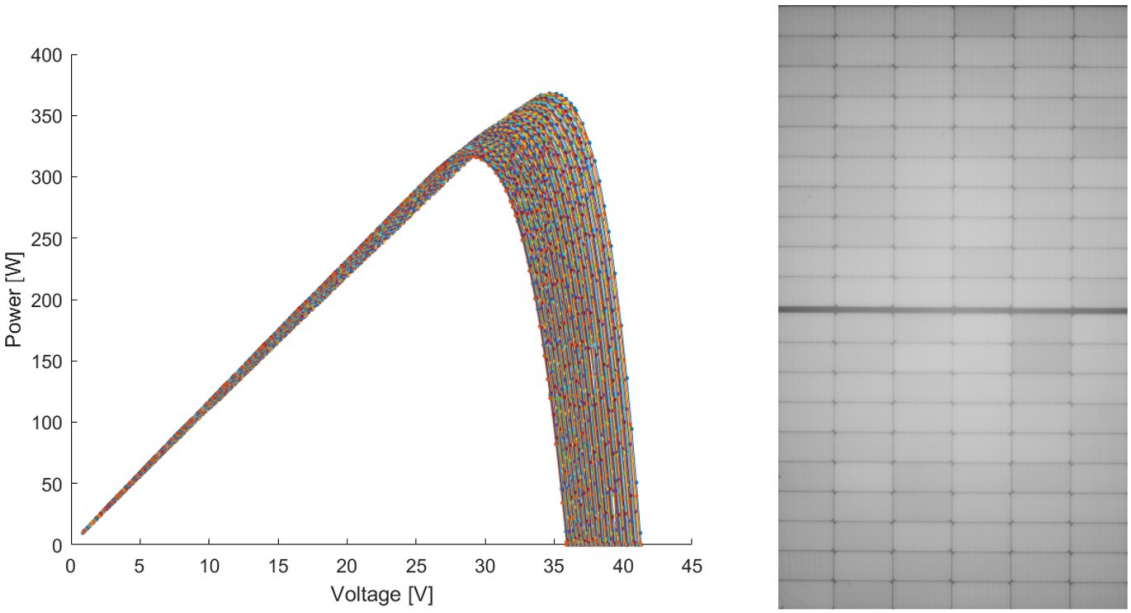

Figure 3.36: Left: Power-Voltage curve, Right: Electroluminescence photo

Monitoring system

Four data loggers are installed on Harmonie. Every data logger can measure and store different parameters. Table 3.7 provides an overview of the data loggers which are installed on Harmonie. The enumeration below explains the different devices.

Table 3.7: Monitoring devices installed on the Harmonie

Data log-ger	Stored parameters	Time inter-val	Accuracy
PV panel	Panel power, voltage and current	10 minutes	Unknown
Wind	Wind speed	5 minutes	±1m/s >5m/s and ±10% <5m/s
GPS	Location data, heading and speed	5 minutes	Speed: ±0.05m/s
Motion	Pitch motion, roll motion and ambient temperature	30 seconds	Motion: 0.03% <5° and 0.17% full range Temp: ±0.5°

- To monitor the PV panel, a data logger is connected to the charge controller, see figure 3.34. Using the communication cable and a pre-installed program from Epever, the stored data can be extracted from the device. The output of this data logger will be compared with the PV energy power and yield estimates of the simulation model, described in section 3.1.
- An Alecto WS-5500 wind data logger is mounted on the opposite side of the PV panel, to prevent shadows on the panel, see figure 3.37. This data logger measures the wind speed and sends it to the website wunderground.com. The stored data on this website can be downloaded.
- A Qstarz BL-1000ST BLE GPS travel recorder is installed on the PV panel, see figure 3.38. Using the communication cable and a pre-installed program from Qstarz the stored data can be extracted.
- A motion data logger is installed on the PV panel, see figure 3.38. In addition to the movements of the panel, the data logger stores the ambient temperature. Using a communication cable, the stored data can be extracted from the device using a mobile phone.

Figure 3.37: Wind data logger with a container vessel in the background

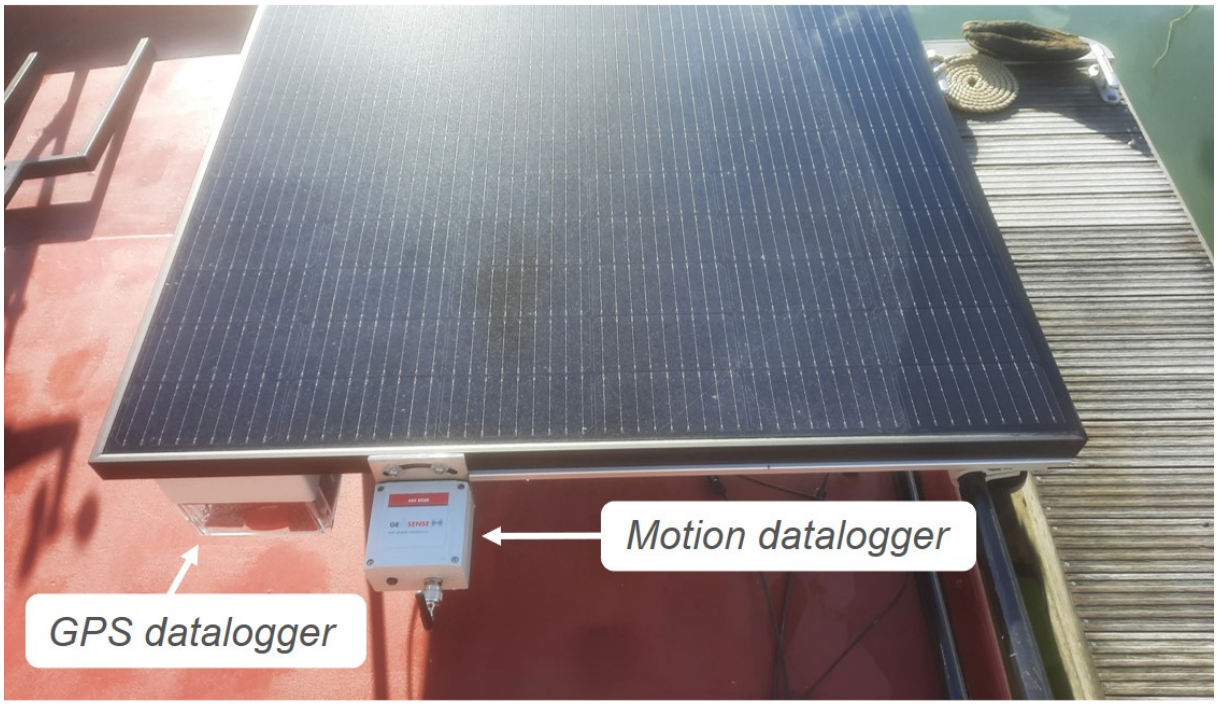

Figure 3.38: GPS and motion datalogger


Vestas
HARMONIE

4 Results

This chapter presents the results of the experiment that was conducted with the test vessel Harmonie and shows the Photovoltaic potential of the Dutch general cargo fleet. The sailing performance, the surroundings and the energy demand of Harmonie and the general cargo fleet are discussed. By means of a linear regression method, the developed model used in the experiment is statistically validated. The photovoltaic energy of the general cargo fleet is analysed and suitable probability distributions are fitted in.

This chapter consists of two sections. In the first section, the results of the experiment are presented. In the second section, the results of the general cargo fleet are discussed.

4.1 Experiment

This section shows the results which are obtained from conducting the experiment. These results will give an indication of the accuracy of the developed model to calculate the photovoltaic energy yield of a vessel.

4.1.1 Sailing behaviour

To analyse the results of the experiment, it is important to know the sailing behaviour of Harmonie, as this is one of the main input parameters in the simulation model. This sailing behaviour is reviewed in this section.

Docking time

During the first week of conducting the experiment, Harmonie was docked in a harbor in Rotterdam, see figure 4.1. The purpose of this one docking week was to measure the energy yield of the Harmonie and compare it with the estimated energy yield of the simulation model, to confirm the accuracy of the model when a vessel is docked.

The harbor is located in the centre of Rotterdam, see the red dot in figure 4.2, as discussed in section 2.2.2, the harbor of Rotterdam is the biggest harbor of the Netherlands. In the ports where general cargo vessels are docked, recreational ships are not allowed. This port was specifically chosen because it is located in an urban area of Rotterdam, therefore the effect of an obstructed horizon on the photovoltaic energy can be analysed. Table 4.1 given various information about the time that Harmonie is docked in Rotterdam.

Table 4.1: Docking information

Latitude and longitude harbor	52.3702 ,4.8952
Panel tilt	8° tilted to port side
Docking period	30-08-2021 12:30 until 06-09-2021 11:30

Figure 4.1: Harbor in Rotterdam

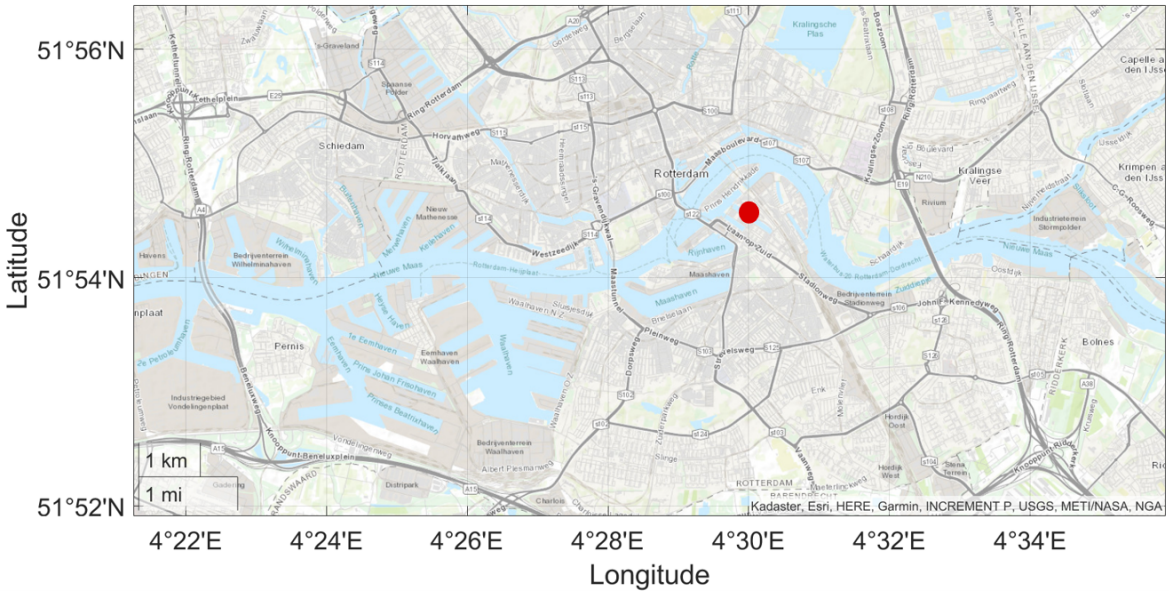

Figure 4.2: Location of the harbor in Rotterdam

Sailing time

During the second and third weeks, Harmonie followed its scheduled route through the Netherlands. The goal of these two weeks was to measure the energy yield of Harmonie and compare it with the estimated energy yield of the simulation model. Table 4.2 gives the travel report of the Harmonie during the experiment. This report shows the route that Harmonie sailed, with corresponding sailing hours, locations and panel tilts. There were two break days in the two weeks, during which no measurements were done.

Table 4.2: Harmonie travel report

	Date	Start time	End time	Sailing hours [h:min]	Start location	End location	Panel tilt [°]
1	7-9-2021	13:47	17:37	3:50	Rotterdam	Schoonhoven	8
2	8-9-2021	15:17	17:47	2:30	Schoonhoven	Nieuwegein	8
3	9-9-2021	11:27	16:27	5:00	Nieuwegein	Wijk bij duurstede	8
4	10-9-2021	10:47	18:57	8:10	Wijk bij duurstede	Arnhem	8
5	11-9-2021	11:57	14:37	2:40	Arhem	Frankerwaad	8
6	12-9-2021	Break	Break	Break	Break	Break	8
7	13-9-2021	11:07	14:47	3:40	Frankerwaard	Deventer	8
8	14-9-2021	14:19	18:59	4:40	Deventer	Kampen	0
9	15-9-2021	12:29	16:19	3:50	Kampen	Ketelhaven	0
10	16-9-2021	10:19	17:59	7:40	Ketelhaven	Lelystad	0
11	17-9-2021	10:09	12:49	2:40	Lelystad	Almere	0
12	18-9-2021	Break	Break	Break	Break	Break	0
13	19-9-2021	13:09	17:19	4:10	Almere	Amsterdam	0
14	20-9-2021	11:19	19:19	8:00	Amsterdam	Leiden	0
15	21-9-2021	08:29	14:59	6:30	Leiden	Rotterdam	0

During the two weeks, the Harmonie sailed for 63 hours and 20 minutes, on average almost 5 hours a day. See table 4.3. The Harmonie always sailed during the day, and most of the time between 12:00 and 17:00 when the sun is at its highest point.

Table 4.3: Sailing information

	Complete trip	**First sailing week PV tilt = 8 [°]**	**Second sailing week PV tilt=0[°]**
Total sailing days	13	6	7
Total rest days	2	1	1
Total sailing hours [h:min]	63:20	25:50	37:30
Average sailing hours per day [h:min]	4:52	4:18	5:21

Sailing route

The trajectory of Harmonie is shown in figure 4.3. Indicated in blue are the locations where the PV panel was tilted eight degrees to port (tilted), and marked in green shows when the PV panel tilt was zero degrees (flat).

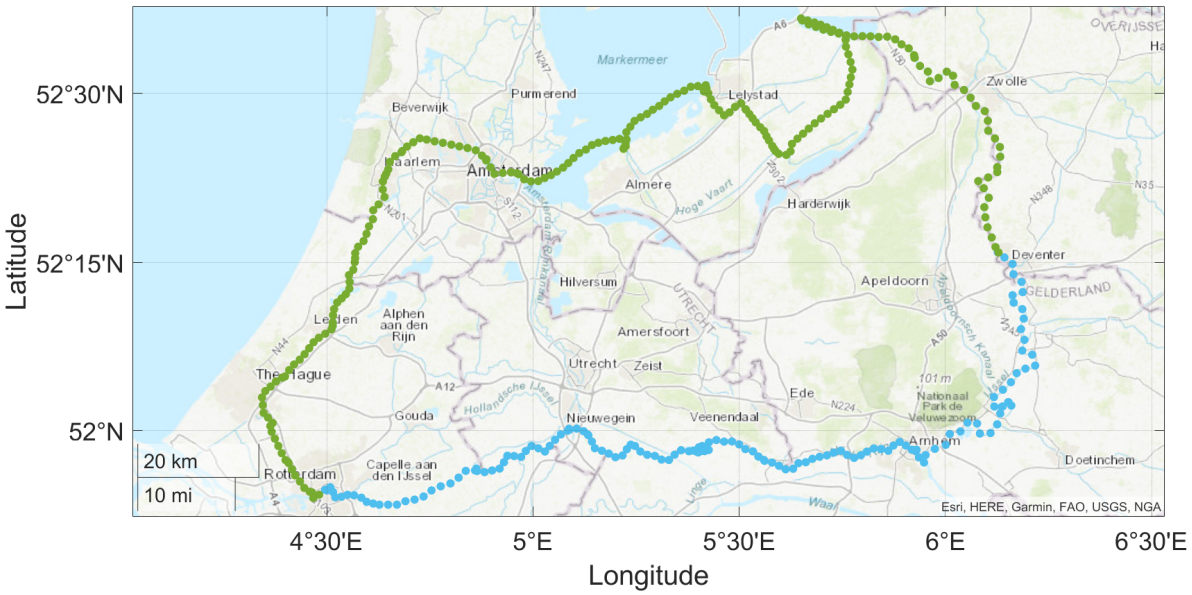

Figure 4.3: Sailing route Harmonie

The figure shows that the location points in the Hollandse IJssel are more distant from each other. This is because on the Hollandse IJssel, the water flows from south to west at 4 $[km/h]$. The Harmonie is a recreational vessel, and can therefore not always follow the same movement patterns as inland shipping vessels. As the goal of these two weeks was to estimate the accuracy of the model when a vessel is sailing, only representative data points of the route were used for the validation, namely the inland waterways that are used by general cargo shipping vessels.

An example of non-representative data are the locations where Harmonie moored at the end of a day. Recreational vessels must dock in an assigned harbor, often these are located outside the inland shipping waters and on branches of the major canals. Another example when the Harmonie couldn't imitate the movement of an inland vessel was on September 16. The initial plan was to cross the IJsselmeer

from the Kettelmeer to Lelystad. But due to a strong rising wind, it was irresponsible to cross the IJsselmeer with a small ship like the Harmonie. As a result, the ship had to sail inwards over small canals only used by recreational vessels to Lelystad.

4.1.2 Surrounding of the sailed waters

Before discussing the photovoltaic energy, the environment of Harmonie is analysed as this is an important input parameter in the simulation model as well.

Figure 4.4 gives the sky view factors (SVF) varying over time, which give an identification of the surrounding of a location point, as discussed in section 3.15. The SVF during the first week of the experiment was fixed, as Harmonie's location did not change during that week. The SVF of the second week is indicated in blue, when the PV panel was tilted 8 degrees to the port side. The SVF indicated in green is calculated for the last experiment week, when the PV panel was placed flat.

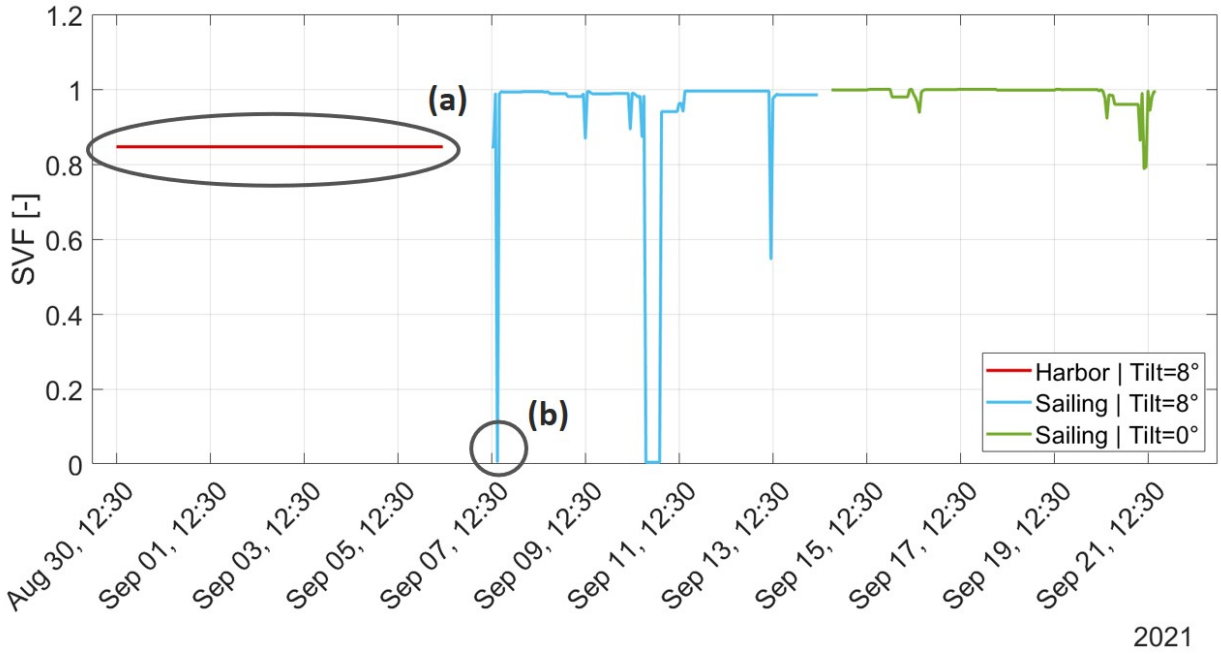

Figure 4.4: Sky view factors during the three weeks of the experiment

Figure 4.5 shows the DSM and skyline profile of the location point in the Harbor of Rotterdam. The corresponding SVF, 0.8465, is indicated with an (a) in figure 4.5. A proportional part of the horizon is blocked. The altitude is a straight line from the azimuth 70 until 100 degrees, this is a limitation of the usage of the DSM. Vessels in the Harbor do have masts stretched with lines. The lines are identified as volume blocks that can block the sun.

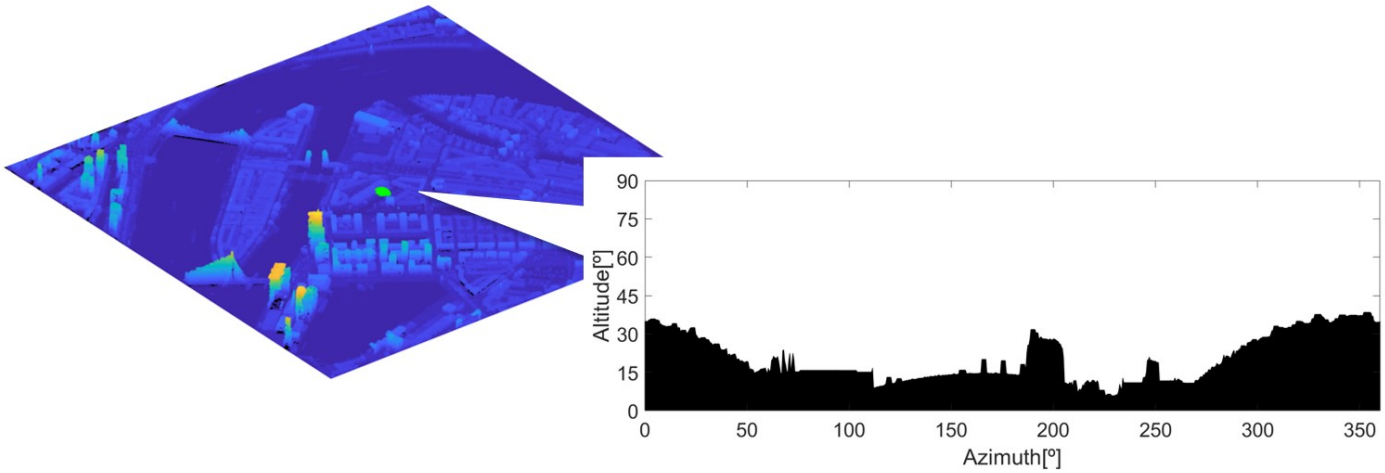

Figure 4.5: DSM and skyline profile in the harbor of Rotterdam (a)

Figure 4.4 shows an SVF of almost zero, 0.005738, at point (b). The DSM and the skyline profile of these points are visualized in figure 4.6. This waterway data point is located under a bridge, which leads to a skyline profile that is almost completely blocked.

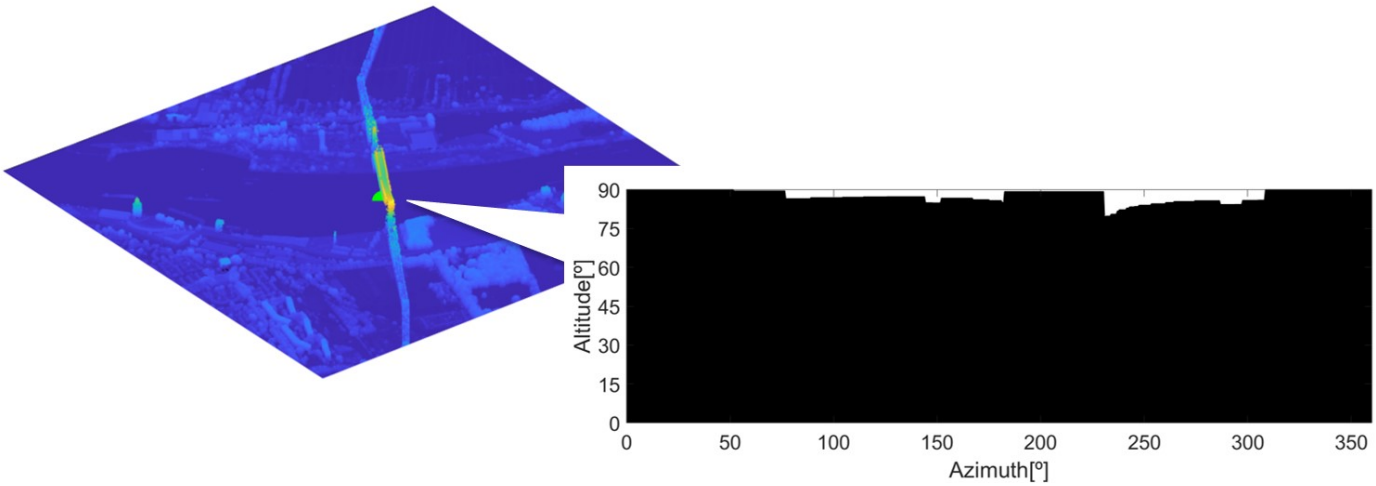

Figure 4.6: DSM and skyline profile of point (b)

4.1.3 Photovoltaic power and energy yield

During the experiment, the PV power generated by the PV panel for every 10 minutes is stored. The PV energy yield is calculated by integration of the power overtime for every hour, as indicated by formula 3.31 in section 3.1.6. The measured and estimated energy yield are compared, see Figure 4.7, which shows the measured energy yield, estimated energy yield and the percentage difference between the two. The measured energy yield is displayed in grey and the estimated energy yield is indicated by the colour of the corresponding week. The black line gives the relative deviation of the estimated yield with respect to the measured energy yield.

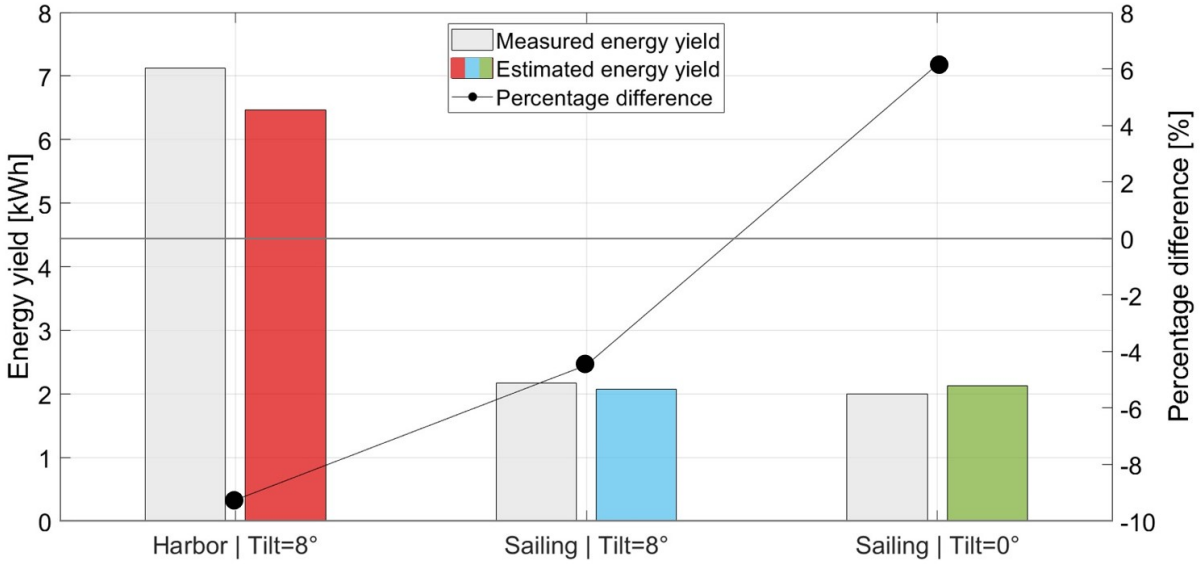

Figure 4.7: Measured and estimated energy yield

The exact values of figure 4.7 are shown in table 4.4. The energy yields of the weeks where the Harmonie was sailing were smaller than the energy yields when it was docked in the Harbor. This is because these weeks have fewer data points, therefore the energy yields are smaller. The accuracy of the simulation lies in a range between -9.26 % and +6.15 % for a weekly time step. Sailing weeks have a lower absolute percentage difference than the harbor week. The simulation results are not biased towards overestimation or underestimations with respect to the measured energy yield. There are more data points for the harbor week than for the sailing weeks. During the harbor week the PV power data point during the entire day are used, for the sailing week only the PV power data points during the sailing hours are taken into account.

Table 4.4: Measured and estimated energy yield

Week	**Measured energy yield [kWh]**	**Estimated energy yield [kWh]**	**Percentage difference [%]**	**RMSE**	**Data points**
Harbor | Tilt 8 [°]	7.12	6.45	-9.26	30.87	104
Sailing | Tilt 8 [°]	2.17	2.08	-2.07	38.87	33
Sailing | Tilt 0 [°]	2.00	2.12	+6.15	31.28	33

4.1.4 Model validation

To validate the developed model a linear regression model is used, to describe the relationship between the measured results, response, and the different predictors. The linear regression model is as follows:

$$Measured \cong \alpha Estimated \tag{4.1}$$

- $Measured$ and $Estimated$ are vectors that combines the 170 data points for the three experiment weeks.
- $Measured$ is a vector of observed PV power values of the response variable.
- $Estimated$ is a predictor variable which contains the values of the estimated PV power.

Table 4.5 shows the regression coefficients α and the P-value. The P-value is used to identify if the predictor is statistically significant or insignificant. The signification level of the model is set to 5%, 0.05. A P value smaller than 0.05 indicates that the predictor is statistically significant, the predictor has an effect on the outcomes of the response variable. A P value larger than 0.05 indicates the predictor is statistically insignificant, the predictor does not have a significant (random) effect on the outcome of the response variable.

Table 4.5: Linear regression model parameters

	Estimate: α	**Pvalue**	**95% confidence interval**
Estimated	1.0173	5.6717e-75	[0.9559 1.0788]

The P-value for the predictor value $Estimated$ is below the signification level, therefore the $Estimated$ is significant and indicates that there is a relation between the measured and estimated PV power. The α is 1.02, therefore the model underestimates the outcomes by 2%. The R^2 of the linear regression model is 0.7156. The simulation model is able to estimate the outcomes close to the measured values. Figure 4.8 shows the linear regression model, the 170 data points and the ideal line where the measured value are equal to the measured values.

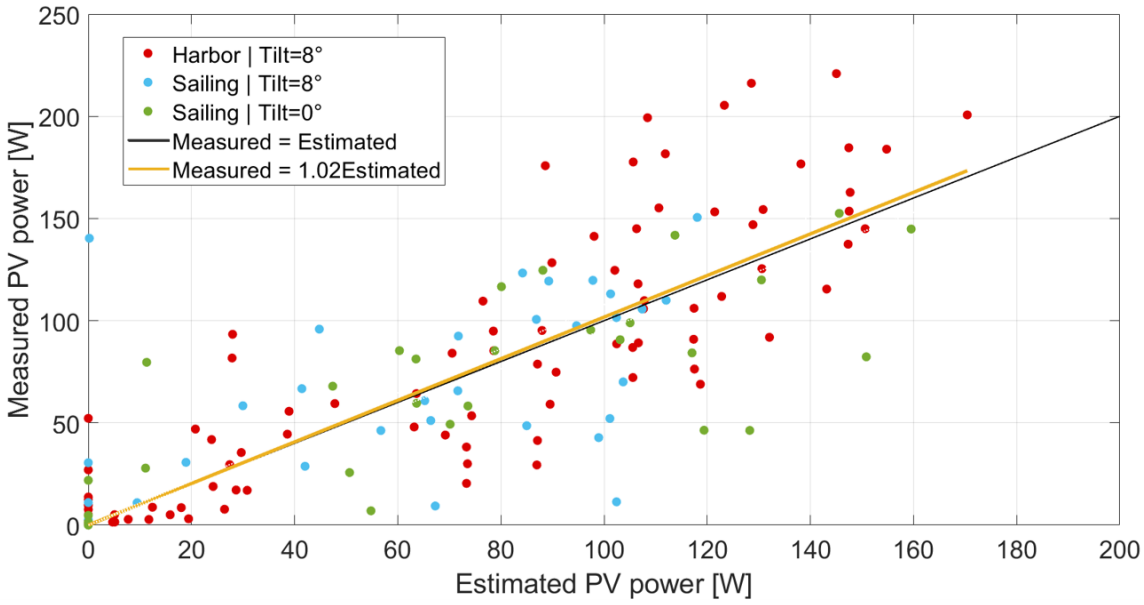

Figure 4.8: Linear regression model

There are various variables that can influence the outcome of the experiment. Variables that are taken into account during the experiment are the difference in PV panel tilt and the sailing and docking status. To estimate the effect of these variables the following co-variance linear regression model is analysed:

$$Measured \cong \alpha Estimated + \beta Sailing + \gamma Tilt8 \quad (4.2)$$

- $Tilt8$ is a binary predictor variable, where 1 indicates if the PV panel is tilted 8 degrees to the port side.
- $Sailing$ is a binary predictor variable, where 1 indicates if the PV panel is tilted 8 degrees to the port side.

Table 4.6 shows the regression coefficients α, β and γ with corresponding P values.

Table 4.6: Co-variance linear regression model parameters

	Estimate: α, β, γ	**Pvalue**	**95% confidence interval**
Estimated	0.96	2.4321e-48	[0.8684 1.0501]
Sailing	-2.08	0.6503	[-11.1355 6.9699]
Tilt angle 8	8.56	0.0273	[0.9692 16.1517]

The $Sailing$ predictor has a P-value above 0.05, which indicates that the outcome of the measured experimental results is not affected if by the sailing or docking behaviour of the vessel.

The $Tilt8$ predictor is statistically significant, the effect of a different tilt on the outcome of the measured PV power is not random, as the P-value is below 0.05. As the $Tilt8$ is a binary vector and γ is 8.56, the measured outcome can be affected by 8.56 $[W]$ for a tilt for 8 degrees compared to a tilt of zero degrees. The $Tilt8$ is significant, but an effect of 8.56 $[W]$ is relatively small as the PV power range is between 0 $[W]$ and 200 $[W]$.

The estimate α is changed to 0.96. The R^2 of this linear regression model is 0.6979. Figure 4.9 shows the linear regression line with and without the effect of different tilts on the outcome.

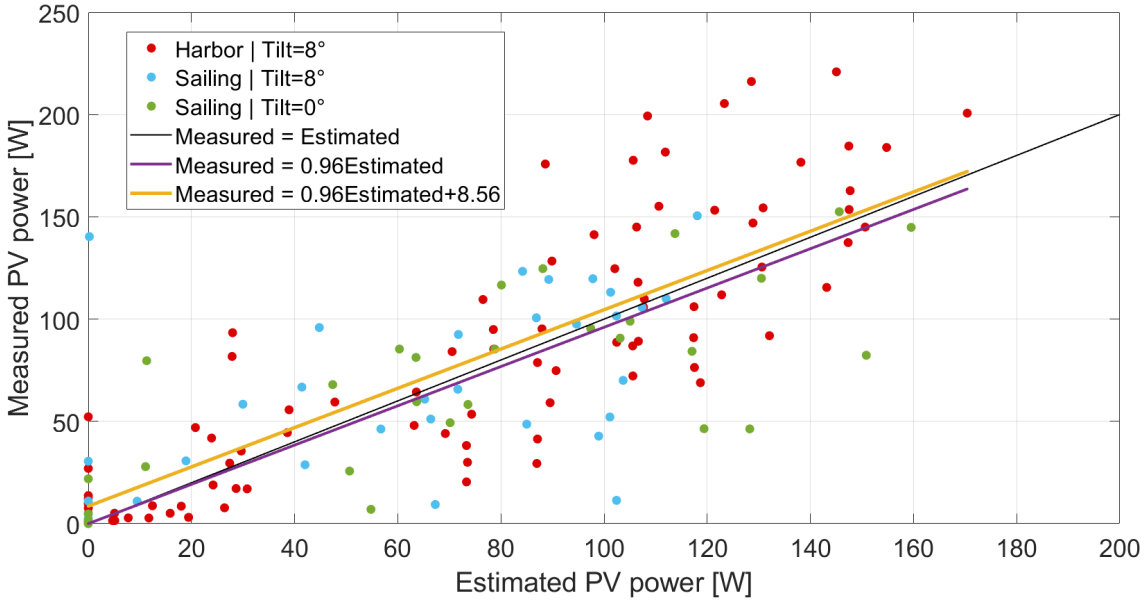

Figure 4.9: Co-variance linear regression model

4.1.5 Energy demand

Figure 4.10 shows the power demand of the engine of the Harmonie. On September 12 and 18 the energy demand is almost zero, as there Harmonie did not set sailing. Most of the energy demand comes from the consumption of the engine. The energy demand the household appliances are not taken into account as these can vary a lot between vessel owners.

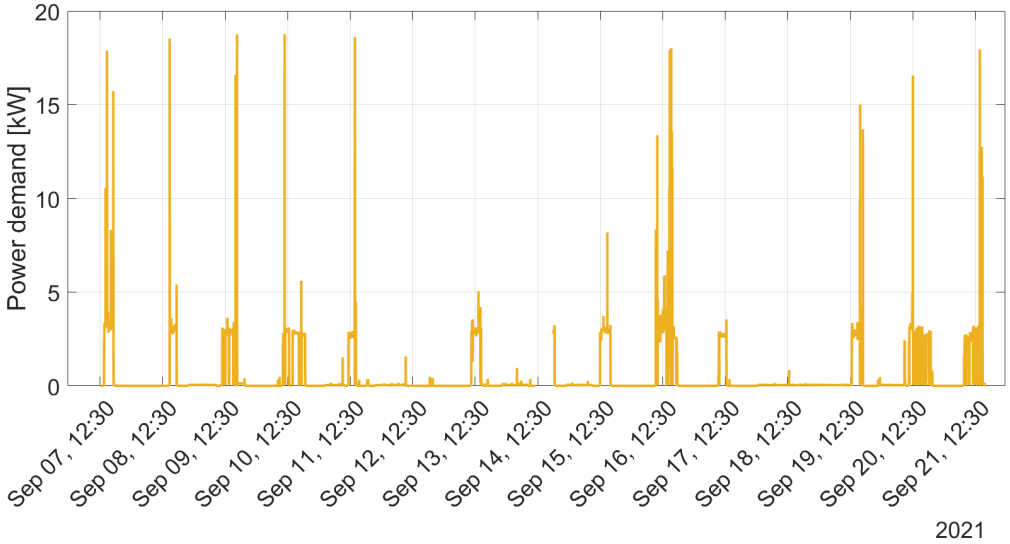

Figure 4.10: Power demand engine Harmonie

Figure 4.11 shows the power demand of the Harmonie on September 11. As indicated in the travel report and shown in figure 4.11, Harmonie set sail from 11:47 to 14:37, during which the power demand was above zero [kW]. Most of the time the engine power was constant around 3 [kW], at this power the vessel speed with respect to the water is around 8 [km/h]. Around 14:20 the energy demand rose to the maximum power of the engine for a period of time. This happens more often when certain actions are performed such as parking, slowing down for a bridge, going through a lock, etc. In this case, the full capacity of the motor was used because the Harmonie got stuck due to inattention. With the help of the engine and pushing from the water, the boat was able to come loose again.

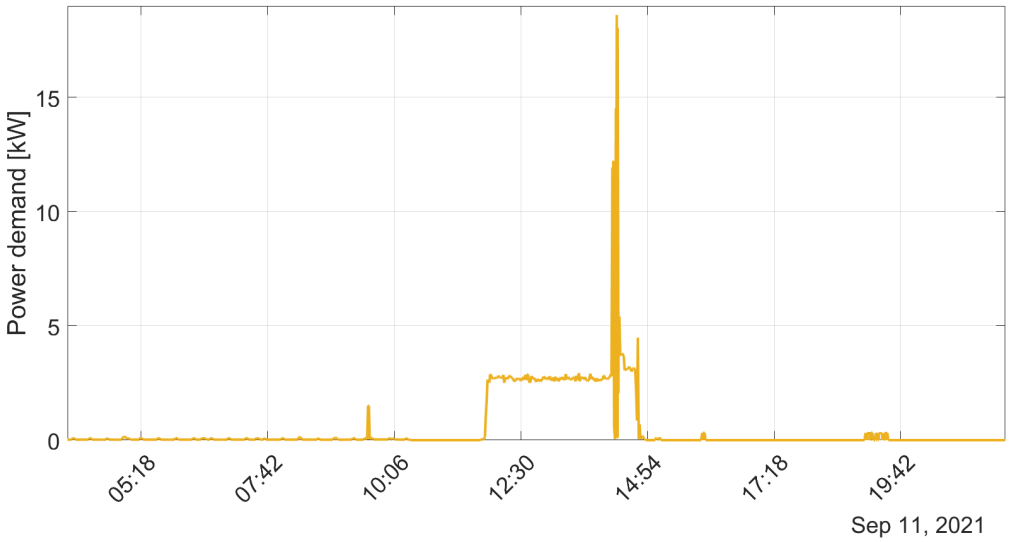

Figure 4.11: Power demand 11 September engine Harmonie

Figure 4.12 shows the engine's power demand for the 20th of September. During this day Harmonie was sailing from Amsterdam to Leiden, across the channels Spaarne and Ringvaart. There are many bridges across these canals, so Harmonie often had to wait at a mooring place before the bridge opened, which can be seen in the figure below.

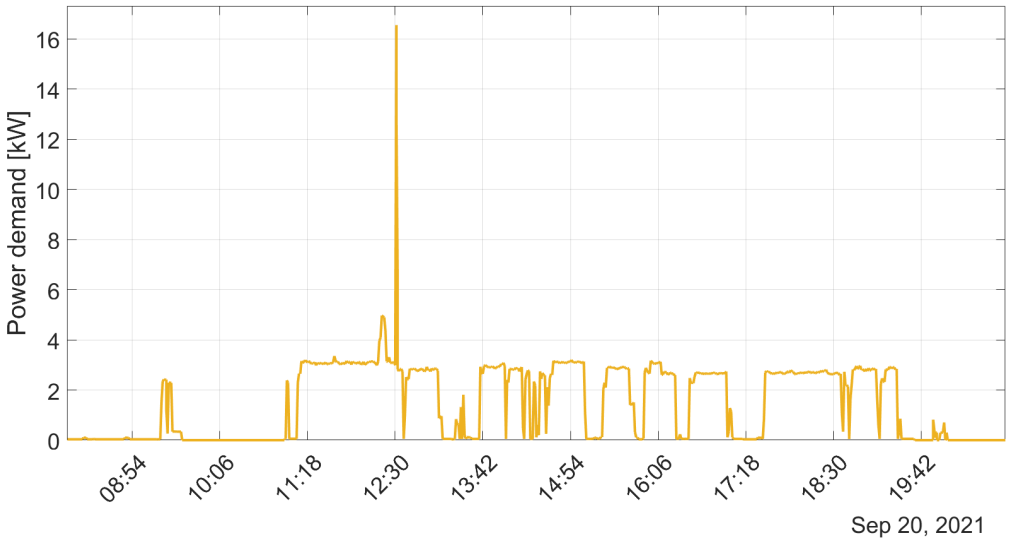

Figure 4.12: Power demand 20 September engine Harmonie

By means of the experiment, the photovoltaic energy yield and the energy demand of the two sailing weeks have been measured. Figure 4.13 shows how much of the energy demand from the engine of the Harmonie can be generated by the one PV panel installed. 6.60% of the energy demand can be supplied by the PV panel and 93.40% needs to come from shore power. The total energy demand of the Harmonie is 162 [kWh] and the photovoltaic energy generation is 11 [kWh].

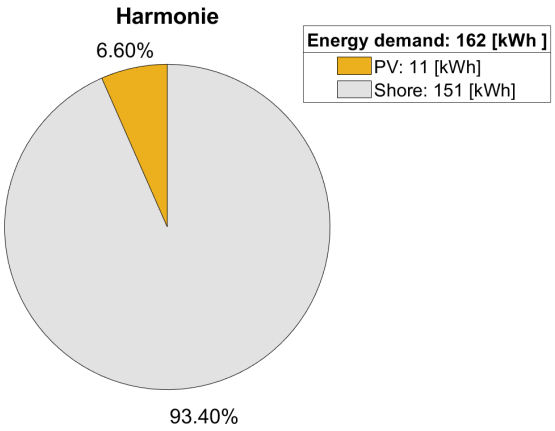

Figure 4.13: Energy demand that can be covered with Photovoltaic energy

The 6.60% of the energy demand that can be generated by the PV energy is from one PV panel. The Harmonie would have the capacity to carry 4 PV panels. The Harmonie is a recreational vessel, and on holidays the vessel would not have the same sailing pattern as during the experiment. When the Harmonie is used during a Holiday, the vessel might only be used every other day for three hours a day. Table 4.10 shows the estimated percentage of which the energy demand can be generated by PV energy for different sailing behaviours and a different number of PV panels installed.

Table 4.7: Energy demand that can be covered for various PV systems

Sailing behaviour over 15 days	**Panels installed**	**Energy demand covert by PV energy**
63:20 hours of sailing: 13 days 4:52 hours of sailing	1	6.60%
63:20 hours of sailing: 13 days 4:52 hours of sailing	4	26.40%
21:00 hours of sailing: 7 days 3 hours of sailing	4	79.61%

4.1.6 Vessel motion

During the experiment, various vessel motion data is collected. There are three ways a vessel can rotate. First, a ship can roll, which is a rotation over the length of the vessel. Second, it can Pitch, which is a rotation over the width of the vessel. The third way to rotate is yaw, this rotation over the cross-section of the vessel.

Pitch motion

Figure 4.14 shows the four different weeks of monitoring the roll motion of the Harmonie. The yellow and red graphs showed the roll motion of the week when the Harmonie was moored in the harbor with a tilt of zero and 8 degrees, respectively. The green and the blue show the roll motion for a sailing week with a PV panel zero and 8 degrees to port side, respectively. Table 4.9 gives an overview of the maximum and minimum pitch values from figure 4.15.

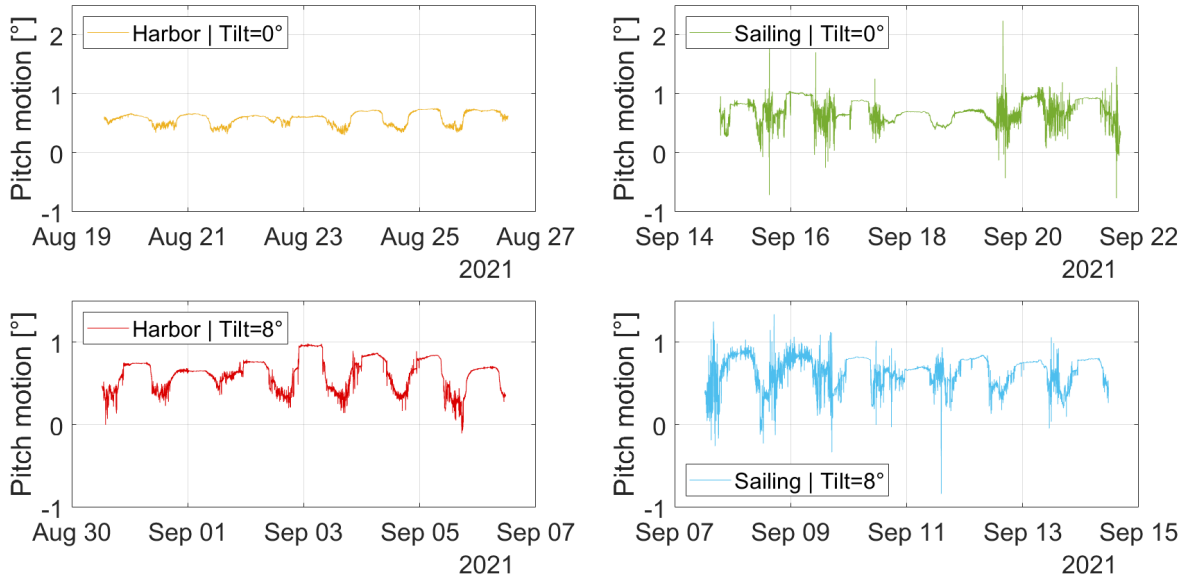

Figure 4.14: Pitch motion

Table 4.8: Minimum and maximum roll angles with maximum differences

Week	**Minimum roll angle [°]**	**Maximum roll angle [°]**	**Maximum roll difference [°]**
Harbor | Tilt 0 [°]	+0.35	+0.75	0.40
Harbor | Tilt 8 [°]	-0.11	+0.98	1.09
Sailing | Tilt 0 [°]	-0.77	+2.24	3,01
Sailing | Tilt 8 [°]	-0.83	+1.33	2.16

The first week when the Harmonie was moored in the harbor, the vessel owner did not enter the vessel during these measurements. During the second week, the owner of the vessel enters the vessel almost every day. Stepping on and off-board the vessel leads to movements of the ship itself. As a result, this week's movements are greater than the motions of the other week. There is no relation between the different PV panel tilts of zero and eight and the pitch motion of the vessel Harmonie. This difference in pitch motion is caused by the other sailing conditions, different routes and different weather conditions. The maximum pitch motion difference is 2.76 times bigger when the Harmonie is sailing compared to being docked.

Roll motion

Figure 4.9 shows four different weeks of monitoring the roll motion of the Harmonie. Table 4.9 gives an overview of the maximum and minimum roll values from figure 4.15.

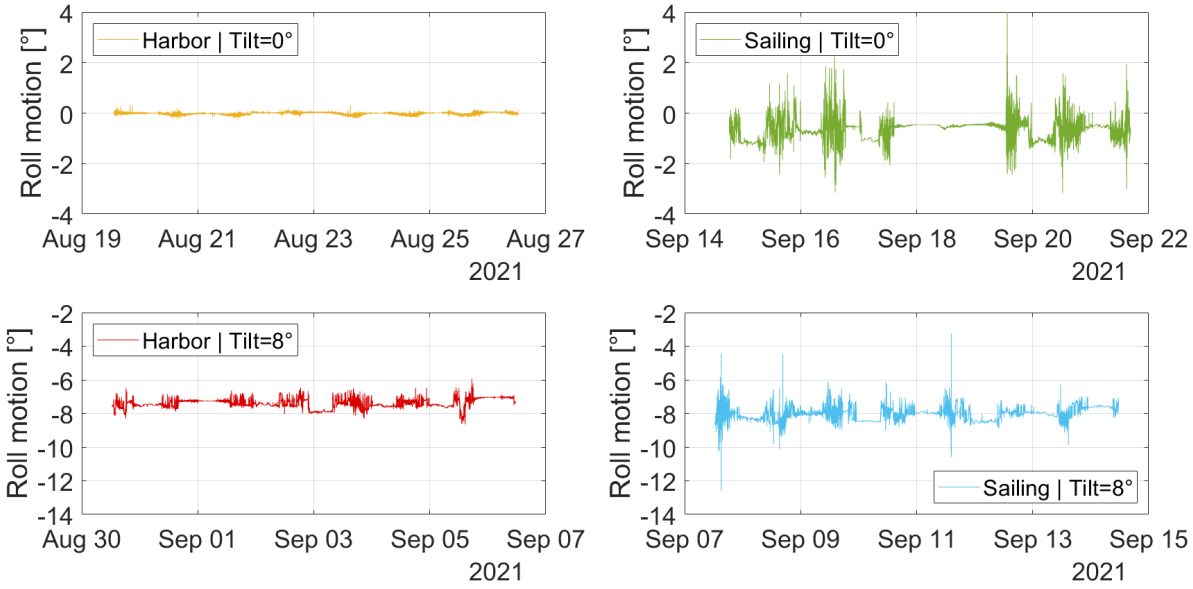

Figure 4.15: Roll motion

Table 4.9: Minimum and maximum roll angles with maximum differences

Week	Minimum roll angle [°]	Maximum roll angle [°]	Maximum roll difference [°]
Harbor | Tilt 0 [°]	-0.25	+0.34	0.59
Harbor | Tilt 8 [°]	-8.65	-5.94	2.71
Sailing | Tilt 0 [°]	-3.17	4.07	7.24
Sailing | Tilt 8 [°]	-12.63	-3.25	9.38

The maximum roll motion difference is large than the maximum pitch motion difference, because of the two seasons. First, most people board a ship from the side of the boat, leading mainly to a roll motion. Second, the other reason the roll motion difference is more significant is because the length of a vessel is always longer than the width of the vessel, leading to a greater buoyancy along with the size of the ship. The maximum roll motion difference is 3.46 times bigger when the Harmonie is sailing compared to being docked.

4.2 Dutch shipping fleet

This section provides an overview of the results for the general cargo vessels. The different discussed topics will give an idea of the photovoltaic potential of the general cargo fleet.

4.2.1 Sailing behaviour

The sailing behaviour of the general cargo vessels is an important factor when determining the photovoltaic energy yield of the fleet.

Table 4.10: Number of container and bulk vessels

Number of general cargo vessels	2746
Number of vessel which transport containers	600
Number of vessel which transport bulk	2146

Sailing time

Figure 4.16 shows the sailing distribution of the general cargo vessel during an average day. The graph gives an estimate of the sailing times of the general cargo fleet. Between 08:30 and 16:30 the probability that a vessel is sailing is the highest. The probability at night is only slightly lower, a sufficient amount of vessels still sail at night. As discussed in section 2.2.1, there are vessels that sail continuously, with changing crew. The average day in figure 4.16, is calculated for 2,746,365 hours of data. Appendix F shows the sailing distribution of the general cargo vessel during an average 12-hour day.

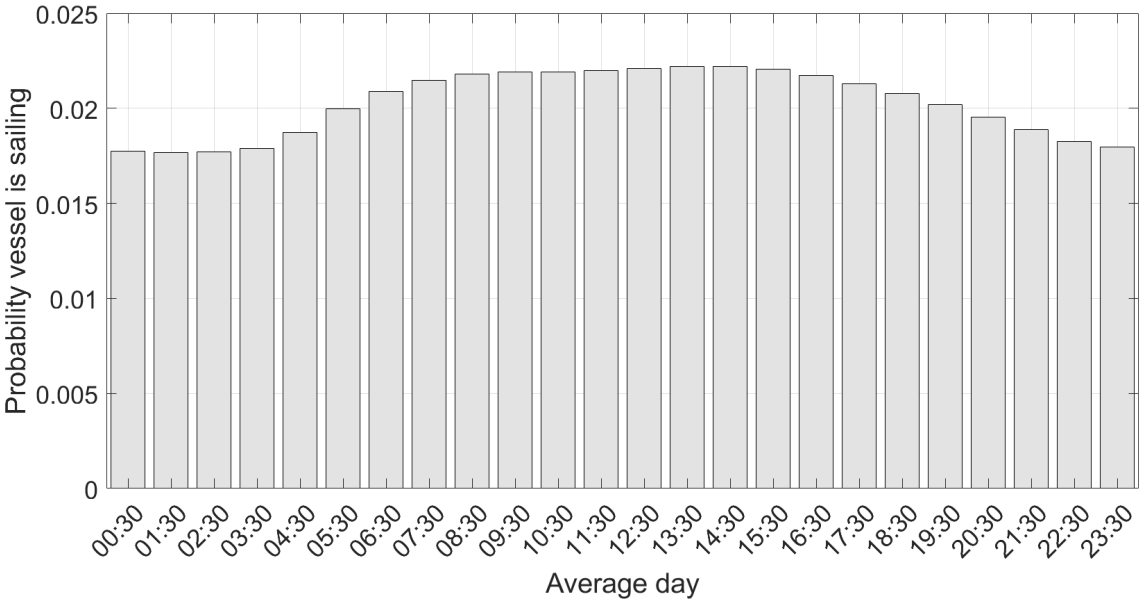

Figure 4.16: Sailing behaviour over an average day

A cargo vessels sails on average for 48.68% of the time, as indicated in table 4.11. In section 3.1.3 an average of 50 % was assumed, this is closed to 48.68%.

Table 4.11: Average sailing day parameters

Number of vessels used for generating the data [-]	2746
Number of data points for generating an average hour [-]	2,746,365
Sailing percentage [%]	48.68
Docking percentage [%]	51.32

Sailing routes

The vessels sail fairly uniformly through the Dutch waterways in the Netherlands. Appendix O shows how the waterway points are scattered through the whole country, and how often a vessel passes through every waterway point.

Figure 4.17 zooms into the area of Rotterdam. The figure shows that the waterway points in the Port of Rotterdam are passed frequently by general cargo vessels. As discussed in section 2.2.2, Rotterdam is the largest port of the Netherlands.

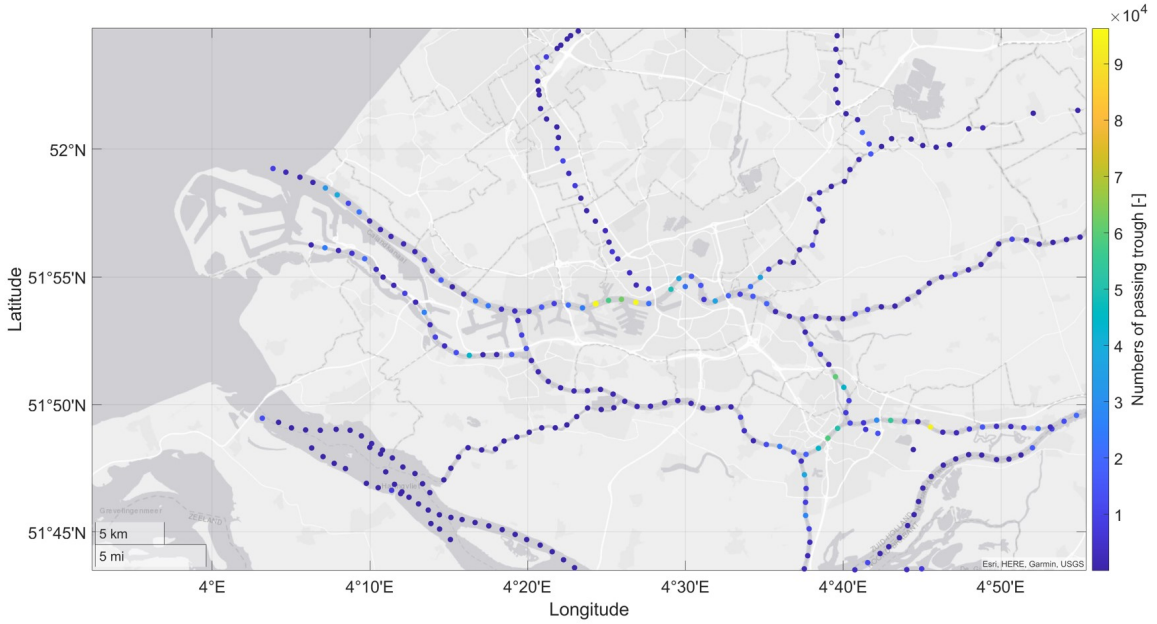

Figure 4.17: Number of times passing through waterways points at Rotterdam

The second-largest port in the Netherlands is the Port of Amsterdam. Figure 4.18 show the waterways of the area of Amsterdam. This graph confirms that there is a relatively large number of vessels sailing through Amsterdam each year.

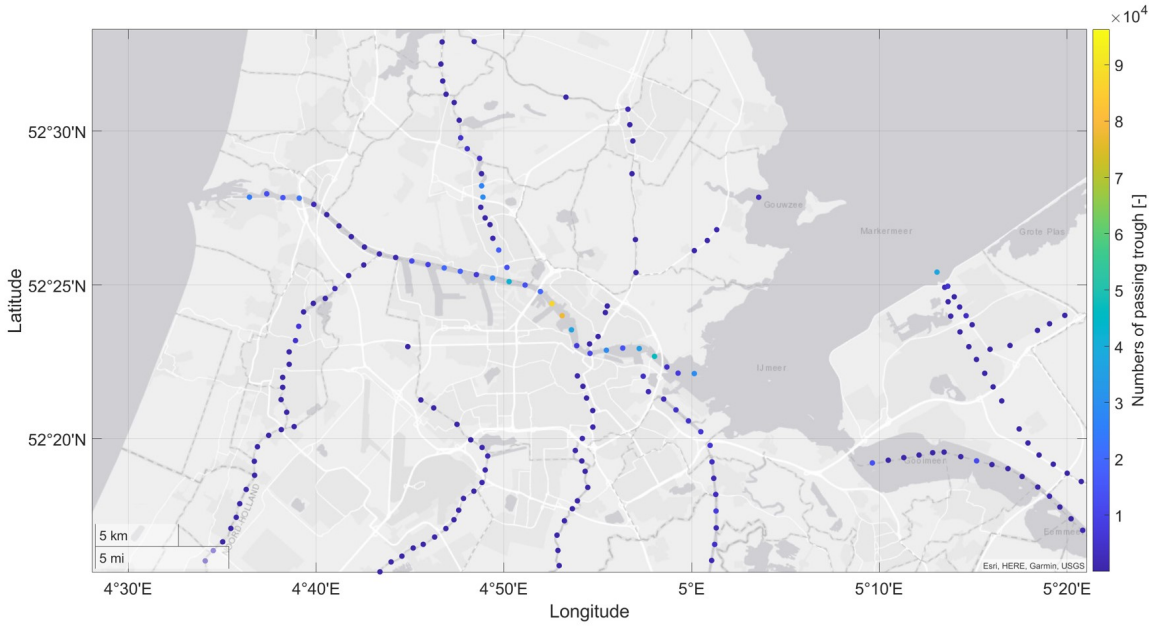

Figure 4.18: Number of times passing through waterways points at Amsterdam

4.2.2 Surrounding of the Dutch waters

Table 4.12: SVF parameters

	Container vessels	**Bulk vessels**	**Bulk vessels**
Panel orientation	Tilted 0 [°]	Tilted 8 [°] to starboard	Tilted 8 [°] to port
Outlier percentage [%]	15.33	16.92	14.99
Number of SVFs [-]	5256000	18798960	18798960
Mean SVF [-]	0.9530	0.9451	0.9449
Max SVF [-]	1.0000	0.9951	0.9951
Min SVF [-]	0.0051	0.0049	0.0049

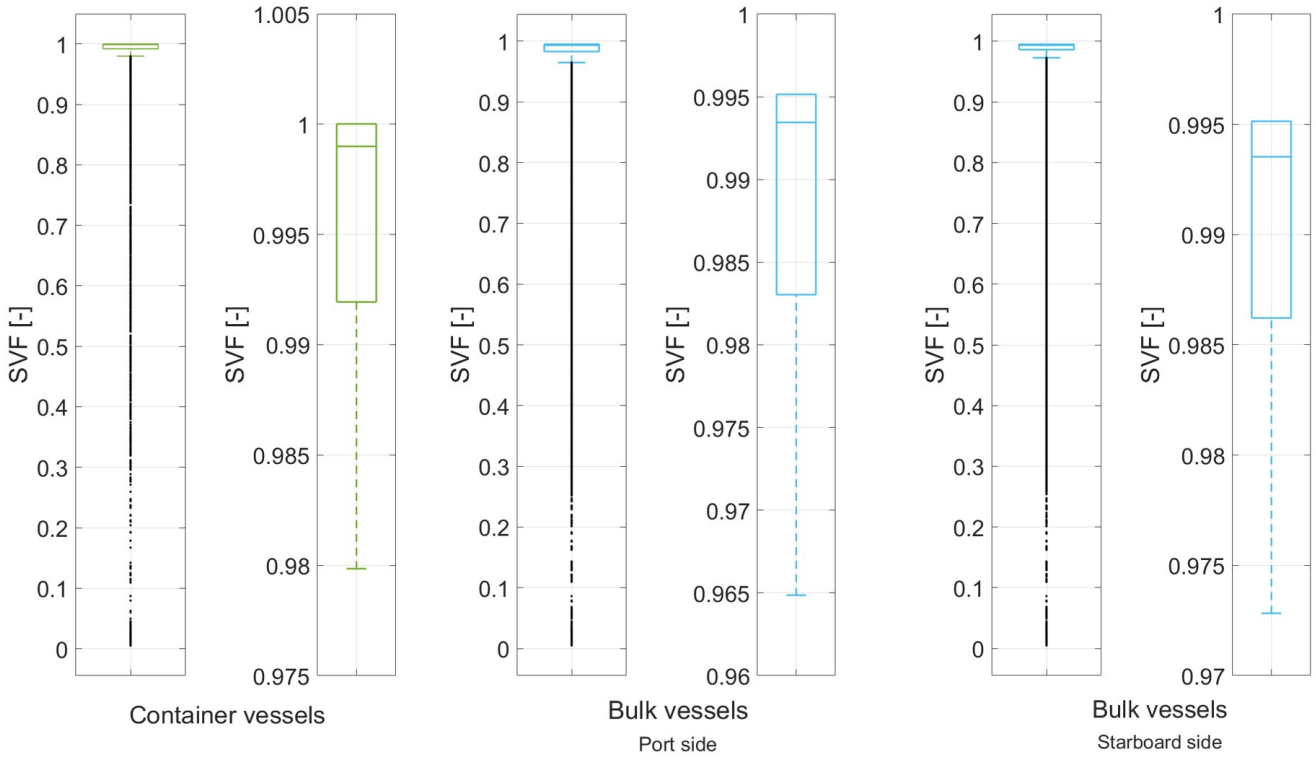

Figure 4.19: Box plots, with and without outliers, for probability distribution of the SVFs

SVF container vessels

Figure 4.19 shows the box plots of the SVFs of all the container vessels of every hour. The distribution of the sky viewing factors cover almost the maximum range, the SVFs varies from 0.0051 to 1.0000. This means that the surroundings vary between an almost completely enclosed surrounding to a complete free horizon. The mean SVF of 0.9530 indicates that on average 95.30% of the skydome around the PV panels is not blocked. Examples of various skyline profiles are indicated in section 4.1.2.

SVF bulk vessels starboard side

The middle two box plots in figure 4.19 correspond to the general cargo vessels with a PV panel tilt of 8 degrees to starboard. The SVFs vary from 0.00491 to 0.9951. Notice that the maximum SVF is smaller than that of the container vessel which was 1.000. The reason for this is the tilt of the PV panels. As the PV panels are tilted, the horizon behind the PV panel is by definition not completely free. Therefore the complete distribution is shifted a little to the lower side of the SVFs. Equation 4.3 confirms that the SVF of 0.9951 is the theoretical maximum of a PV panel titled 8 degrees.

$$0.9951 = \frac{1 + \cos(8°)}{2} \tag{4.3}$$

SVF bulk vessels port side

The last two box plots in figure 4.19 correspond to the general cargo vessels with a PV panel tilt of 8 to the port side. The difference in SVF between the port and starboard side is related to the difference in the heading of the PV panels. The locations of the first, second and third quartile are lower for the port side. This indicates that on average the skyline profiles of the port side panels are somewhat smaller. This difference however is almost zero, -0.0212%.

4.2.3 Surface utilization

The suitable surface for PV panels on the general cargo inland vessels is calculated for every vessel individually. This is an important parameter used to estimate the photovoltaic potential of the Dutch general cargo fleet. Table 3.5 gives an overview of the discussed parameters related to the PV surface of the vessel.

Table 4.13: PV surface and installed panels

	Container vessels	**Bulk vessels**	**General cargo fleet**
Number of vessels [-]	600	2146	2746
PV surface area mean[m^2]	599.45	461.38	495.19
PV surface area total [m^2]	369,670.00	990,124.00	1359794
PV surface utilisation mean [$\%$]	60.49	50.83	52.94
PV installed peak power mean [kW]	118.46	91.18	97.14
PV installed peak power total [MW]	71.08	195.67	266.75
PV installed panels mean [-]	329.06	253.27	269.83
PV installed panels total [-]	197,438	543,520	740,958

PV surface area

The suitable PV surface area for the 600 container vessels and the 2146 bulk vessels individually is indicated in appendix I. The total PV surface of the complete general cargo fleet is 1,359,794 [m^2], which is 1.6 [km^2]. The PV surface on average for a general cargo inland vessel is 495.19 [m^2].

PV surface utilisation

The PV surface utilisation of the vessels is the percentage of suitable PV surface with respect to the vessels surface. The surface utilisation of an average general cargo

vessel is 52.94%. The surface utilisation of an average container and bulk vessel is 60.49% and 50.83% respectively. The utilisation distribution of the container vessel is shifted towards the right side with respect to the bulk vessel, indicating more vessels with higher surface utilisation, see figure 4.20 and 4.21. For bulk vessels, the PV panels are installed on the hatches of the holds, which contain a corridor and therefore have a smaller average PV surface utilization

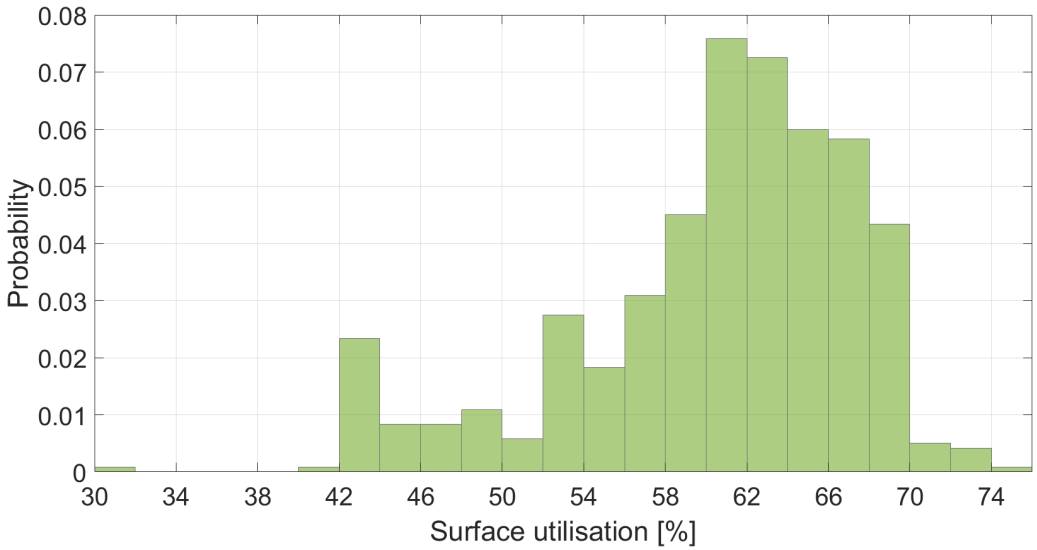

Figure 4.20: Surface utilisation distribution for container vessels

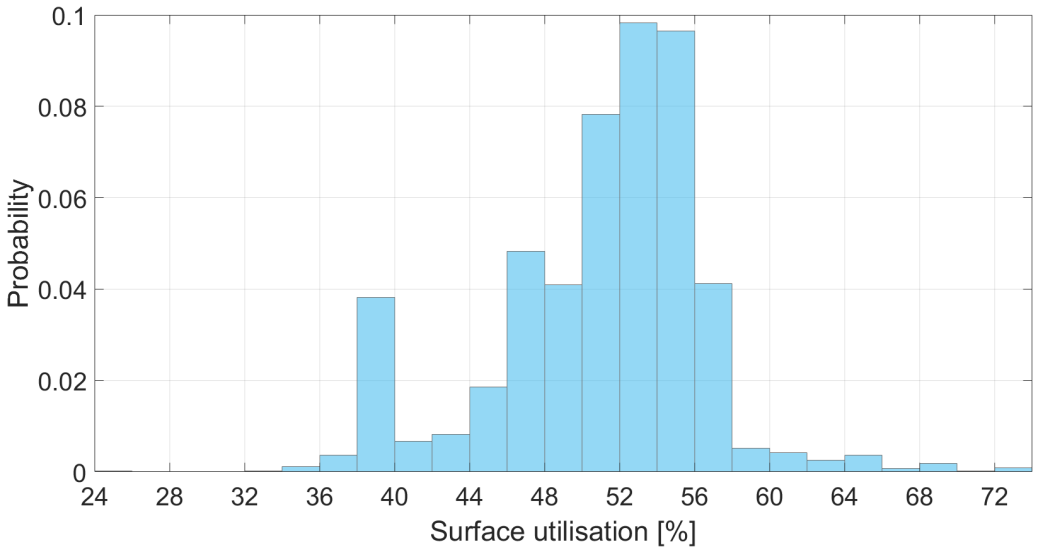

Figure 4.21: Surface utilisation distribution for bulk vessels

PV installed power

The PV panels that are simulated in the developed model are 360 Watt peak monocrystalline silicon PV panels, see appendix B for the datasheet. The total installed peak power on the general cargo fleet is 266.74 $[MWp]$, which comprises 740,958 installed PV panels. On an average general cargo vessel, 270 panels can be installed.

Figure 4.22 shows the box plots of the distribution of the PV installed peak power for the bulk and container vessels. When comparing the bulk vessels with the container vessels, the bulk vessel has very high outliers. this is caused by linkage when multiple vessels are connected to each other. These connected vessels are indicated as one vessel, therefore the PV installed power on the vessels is relatively large.

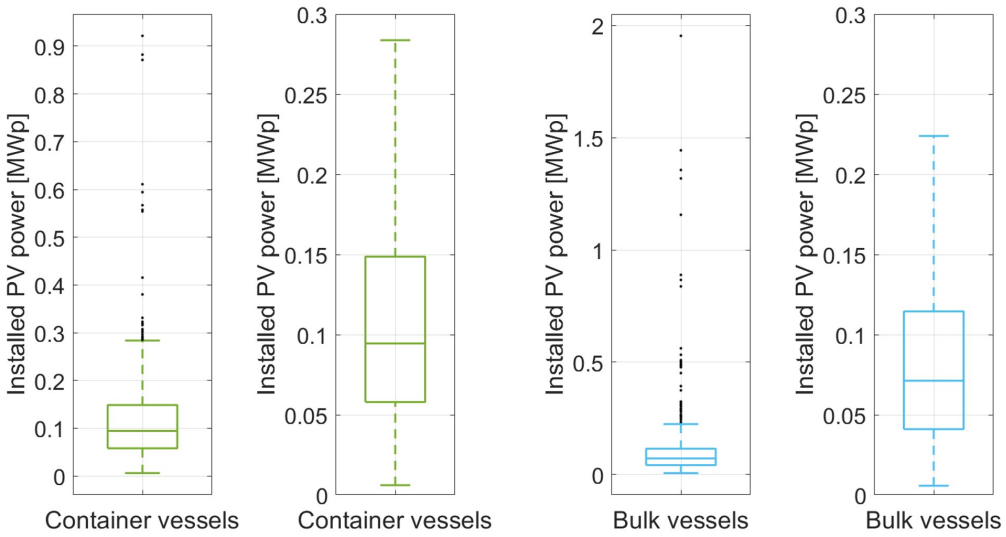

Figure 4.22: Installed PV power distribution

4.2.4 Photovoltaic energy yield

The simulated photovoltaic energy yield gives an estimation of the photovoltaic energy potential of the general cargo fleet.

Table 4.14: Annual photovoltaic energy yield

	Container vessels	**Bulk vessels**	**General cargo fleet**
PV annual energy per unit area mean [kWh/m^2]	170.73	168.43	168.93
PV annual energy total [GWh]	61.97	168.25	230.22
PV annual energy mean [MWh]	103.28	78.58	83.98
PV annual energy max [MWh]	826.78	1725.91	1725.91
PV annual energy min [MWh]	3.18	174.82	3.18

PV annual energy per unit area

The average energy generated over a year for a square meter is 168.93 for the general cargo fleet [kWh/m^2], see table 4.14. The energy per unit area for a container vessel is 170.73 [kWh/m^2] and for a bulk vessel 168.43 [kWh/m^2]. According to these values, placing a PV panel flat is more efficient than placing the PV panel under a tilted angle of 8 degrees to port and starboard side. The energy per unit area for the container and bulk vessels individually is displayed in appendix L.

Figure 4.23 shows the distribution of the monthly PV energy per unit area for the general cargo vessels. December and January have the lowest energy generation per unit area and May and June are the largest.

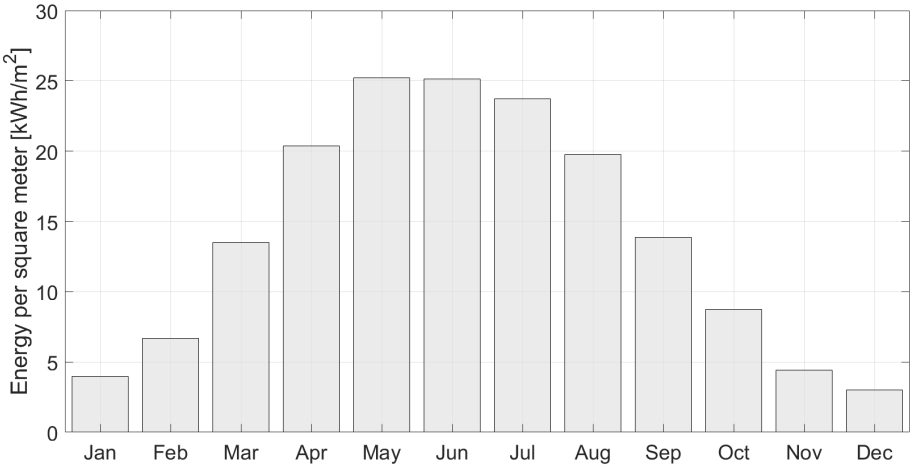

Figure 4.23: Monthly PV energy per unit area distribution

PV annual energy

Figure 4.24 shows the box plot of the distribution of the container and bulk vessel energy yield. The total annual energy generated when installing PV panels on general cargo vessels is 230.22 [GWh]. On average the annual energy yield of a container vessel is 103.28 [MWh] and 78.58 [MWh] for bulk vessels.

The minimum generated energy yield for container vessels is 3.18 [MWh] which is relatively small compared to the 174.82 [MWh] for the bulk vessel. This annual PV energy is related to a small surface area of a container vessel, 30 [m^2]. The vessel is 34 meters in length and 3 meters in width.

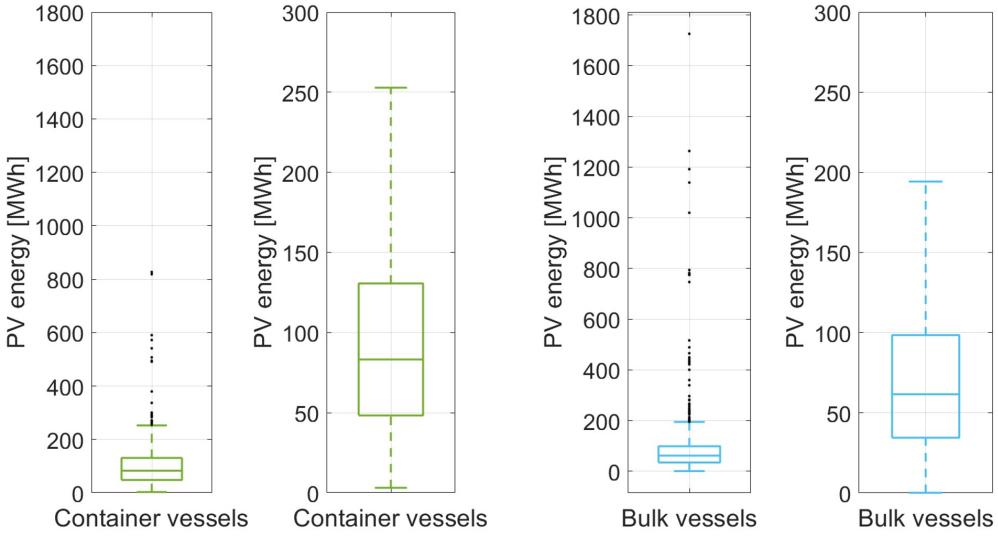

Figure 4.24: Annual PV energy distribution

4.2.5 Photovoltaic energy per installed power

The energy per installed power is a good parameter to estimate the photovoltaic energy potential.

Table 4.15: Energy per installed power parameters

	Container vessels	Bulk vessels	General cargo fleet
PV energy per installed power mean [Wh/Wp]	863.95	852.31	854.85
PV energy per installed power max [Wh/Wp]	949.79	939.80	949.79
PV energy per installed power min [Wh/Wp]	81.96	6.68	81.96

The average energy per installed power over a year is 854.85 [Wh/Wp], see table 4.15. Figure 4.25 shows the box plots of the distribution of the energy per installed power over a year for container and bulk vessels.

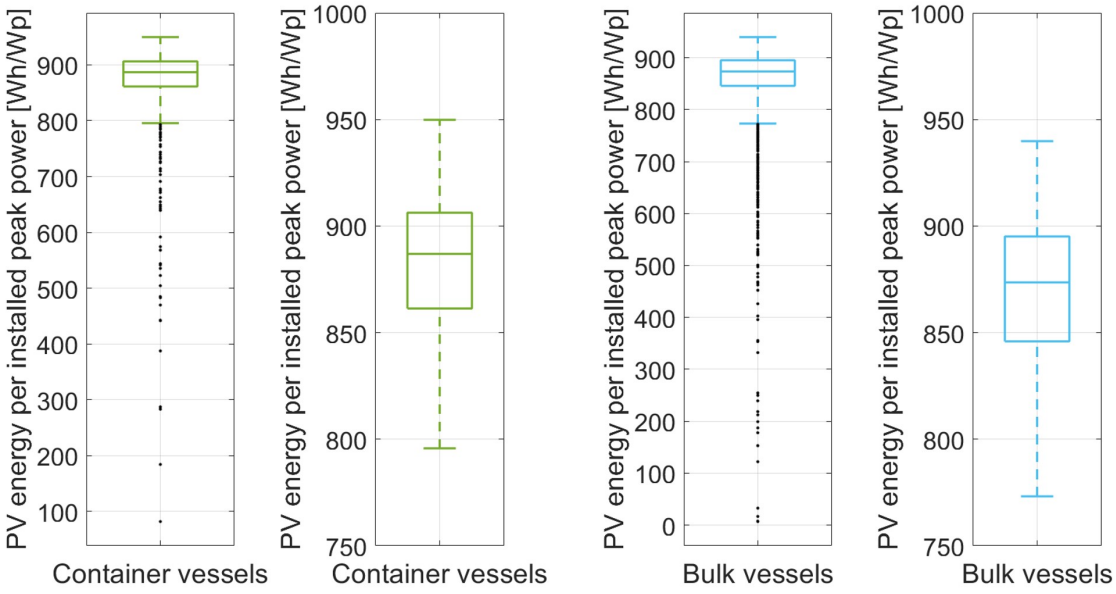

Figure 4.25: PV energy per installed power

Annual probability distribution

For further research, it is useful to know the probability distribution of the PV energy generation of the general cargo vessel. Finding a good probability distribution fit is done by studying 17 different possible continuous distributions. For every probability distribution, four statistic weighting factors are calculated and compared: NLogL (Negative of the log-likelihood), BIC (Bayesian information criterion), AIC (Akaike information criterion), AICc (Akaike information criterion for small sample size) (Yoav Aminov, 2021). These factors test the goodness of fit specific for probability distributions. Appendix Q en R shows the values of the weighting factors for the different fitted distributions.

The best fitting probability function for the annual PV energy per peak power is the t location-scale distribution. Figure 4.26 and 4.27 show the empirical distribution and the t location-scale probability distribution of the annual PV energy per installed power source. The location, scale and shape parameters corresponding

to the t location-scale probabilities are given in the legend of the figures. Equations 4.4 give the t location-scale continuous probability function, with the gamma function given in equation 4.5 for complex numbers with a positive real part (WolframMathWorld, 2021) (MathWorks, 2021).

$$f(x;\Gamma,\nu,\sigma,\mu) = \frac{\Gamma\left(\frac{\nu+1}{2}\right)}{\sigma\sqrt{\nu\pi}\Gamma\left(\frac{\nu}{2}\right)}\left[\frac{\nu+\left(\frac{x-\mu}{\sigma}\right)^2}{\nu}\right]^{-\left(\frac{\nu+1}{2}\right)} \tag{4.4}$$

$$\Gamma(z) = \int_0^\infty x^{z-1}e^{-x}dx \tag{4.5}$$

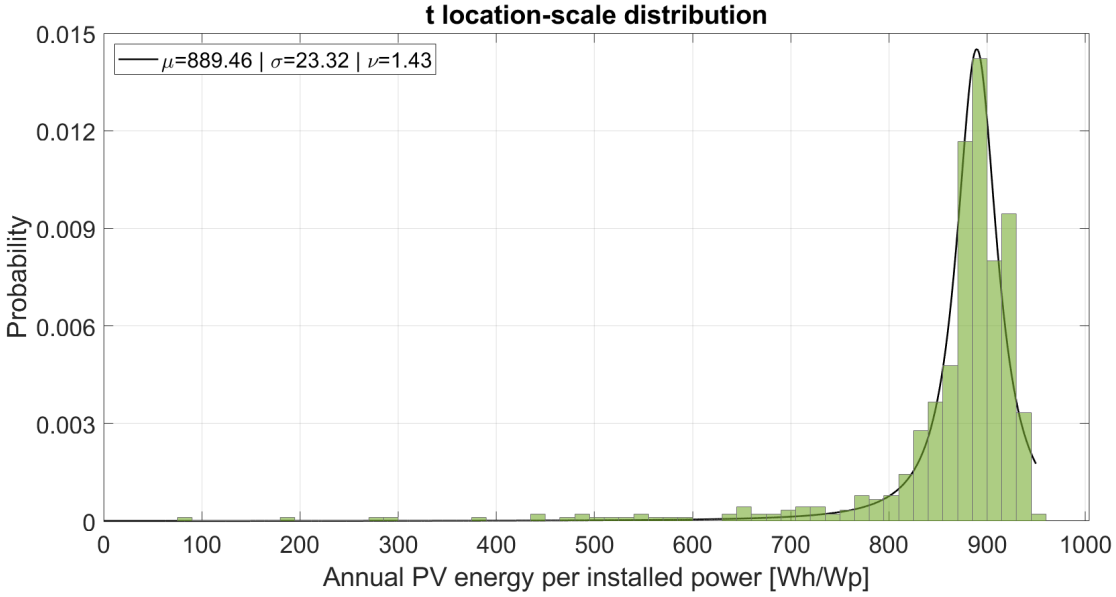

Figure 4.26: t location-scale distribution for the container vessels

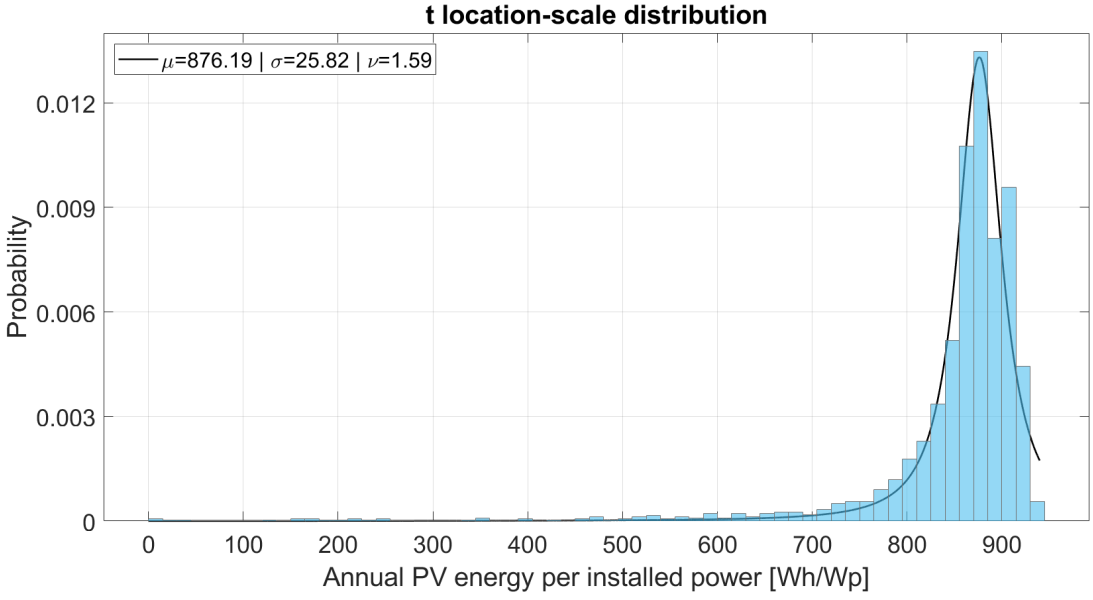

Figure 4.27: t location-scale distribution for bulk vessels

Figure 4.28 and 4.29 shows a number of relatively small outliers. The potential of some vessels is small as the vessel was not sailing during the year 2019 and its location was in an unfavorable place, with a large part of the horizon blocked. Findings from other research show that an energy per installed power below the 650 $[Wh/Wp]$ is not economically feasible (de Vries et al., 2020). Therefore the energy per installed power is analysed while leaving out the outliers below 650 $[Wh/Wp]$. These outliers contain 3.67 % of the dataset for container vessels and 3.40 % for bulk vessels. When removing the outliers out of the data set the best distribution fit changes to a Weibull distribution, according to the same 17 possible continuous distributions and the four statistic weighting factors. Figures 4.28 and 4.29 shows the Weibull distribution for both container and bulk vessels, with the corresponding scale and shape parameters depicted in the legend of the figures. Equations 4.6 give the continuous probability function when the scale and shape factor are bigger than zero.

$$f(x;\lambda,k) = \frac{k}{\lambda}\left(\frac{x}{\lambda}\right)^{k-1} e^{-(x/\lambda)^k} \tag{4.6}$$

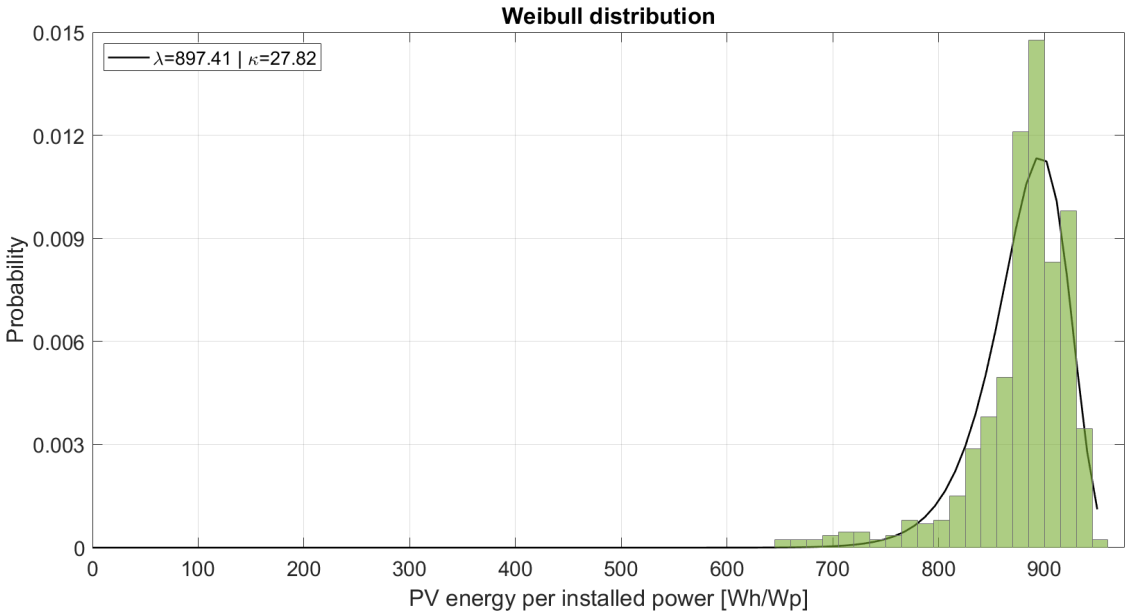

Figure 4.28: Weibull distribution for container vessels

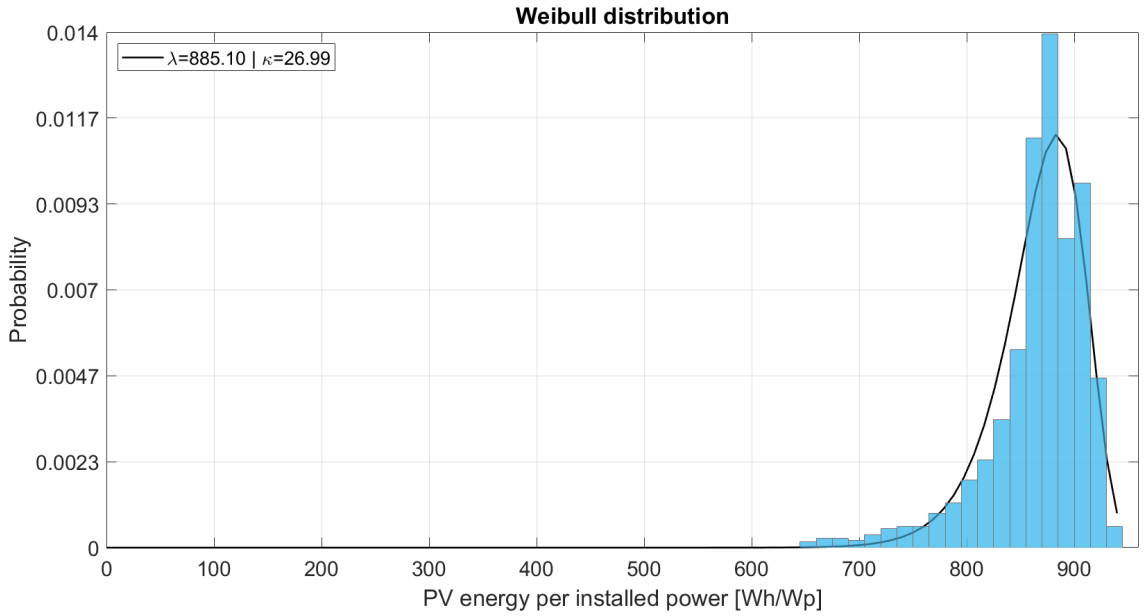

Figure 4.29: Weibull distribution for bulk vessels

Monthly and weekly probability distribution

Figure 4.30 and 4.31 shows the t location-scale distribution for data sets which contains winter and summer, months and weeks. Usually in statistics, the t location-scale distribution is used for smaller data sets with heavier tails, containing more outliers (MathWorks, 2021). Therefore the Weibull distribution becomes a better fit when the outliers are removed from the data set.

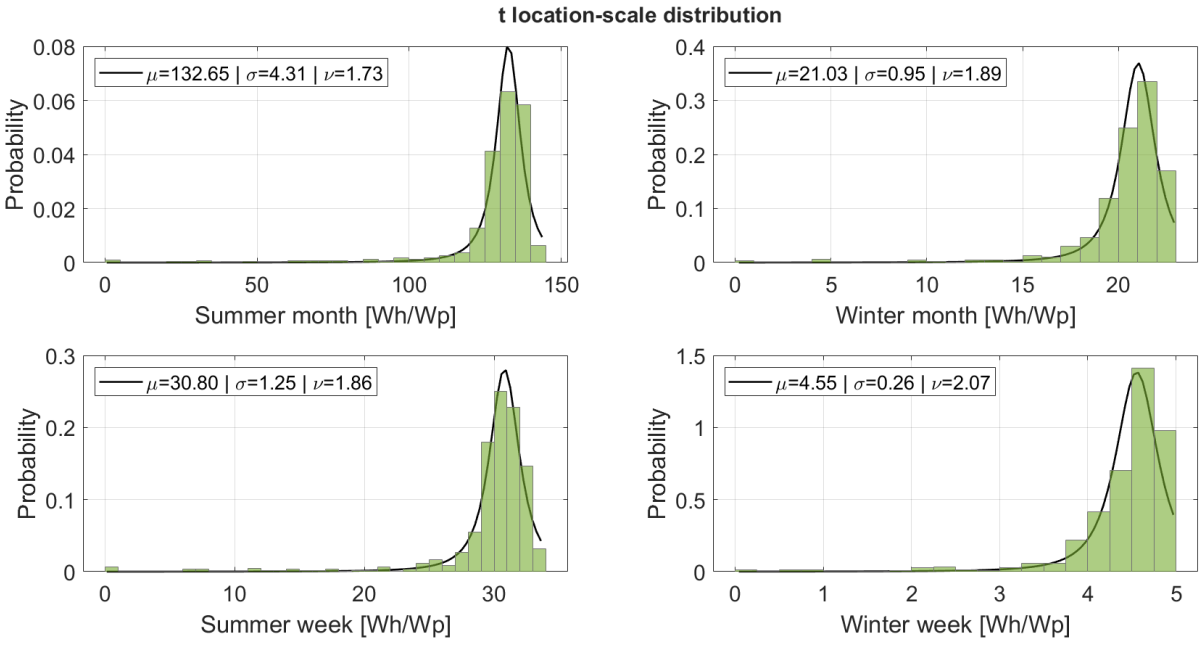

Figure 4.30: Summer and winter, months and weeks for container vessels

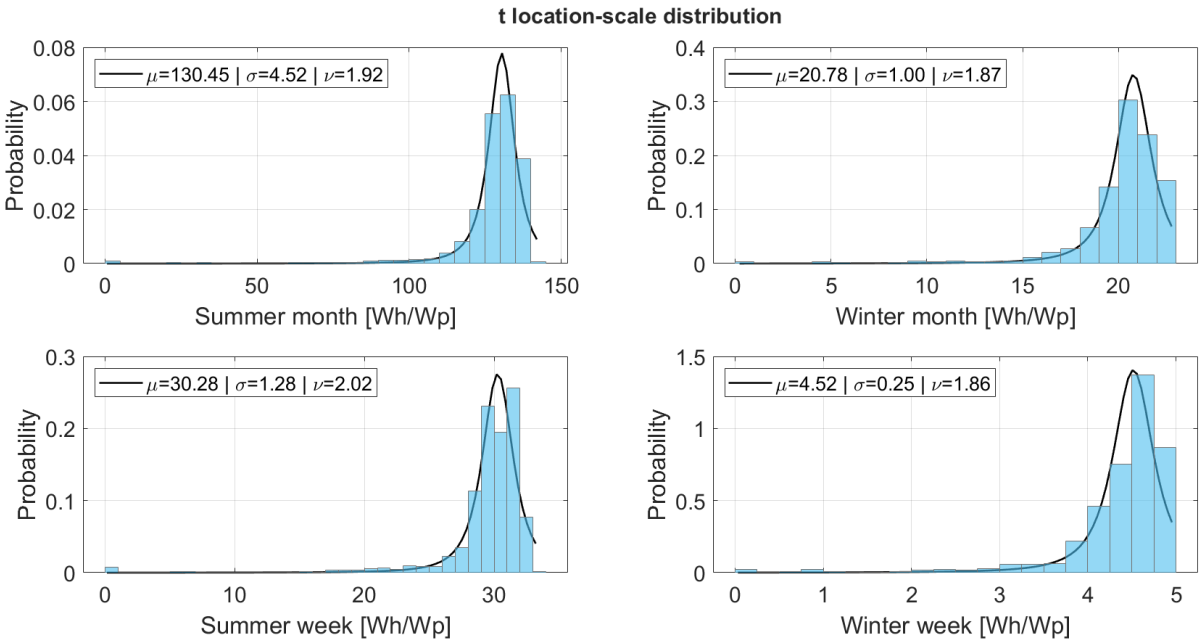

Figure 4.31: Summer and winter, months and weeks for bulk vessels

4.2.6 Energy demand

The energy demand of a general cargo vessel is depending on the length. The typical engine powers for every class of general cargo vessel are indicated in table 4.16 (Rijkswaterstaat, 2020). The annual energy demand of a 110 meter inland shipping vessel, according to the research of Panthei, is 2500 $[MWh]$ (van de Geest & Menist, 2019). This number is cross-validated in a conversation with an inland shipping vessel expert of the Technical University of Delft, Dr.ir. H.J. de Koning Gans.

Table 4.16: Energy demand of general cargo vessels

Vessel length [m]	<50	51-67	68-80	81-105	106-135	>135
Engine power[kW]	175	270	565	910	1562.50	2400
Vessels energy demand [MWh/year]	280	432	904	1456	2500	3840

The average energy demand of a general cargo vessel, for a specified length class, can be calculated by scaling the energy demand of 2500 $[MWh]$ with the engine powers of the different classes. Figure 4.32 and 4.33 shows the distribution of the number of vessels in every length class.

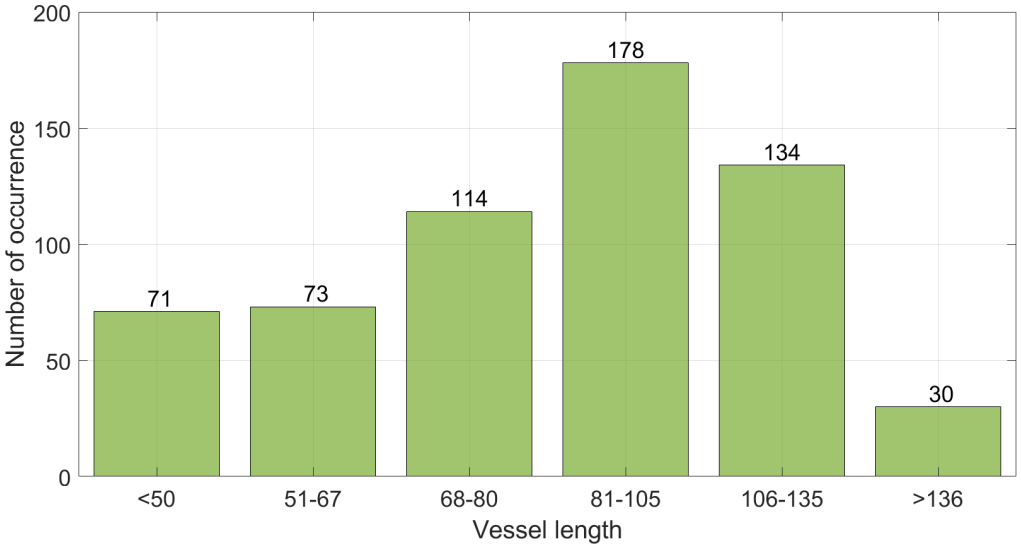

Figure 4.32: Distribution of the length of container vessels

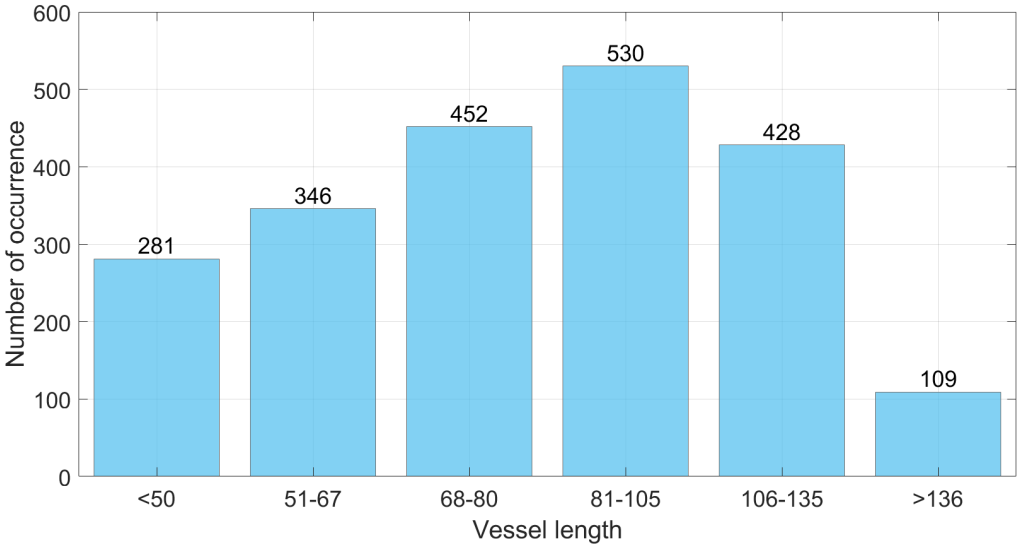

Figure 4.33: Distribution of the length of bulk vessels

This energy demand can then be compared with the PV energy that is generated by the PV panels installed on the vessels. For container vessels, the average annual energy demand is 1440 $[MWh]$ and the annual PV generation is 103 $[MWh]$, as indicated in section 4.2.4. The PV energy generated can supply 7.17% of the energy demand. The average energy demand of a bulk vessel is 1350 $[MWh]$ and the average energy generated by the PV panels is 79 $[MWh]$ which can supply 5.82% of the energy demand, see figure 4.34

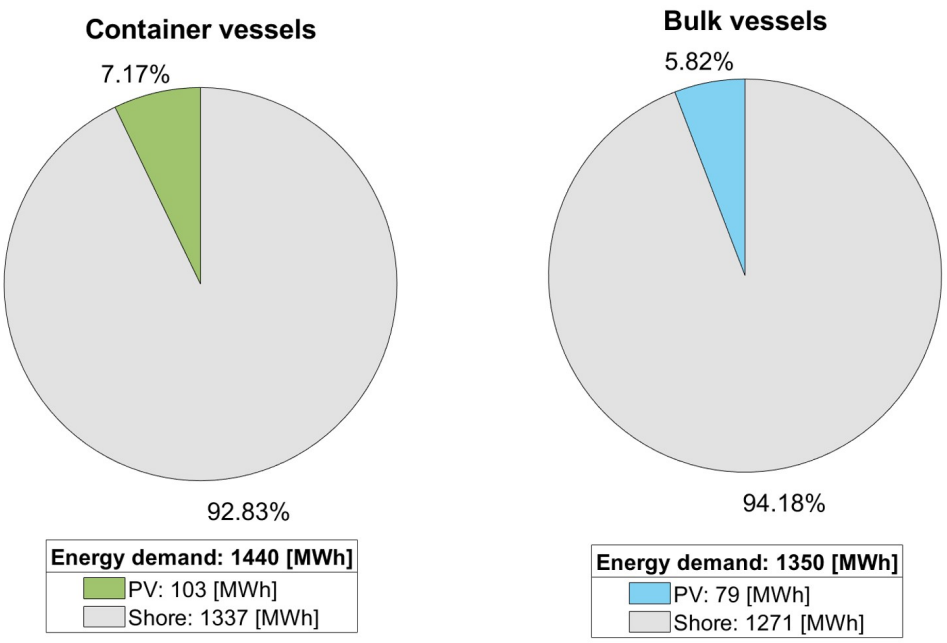

Figure 4.34: Energy demand

5 | Discussion

This chapter discusses the results and possible implications of the research. The chapter is organized in the four research topics discussed in section 1.2. At the end of this chapter, future applications of the research are discussed.

5.1 Feasibility of the concept

This research is carried out to estimate the photovoltaic potential of the general cargo inland fleet. The general cargo fleet consists of two types of vessels: container and bulk vessels. For the container vessels, it is assumed that PV panels can be installed on top of the container. After executing the experiment and field research it is noticed that there are container vessel sailing with unequal stacked containers, see figure 5.2. Some bulk vessels are also sailing without hatches or having the hatches stacked when sailing, see figure 5.1. These two findings may prevent some ships from implementing solar panels on the ship.

Figure 5.1: Hatches are stacked on top of each other

Figure 5.2: Containers are placed unevenly in the hold

To understand the feasibility of the concept, during this research a meeting with the company Wattlab is scheduled. Wattlab is implementing PV panels on the inland shipping vessel Ms Oleander, as discussed in section 2.2.3. During this meeting, Wattlab said that the company only uses foil to foil solar panels because the solar panels should not be too thick when the hatches are stacked.

5.2 Simulation model

Input variables have an important effect on the output of a simulation model. An important input variable is the waterway data points. These waterway points are implemented in the simulation model, to generate skyline profiles and simulate the routes of the vessels together with the AIS data. The vessels movements are continuous when sailing. The model simulates the movements and the surroundings of the vessel as a discrete parameter, to decrease the computational time of the simulation. The distance between the waterway points is 1000 meters. The points are placed in the middle of the waterways. The locations of the waterways and the discrete modelling of the movement of the vessel and hourly time step, will lead to estimation errors. The smaller the time steps and the more waterway data points are simulated, the more accurate the continuous motion of the vessel can be simulated. The experiment however indicates that the simulation model for this experiment is still accurate, as discussed in section 4.1.4.

The LIDAR height data set AHN3 data set is used to generate the skylines of the waterway points. This dataset contains height data over the years 2014 and 2019 (Rijkswaterstaat, 2021). In an urban area the skyline profiles can change between 2014 and 2021. The experiment is executed in the year 2021. The simulation of the photovoltaic power uses AHN3 but is still able to estimate Harmonie's energy potential accurately.

AIS data, for the months January, April, July and October, is used to simulate the locations of the general cargo vessels. For the other months, it is assumed that the vessel sails the same routes as in the mentioned months. As discussed in section 2.2.2, there are vessels that transport goods continuously on contract and ships that sail on the spot market. For the latter, sailing routes can be random and so the made assumption may not be entirely accurate. This can change the photovoltaic potential of these vessels, as the vessels locations of 8 out of the 12 months are based on assumptions. According to the AIS data the general cargo fleet consist out of 2746 vessels, but according to the data of IVR, discussed in section 2.2.1, there are 3988 vessels in this fleet. Resulting in a difference of 1242 vessels. The registered vessels from IVR may no longer be in service over the years or it is possible that ships are sailing without their AIS system on, but this is illegal. In the simulation model is simulated that when a vessel is crossing the border of the Netherlands, its location is assumed to be at the waterway points close to that border. In reality, this is not the case, but no height data of the aligning country is available and used in this model.

A general cargo vessel has its wheelhouse located at the back of the vessel. When the PV panels receive irradiance from the sun behind the vessel, it is possible that the wheelhouse is causing shading on the PV panels themselves. This shading effect is not taken into account in the simulation model and can lower the photovoltaic energy generated by the PV panels.

The skyline profiles of the PV panels installed on the vessel are corrected from the skyline profiles of the waterways. This height correction takes into account the load transported by the vessel. Assumed is that 50% of the time the vessel is transporting goods. This is similar to the sailing percentage of 51%, calculated in section 4.2.1. In this assumption, the weight of the PV panels is not taken into account when estimating the draft of the ship. The weight of the PV panels can be important if this weight will significantly effect the draft of the vessel. Appendix S indicates that for a container vessel on average the weight of the PV panels installed are 0.25% of the weight of the vessel itself, for bulk vessels this is 0.12%. These numbers are small and will therefore not significantly effect the draft and thus the skyline profiles of the vessels.

5.3 Model validation

The experiment is executed using the test vessel Harmonie. Harmonie is not a general cargo vessel, therefore it also behaves differently, which can cause experiment uncertainties. For inland shipping vessels, the vessel movements are negligible, as the roll and pitch motion of inland shipping vessels when sailing is below 1 [°], according to Dr. ir. H.J. de Koning Gans from the study Maritime Technology of the technical university of Delft. The motion range of the Harmonie is bigger than the motion of inland shipping vessels. The roll motion various ± 1.09 [°] and ± 3.0 [°] when the Harmonie is docked and sailing, respectively. The pitch motion when Harmonie is docked varies ± 2.71 [°] and when Harmonie is sailing ± 9.38 [°]. Therefore, the accuracy of the experiment can differ if a general cargo vessel is used to validate the model. The accuracy is not expected to differ proportionally, but how much it in reality is unknown as no model has been performed in which the PV energy can be scaled up on the basis of the motion of a PV panel. For further study, and in case this developed model is going to be adapted to recreational ships, the motion results of the experiment can be used.

During the experiment the airspeed around the PV panel is measured, this airspeed effects the module temperature. Figure 5.3 shows the measured air speed and the module temperature that is simulated according to this airspeed. Figure 5.4 shows the simulated air speed, calculated from the simulated corrected wind speed and the vessels speed, according to equations 3.21.

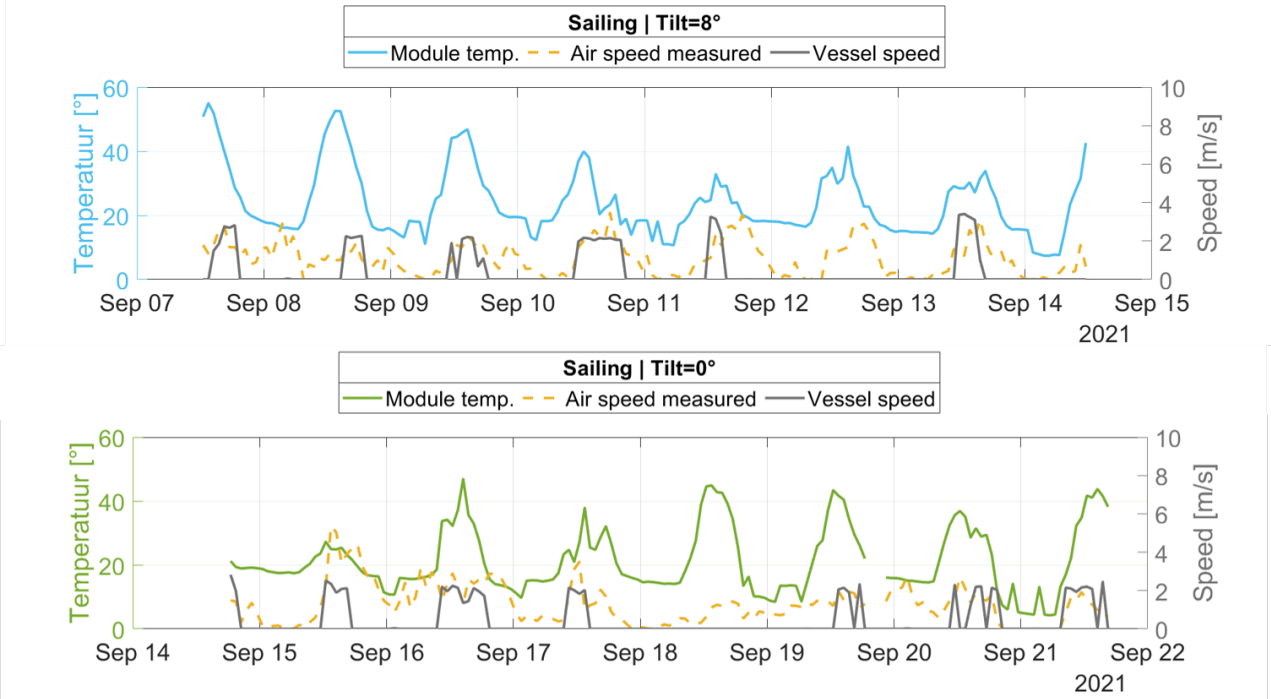

Figure 5.3: Measured air speed

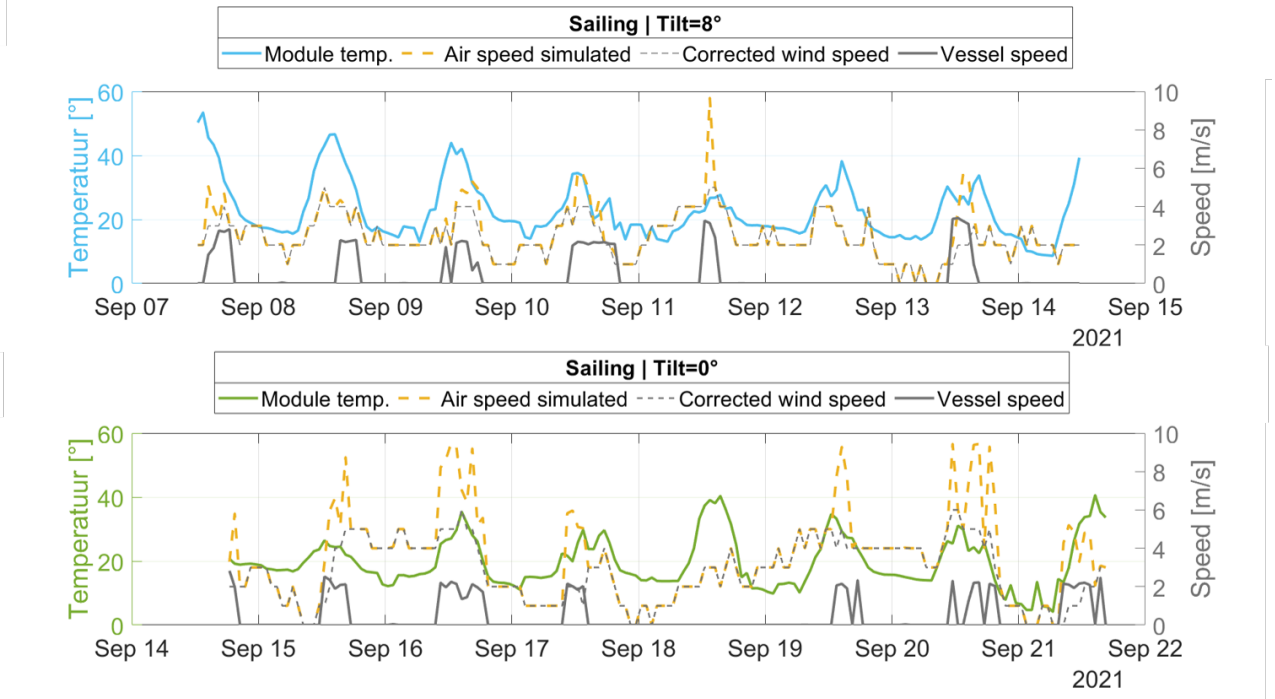

Figure 5.4: Simulated air speed

When comparing the graphs, it can be noticed that the airspeed measured is most of the time smaller than the airspeed simulated. The location of Harmonie's wheelhouse is at the front of the vessel, leading the airflow around the PV panel. This sheltered effect caused a lower measured airspeed than the simulated airspeed. This sheltered effect by the wheelhouse, during forward movement, of the vessel does not count for general cargo vessels, as the wheelhouse is placed in the back of the ship. However, the wheelhouse of general cargo vessel will block wind coming from behind. This wind blocking effect of the wheelhouse is not taken into account in simulating the module temperature of the general cargo vessels, therefore the simulated module temperature can be higher than it is in reality.

5.4 Photovoltaic potential

For a rooftop PV installation, the average PV's annual energy per installed power is 877 ± 137 $[Wh/W_p]$ in the Netherlands (van Sark et al., 2014). The average annual energy per installed power of a general cargo vessel is 854 $[Wh/W_p]$, which is somewhat lower than a rooftop installation. A possible cause is the raised and changing horizon of the general cargo vessels, as the PV panel height is lower than installed on a rooftop. On a roof, the PV panel tilt can be more favourable as well. The potential is lower even though the PV panel installed on the vessels depict additional cooling because of the movement of the vessel. The annual energy per installed power, when considering the outliers of the dataset, can be modelled as a t location-scale distribution. The t location-scale distribution is based on a normal distribution but can be distributed better for heavier tails. These distributions are mirrored on the mean of the distribution, the shapes of the left and right tails are the same. In this research the right tail of the t location-scale distribution has a limit at the maximum of the annual energy per installed power. Table 5.1 gives an overview of the right-side limits of the probability distribution for a year, month and week.

Table 5.1: t location-scale distribution maximum limits

	Container vessel	**Bulk vessel**
Year $[Wh/W_p]$	950	940
Summer month $[Wh/W_p]$	144	142
Winter month $[Wh/W_p]$	23	23
Summer week $[Wh/W_p]$	34	33
Winter week $[Wh/W_p]$	5	5

The annual energy potential of the general cargo fleet is 230 $[GWh]$. The energy demand of an average household in the Netherlands is 2.73 $[MWh]$ (Milieu centraal en CBS, 2021). The energy generated by the general cargo fleet can supply the energy demand of 84 thousand households. The biggest solar park of the Netherlands has an installed power of 103 $[MW_p]$, which is 2.6 times smaller than the solar capacity of the general cargo fleet (Goldbecksolar, 2019).

The average energy demand of a general cargo vessel that can be covered with PV energy is 6.12 %. From this point of view, energy potential is relatively small. Either way, this energy must be delivered to the ship. The energy can be delivered by a diesel generator or if this is not generated on the ship, this energy must come from further away: from solar parks, wind parks or from nonrenewable energy generators, which will still lead to transportation losses. However, it must be taken into account that the energy demand is calculated on the basis of the consumption of a

diesel engine. The efficiency of an electrical engine is higher and according to the research of Panthei, see section 1.1, inland vessels will switch to an electric engine for propulsion.

The company Wattlab claims that the PV panels placed on the vessel Ms Oleander, can generate annual 63.8 [MWh] and can cover around 10 % or 12 % of its energy demand (Solar magazine, 2021). The installed capacity of the PV panels or the PV surface corresponding to this energy potential is unknown. Comparison between the estimated energy potential and the energy potential of this developed model is therefore not entirely accurate. However, according to this research an average bulk vessel has an annual energy potential of 78.58 [MWh] and 5.85 % of the energy demand can be covered by PV panels. These are average values and depend strongly on the size of the PV surface area. The PV panels placed on the Ms Oleander, see figure 2.16, are placed less efficient than is simulated in this developed model. In this developed simulation model the PV panels are placed next to each other, without spacing, except for the mounting and corridor spacing.

5.5 Applications of the research

The goal of this research is to estimate the photovoltaic potential of the general cargo inland shipping fleet. This research can be used for further and other studies. From this research, the inland shipping industry can benefit when choosing the right size of batteries onboard of electrically propelled vessels, as this model is developed based on PV power calculations and not an average energy yield over time.

This developed model can be used to optimize the tilt angle of a PV system installed on a vessel. Different routes can be simulated for a vessel to optimize the energy yield of PV system.

The fitted t location-scale and Weibull distributions for the potential PV energy per installed power can be used to calculate the payback time of an installed PV energy system on board of a vessel and estimate the economical feasibility of the PV system installed.

The developed model can convenient adapted to a simulation model which estimated the photovoltaic potential of other types of vessels, such as recreational vessels.

6 | Conclusion

The world population is growing, therefore increasing the demand for energy and resources. Fossil fuels are becoming scarce and are polluting the environment. Both the implementation of renewable energy generation and more sustainable consumption behaviour is necessary. Renewable energy generation is volatile and causes problems to the electric energy network. Electrification is leading to an increase in electrical energy demand at the source of consumption. The generation of the decentralized photovoltaic energy systems on board of general cargo vessels can be one of the solutions for these challenges. To know the potential of the decentralized energy system, an accurate simulation model is needed.

The objective of this research is to **determine the photovoltaic potential of the Dutch general cargo inland shipping fleet.** The conclusion of this research and the answers to the research questions, which were formulated in section 1.2, are provided in this chapter.

6.1 Feasibility of the concept

The holds of the general cargo vessels are a suitable area to implement photovoltaic panels. Between general cargo inland vessels, two types of ships can be distinguished: container vessels and bulk vessels. For container vessels the PV panels can be placed on top of the containers. The containers have standard sizes and are made to be stacked on top of each other. Therefore, PV panels can be easily connected and systematically placed. Bulk vessels have hatches that cover the holds, PV panels can be installed on the hatches of these vessels.

On average, the photovoltaic surface to integrate photovoltaic panels is 599 [m^2] for a container vessel and for a bulk vessel is 461 [m^2]. The surface utilisation of a container vessel is 60 % and for a bulk vessels 51 %. The total potential surface area of the general cargo inland fleet that can be used to integrate photovoltaic systems is 1.36 [km^2].

6.2 Simulation model

In the simulation model, the hourly energy yield of a moving vessel is simulated. The developed simulation model is an irradiance model framework that estimates the energy yield on hour dependent power calculations. This simulation model consists of a skyline model, vessel model, irradiance model, PV module temperature model and a power and energy model.

The surroundings of a vessel have an impact on the photovoltaic energy yield and are simulated in the skyline model. The computational time needed for generating a skyline profile for every vessel for every time step is high, averaging 10 seconds per skyline. Hence, a method is developed to estimate the surroundings of the waterways in which the vessel is sailing. With LIDAR height data a skyline

profile for 3036 waterway points is generated. The path of the vessel is related to these waterways points. The waterway skylines are corrected for every vessel individually. This method lowers the simulation time significantly. On average the sky view factor of the general cargo vessels is 0.945. The minimum and maximum sky view factor of the photovoltaic system installed on a general cargo vessel are 0.005 and 0.995, respectively.

The sailing behaviour is an important factor when determining the photovoltaic potential of the general cargo fleet and is simulated in the vessel model. By the means of AIS data, the sailing behaviour of 2746 general cargo vessels is simulated. General cargo vessels sail uniformly through the Netherlands, but at the seaports the sailing traffic is heavier. The probability that a general cargo vessel is sailing, is highest between 08:30 and 16:30. The difference in sailing behaviour during the day and night is relatively small since a sufficient amount of vessels are also sailing during the night. On an average 24-hour day, a general cargo vessel is sailing 51 % of the time, the vessel is docked for the remainder of the time.

In the irradiance model, the diffused, direct and ground reflection irradiance received by the PV panel are simulated. The model uses the BRL decomposition model to decompose the DNI and DHI from the GHI. The diffused irradiance is calculated according to the Perez model. The PV module temperature affects the performance of the PV panel. The PV module temperature is estimated according to the fluid-dynamic model. The additional air caused by the forward movement of the vessel and the water temperature is taken into account. The photovoltaic energy yield is calculated by the received irradiance, the suitable PV surface and a corrected PV module efficiency.

6.3 Model validation

To validate the developed model an experiment is performed, where a PV panel is installed on the test vessel Harmonie. Harmonie is monitored by the installed equipment during one docking week and two sailing weeks. A co-variance linear regression model is used, to describe the relationship between the perceived PV power and the different predictors, simulated PV power, sailing or docking behaviour and the difference in PV panel tilt. According to the co-variance linear regression model, the simulated PV powers, for this experiment, is statistically significant and overestimates the PV power by 5% with a 95% confidence interval between 0.8684 and 1.0501. The effect of various PV panel tilt influences the relationship between the estimated and measured PV power by 8.56 $[W]$. The sailing and docking behaviour of the vessel does not significantly effect the relationship between the measured en estimated PV power. The roll motion of Harmonie various ± 1.09 [°] and ± 3.0 [°] when the vessel is docked and sailing, respectively. The pitch motion when Harmonie is docked varies ± 2.71 [°] and when Harmonie is sailing ± 9.38 [°].

6.4 Photovoltaic potential

By tracking the yearly motion of the general cargo fleet it is concluded that 740,958 PV panels can be installed on the vessels of the fleet. These panels together have an installed peak power of 267$[MW]$. The estimated annual photovoltaic energy potential of the general cargo fleet is 230 $[GWh]$.

The annual photovoltaic energy per unit area of a container vessel is 171 [kWh/m^2] and for a bulk vessel 168 [kWh/m^2]. The photovoltaic annual energy per installed power for a container vessel is 864 [Wh/W_p] and for a bulk vessel 852 [Wh/W_p]. The research enables to identify the probability distribution of the PV energy generation of a Dutch general cargo vessel. The probability distribution function which can describe the annual PV energy per peak power is the t location-scale and the Weibull distribution if the outliers are considered and removed, respectively. Table 6.1 shows the parameters of these two distributions for both container and bulk vessels.

Table 6.1: Distribution annual photovoltaic energy per installed power

Vessel type	**t location-scale**	**Weibull**
Container	μ=889.46, σ=23.32, ν=1.43	λ=897.41, κ=27.82
Bulk	μ=876.19, σ=25.82, ν=1.59	λ=885.10, κ=26.99

The annual energy demand of general cargo vessels is larger. The average annual energy demand of a container vessel is 1440 [MWh], 7.17 % of this demand can be supplied by the photovoltaic panels installed on the vessel. Bulk vessels demand 1350 [MWh] on average, the installed photovoltaic panels can cover 5.82 % of this energy demand.

7 Recommendations

This chapter recommends various adjustments for the developed simulation model. Future applications and implementations are recommended.

7.1 Feasibility of the concept

As mentioned in chapter 5 discussion, the hatches on the bulk vessel are sometimes needed to be stacked on top of each other, therefore the PV panels installed on the hatches need to be thick. It would be interesting to run the developed model also for thin film or foil to foil PV modules and compare the different photovoltaic energy potentials.

The energy demand that can be covered by photovoltaic energy, when installing PV panels on general cargo vessels, is relatively small as general cargo vessels have a very high energy demand. The high demand is caused by the heavyweight that a general cargo vessel has to propel. The weight of a recreational vessel is smaller in proportion to the surface of the ship. Therefore, it would perhaps be more feasible to implement PV panels on recreational vessels. The simulation model which is developed can be adapted for estimating the photovoltaic potential of a recreational vessel in the Netherlands. Recreational vessels sail through smaller canals, for these canals extra skylines need to be generated. As these vessels have a bigger roll and pitch motion, discussed in section 4.1.6, it is advised to take the movement into account.

The simulation model is developed to estimate a complete fleet of 2746 vessels, therefore a discrete-time step size of one hour is set. For further research and for the vessel industry it would be really interesting to adapt the developed model to a model which estimates the photovoltaic potential of one vessel. The simulation computational time of one vessel is smaller than the complete fleet. The simulation time of one container vessel 5 minutes and 10 minutes for a bulk vessel. When simulating one vessel it is possible to adapt the simulation model to a smaller time step size and make the developed model even more accurate.

7.2 Simulation model

The skylines in the simulation model are generated by the LIDAR AHN3 data. AHN4 was recently released. When this model is used in future studies, it will be accurate to use this dataset. The model has been developed in such a way that the new dataset can be used easily to generate new skylines.

In this simulation model, 4 months of AIS data is used to generate the routes of the general cargo vessel over one year. Only 4 months of AIS data is processed, as the size of this dataset is large. AIS data of a few, for example 20, general cargo vessels for one year, could be queried and simulated.

A comparison between the simulated year for 4 months of AIS data and the simulated year for 12 months of AIS data, will give information about the accuracy of the simulated routes.

The length of a general cargo vessel is relatively large, some vessels are 135 meters in length. In this simulation model, the PV panels installed on the vessel are simulated as single systems. In reality, this is not the case, the front PV panels can experience a different surrounding and temperature than the PV panels close to the wheelhouse. Simulating the PV system installed as individual PV panels will increase the accuracy of the simulation. This simulation model has calculated the DC yield of the PV system, in the future, the AC yield of the system can also be calculated.

In the module temperature model, the deck temperature is assumed to be the same as the water temperature. It is better to estimate the deck temperature for every hour and implement this value in the model.

The wind speed used in this model is assumed to be the same as the wind measured at the KNMI weather stations. These weather stations measure the wind at a height of 10 meters. The PV panels are placed on top of the vessels and therefore experience a lower wind speed, as the height is lower. This wind speed can be scaled down with equation 7.1 (Smets et al., 2016). Where w and w_r are the wind at module height and measured wind. y_m and y_r are the height of the module and the measured wind.

$$w = w_r(\frac{y_m}{y_r})^{\frac{1}{5}} \tag{7.1}$$

It is also advised to implement the effect of the wheelhouse on the received wind and light. Figure 7.1 shows that when the sunlight and wind direction is between - 90 and + 90 degrees on the heading of the vessel, the wind and light received by the PV panels needs to be adjusted. The module temperature in the developed model is probably simulated too low. The three adjustments mentioned above will estimate a more accurate module temperature.

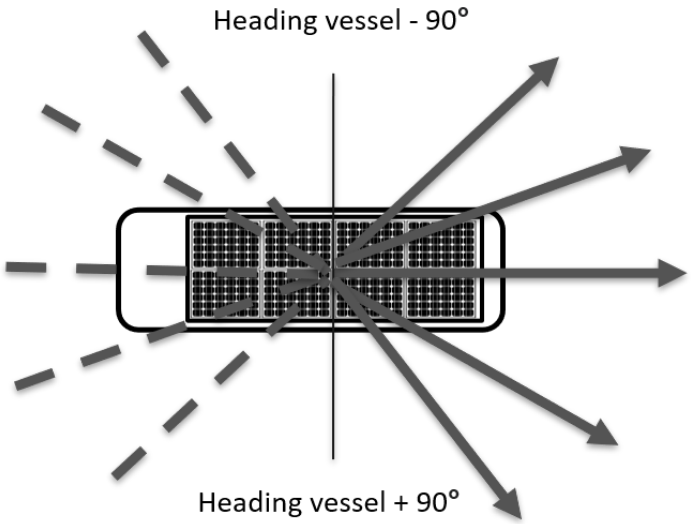

Figure 7.1: Effect of the wheelhouse

The mounting structure of the PV panels are simulated as a standoff system, whereby the PV panels are placed 2.5 centimetres from the containers and hatches. This is approximately the case for the mounting structure of the container vessels. But for the bulk vessels, the PV panels are placed more direct to the hatches. The PV panel placed on Harmonie are placed as a rack mount. Because of these differences, it is recommended to simulate the mounting structure for every vessel differently.

7.3 Model validation

The developed model is validated during a three-week lasting experiment. During the first week, the wind speed measurement set up was not yet installed. This experiment can be performed again, but with the wind speed sensor installed.

The experiment is executed with test vessel Harmonie. This vessel has a different movement than a general cargo vessel. To validate the model for general cargo vessels, it will be useful to correct the photovoltaic power with the roll and pitch motion of the vessels and the PV panel installed.

Bibliography

Amin, N., Shahahmadi, S. A., Chelvanathan, P., Rahman, K. S., Hossain, M. I., & Akhtaruzzaman, M. (2017). Solar photovoltaic technologies: From inception toward the most reliable energy resource. *Reference Module in Earth Systems and Environmental Sciences from Encyclopedia of Sustainable Technologies*, *153 pp.11-26*.

Balaji, N., Shanmugam, D. L. V., Basu, P. K., Khanna, A., Duttagupta, S., & G.Aberle, A. (2021). Pathways for efficiency improvements of industrial perc silicon solar cells. *Solar Energy*, *214 pp.101-109*.

Blommaert. (2021). *Friesche kap luiken.* Retrieved from https://www.blommaertalu.com/nl/home (Accessed: May 2021)

Blue 21. (2019). *Innozowa.* Retrieved from https://www.blue21.nl/portfolio/innozowa/ (Accessed: May 2021)

Boland, J., Huang, J., & Ridley, B. (2013). Decomposing global solar radiation into its direct and diffuse components. *Renewable and Sustainable Energy Reviews*, *28 pp.749-756*.

Bureau voorlichting binnenvaart. (2018). *Bureau voorlichting binnenvaart.* Retrieved from https://www.bureauvoorlichtingbinnenvaart.nl/ (Accessed: January 2021)

Calacabrini, A., adn Olindo Isabella, H. Z., & Zeman, M. (2019). A simplified skyline-based method for estimating the annual solar energy potential in urban environments. *Nature Energy*, *4 pp.206-215*.

CBS. (2019a). *Binnenvaart vervoerde minder droge bulkgoederen in 2019.* Retrieved from https://www.cbs.nl/nl-nl/nieuws/2020/13/binnenvaart-vervoerde-minder-droge-bulkgoederen-in-2019 (Accessed: Feb 2020)

CBS. (2019b). *Welke zeehavens zijn er in nederland?* Retrieved from https://www.cbs.nl/nl-nl/visualisaties/verkeer-en-vervoer/vervoermiddelen-en-infrastructuur/zeehavens (Accessed: Nov 2021)

CBS. (2020). *Sharp rise in green electricity production.* Retrieved from https://www.cbs.nl/en-gb/news/2020/10/sharp-rise-in-green-electricity-production (Accessed: May 2021)

CBS. (2021). *11 percent of energy consumption from renewable sources in 2020.* Retrieved from https://www.cbs.nl/en-gb/news/2021/22/11-percent-of-energy-consumption-from-renewable-sources-in-2020 (Accessed: Dec 2021)

CCR. (2019). *Europese binnenvaart marktobservatie jaarverslag 2019*. Netherlands: Centrale Commissie voor de Rijnvaart.

Cuelenaere, R., Verbeek, R., Harmsen, J., de Ruite, J., van Mensch, P., van Eijk, E., … Smoker, R. (2021). *Achtergrondnotitie over beprijzings- en normeringsmaatregelen voor reductie van de nox emissies in de mobiliteit*. Netherlands: TNO.

Delta TU Delft. (2020). *Start-up tests solar hatch for inland navigation.* Retrieved from https://www.delta.tudelft.nl/start-tests-solar-hatch-inland-navigation# (Accessed: Nov 2021)

de Vries, T. N., Bronkhorsta, J., Vermeera, M., C.B.Donkerb, J., Brielsc, S. A., Ziar, H., … Isabella, O. (2020). A quick-scan method to assess photovoltaic rooftop potential based on aerial imagery and lidar. *Solar Energy*, *209 pp. 96-107*.

Elgouacem, A., & Jourmeay-Kaler, P. (2020). *The netherlands's effort to phase out and rationalise its fossil-fuel subsidies*. Netherland: OECD/IEA.

Fence4Events. (2021). *Ozonnepanelen.* Retrieved from https://www.evenementenhekken.nl/zonnepanelen (Accessed: Nov 2021)

Glykas, A., Papaioannou, G., & Perissakis, S. (2010). Application and cost–benefit analysis of solar hybrid power installation on merchant marine vessels. *Ocean Engineering*, *37 p592–602*.

Goldbecksolar. (2019). *Het grootste zonnepark van nederland is nu operationeel in midden-groningen.* Retrieved from https://goldbecksolar.com/nl/solarpark-midden-groningen/ (Accessed: nov 2021)

Gopal, K., Groenemeijera, L., van Leeuwen, G., Omtzigt, D., & Faessen, W. (2020). *Primos 2020 rapportage*. Netherlands: abfrearch.

HAY, J. E. (1993). Calculating solar radiation for inclined surfaces: Practical approaches. *Renewable energy*, *3 pp. 373 380*.

Hoogheemraadschap. (2020). *Het juiste waterpeil kiezen?* Retrieved from https://www.hhdelfland.nl/ontdek-werk/juiste-waterpeil/juiste-waterpeil// (Accessed: April 2020)

International Maritime Organization. (2019). *Ais transponders.* Retrieved from https://www.imo.org/en/OurWork/Safety/Pages/AIS.aspx (Accessed: Nov 2021)

IVR. (2018). *Binnenvaartcijfers.* Retrieved from https://binnenvaartcijfers.nl/ (Accessed: May 2021)

IVR. (2020). *Scheepsdata nederlandse binnenvaart vloot*. Netherlands: Internationale Vereniging het Rijnschepenregister. (Excel dataset)

Keijzer, M. (2019). *A multi-surface reflected irradiance model for pyranometer corrections and pv yield calculations in complex urban geometries.*

Kim, S., Hoang, V. Q., & Bark, C. W. (2021). Silicon-based technologies for flexible photovoltaic (pv) devices: From basic mechanism to manufacturing technologies. *Nanomaterials*, *11 pp.2944*.

Klein, A., Hilster, D., Scholten, P., van Wijngaarden, L., Tol, E., & Otten, M. (2021). *Stream goederenvervoer 2020 emissies van modaliteiten in het goederenvervoer*. Netherlands: CEDelft.

KONGSBERG MARITIME. (2021). *Maritime surveillance.* Retrieved from https://www.kongsberg.com/maritime/ (Accessed: June 2021)

Lan, H., Wen, S., Hong, Y.-Y., Yu, D. C., & Zhang, L. (2015). Optimal sizing of hybrid pv/diesel/battery in ship power system. *Applied Energy*, *158 p26-34*.

Liu, B. Y., & Jordan, R. C. (1960). The interrelationship and characteristic distribution of direct, diffuse and total solar radiation. *Solar Energy*, *44 pp.1-19*.

Maritiem Nederland. (2021). *25 miljoen eu-subsidie voor green port project.* Retrieved from https://www.maritiemnederland.com/nieuws/25-miljoen-eu-subsidie-voor-green-port-project-rotterdam (Accessed: Nov 2021)

MathWorks. (2021). *t location-scale distribution.* Retrieved from https://nl.mathworks.com/help/stats/t-location-scale-distribution.html (Accessed: dec 2021)

Milieu centraal en CBS. (2021). *Energie en water.* Retrieved from https://www.nibud.nl/consumenten/energie-en-water/ (Accessed: dec 2021)

Nieuwsblad Transport. (2021). *436.000 euro subsidie voor walstroom in moerdijk.* Retrieved from https://www.nt.nl/havens/2021/08/27/436-000-euro

-subsidie-voor-walstroom-in-moerdijk/ (Accessed: Nov 2021)
Panteia. (2020). *Middellange termijn prognoses voor de binnenvaart vervoer in relatie tot nederland, periode 2020 - 2025*. Netherlands: Author.
Perez, R., Stewart, R., Seals, R., & Guertin, T. (1988). *The development and verification of the perez diffuse radiation model*. United States.
Port Liner. (2020). *Ships.* Retrieved from https://www.portliner.nl/ships (Accessed: March 2020)
PVPMC. (2018). *Plane pf array(poa) irradiance.* Retrieved from https://pvpmc.sandia.gov/modeling-steps/1-weather-design-inputs/plane-of-array-poa-irradiance/ (Accessed: nov 2021)
PVPS, I. (2021). Modeling daylight availability and irradiance components from direct and global irradiance. *Task 1 Strategic PV analysis and outreach report*, *IEA-PVPS T1-37*.
Rijkswaterstaat. (2020). *Dataset: Nationaal wegen bestand (nwb).* Retrieved from https://www.pdok.nl/geo-services/-/article/nationaal-wegen-bestand-nwb- (Accessed: Feb 2020)
Rijkswaterstaat. (2020). *Richtlijnen vaarwegen 2020*. Netherland: Author.
Rijkswaterstaat. (2021). *Dataset: Actueel hoogtebestand nederland (ahn3).* Retrieved from https://www.pdok.nl/introductie/-/article/actueel-hoogtebestand-nederland-ahn3- (Accessed: Nov 2021)
Scholz Solar. (2020). *Solar panels: The role of photovoltaics (pv).* Retrieved from https://scholzsolar.com.au/solar-panel-pv-tariffs-rebates/ (Accessed: May 2021)
Schuttevaer. (2020). *Noord-holland: 4 miljoen subsidie voor walstroom en elektrische binnenvaart.* Retrieved from https://www.schuttevaer.nl/nieuws/actueel/2020/11/23/noord-holland-4-miljoen-subsidie-voor-walstroom-en-elektrische-binnenvaart/ (Accessed: Nov 2021)
Sharma, D., Mehra, R., & Raj, B. (2021). Comparative analysis of photovoltaic technologies for high efficiency solar cell design. *Superlattices and Microstructures*, *153*.
Smets, A. H., Jager, K., Isabella, O., van Swaaij, R. A., & Zeman, M. (2016). *Solar energy*. England: UIT Cambridge.
Solar magazine. (2020). *Oleander eerste nederlandse binnenvaartschip met luik van zonnepanelen.* Retrieved from https://solarmagazine.nl/nieuws-zonne-energie/i23093/oleander-eerste-nederlandse-binnenvaartschip-met-luik-van-zonnepanelen (Accessed: March 2021)
Solar magazine. (2021). *Wattlab en blommaert: na zomer start verkoop luiken met zonnepanelen voor binnenvaartschepen.* Retrieved from https://solarmagazine.nl/nieuws-zonne-energie/i24792/wattlab-en-blommaert-na-zomer-start-verkoop-luiken-met-zonnepanelen-voor-binnenvaartschepen (Accessed: Nov 2021)
Steyn, D. (1980). The calculation of view factors from fisheye-lens photographs. *Research Note*, *18:3 pp. 254-258*.
Swinburne University of Technology. (2021). *Swinburne astronomy online.* Retrieved from https://astronomy.swin.edu.au/cosmos/a/Angular+Diameter (Accessed: Nov 2021)
Tegio, R. A. (2018). *The difference between standard and perc solar cells.* Retrieved from https://www.azom.com/article.aspx?ArticleID=16715 (Accessed: May 2021)
van de Geest, W., & Menist, M. (2019). *Opweg naar een klimaatneutral binnenvaart per 2050 transitie- en rekenmodel binnenvaart*. Netherlands: Panteia.

van Norel, R. (2018). *Eindrapport green deal cobald*. Netherlands: Rijksdienst voor Ondernemend Nederland.

van Sark, W. G., Bosselaar, L., Gerrissen, P., Esmeijer, K., Moraitis, P., van den Donker, M., & Emsbroek, G. (2014). Update of the dutch pv specific yield for determination of pv contribution to renewable energy production: 25% more energy! *European Photovoltaic Solar Energy Conference and Exhibition*, *29th*.

WolframMathWorld. (2021). *Gamma function.* Retrieved from https://mathworld.wolfram.com/GammaFunction.html (Accessed: Dec 2021)

Yoav Aminov. (2021). *Fbd - "find the best distribution" tool.* Retrieved from https://www.mathworks.com/matlabcentral/fileexchange/36000-fbd-find-the-best-distribution-tool (Accessed: nov 2021)

ZES. (2021). *First emission-free inland shipping vessel on energy containers in service.* Retrieved from https://zeroemissionservices.nl/en/zero-emission-services-commences-operation/ (Accessed: Nov 2021)

Ziar, H., Prudon, B., Lin, F.-Y. V., Roeffen, B., Heijkoop, D., Stark, T., … Isabella, O. (2020). Innovative floating bifacial photovoltaic solutions for inland water areas. *Prog Photovolt*.

A | Transportation emissions

Table A.1: Emissions per type of carrier for the transportation of bulk cargo (Klein et al., 2021)

Modaliteit	Voer-/vaartuig	Type goederen	CO_2 (g/tkm) (WTW)	PM_v (g/tkm) (TTW)*	NO_x (g/tkm) TTW)*
Weg	Bestelauto LG 2.000-2.500 kg	Licht	1.326	0,078	4,35
	Vrachtauto middelzwaar	Middelzwaar	256	0,015	1,40
	Trekker-oplegger licht	Middelzwaar	178	0,002	0,53
	Trekker-oplegger zwaar	Middelzwaar	88	0,002	0,22
Spoor	Middellange trein (elektrisch 73%: diesel 27%)	Zwaar	12	0,001	0,05
Binnenvaart	R.H.K. (Rijn-Herne-Kanaal)	Zwaar	38	0,014	0,40
	Groot Rijnschip	Zwaar	24	0,010	0,26
Zeevaart	Kustvaart: General Cargo 10-20 dwkt	Zwaar	22	0,009	0,40
	Deep sea: Bulkcarrier 35-60 dwkt	Zwaar	6,6	0,003	0,13
Luchtvaart	Lange afstand (full-freight)	Licht	544	0,015	1,98

* De emissiekentallen van luchtvervuilende stoffen geven geen indicatie voor de schadelijkheid van de verschillende modaliteiten. De schadelijkheid hangt samen met de locatie van uitstoot.

Table A.2: Emissions per type of carrier for the transportation of containers (Klein et al., 2021)

Modaliteit	Voer-/vaartuig	Type goederen	CO_2 (g/tkm) (WTW)	PM_v (g/tkm) (TTW)*	NO_x (g/tkm) (TTW)*
Weg	Trekker-oplegger zwaar (2 TEU)	Middelzwaar	121	0,003	0,30
Spoor	Lange trein (elektrisch 73%: diesel 27%)	Middelzwaar	18	0,0018	0,08
Binnenvaart	R.H.K. (Rijn-Herne-Kanaal) (96 TEU)	Middelzwaar	52	0,019	0,55
	Groot Rijnschip (208 TEU)	Middelzwaar	32	0,013	0,34
Zeevaart	Kustvaart: Containerschip 1.000-1.999 TEU	Middelzwaar	32	0,013	0,57
	Deep sea: Containership 8.000-11.999 TEU	Middelzwaar	12	0,005	0,23

* De emissiekentallen van luchtvervuilende stoffen geven geen indicatie voor de schadelijkheid van de verschillende modaliteiten. De schadelijkheid hangt samen met de locatie van uitstoot.

B | Data sheet PV module

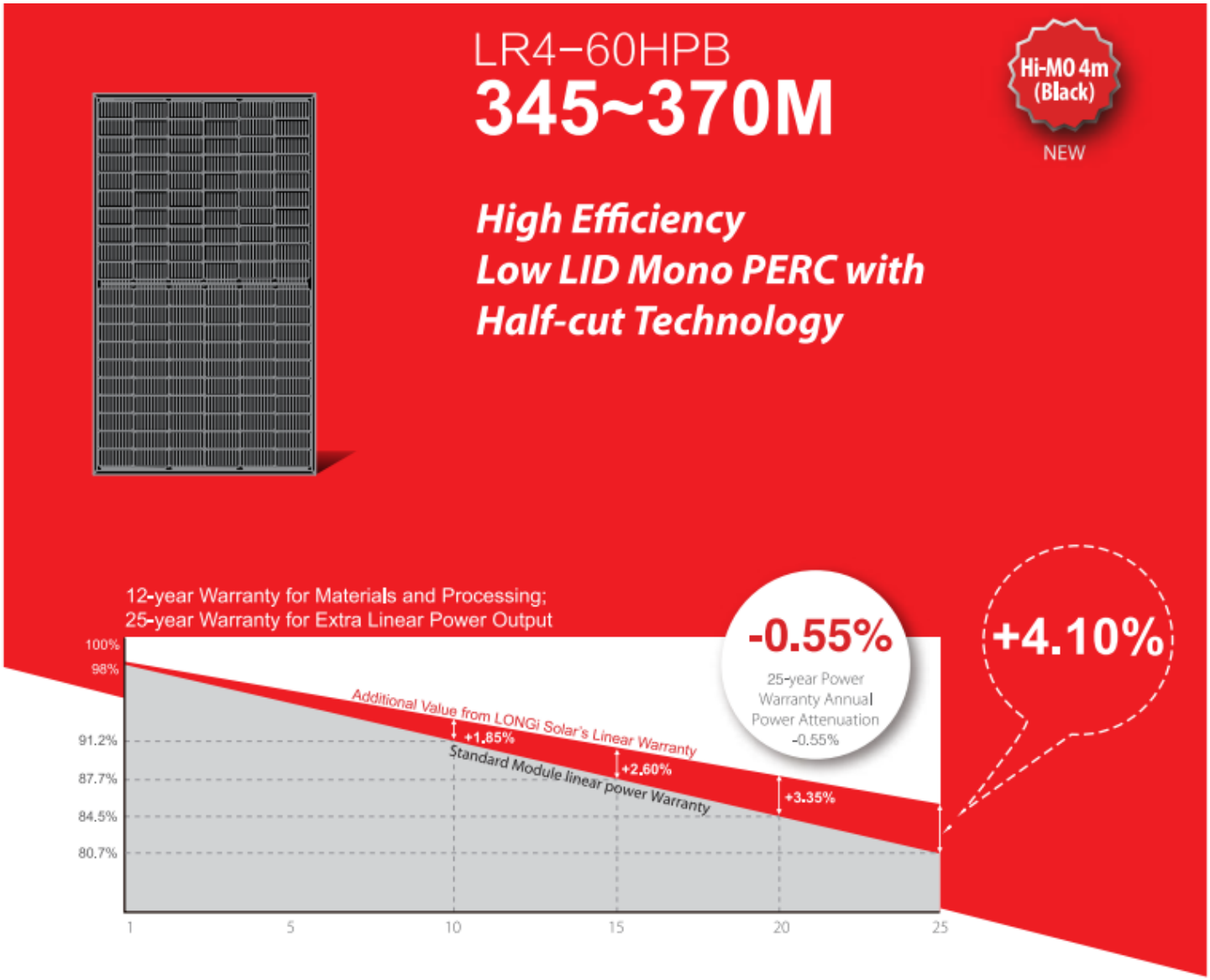

Complete System and Product Certifications

IEC 61215, IEC 61730, UL 61730

ISO 9001:2008: ISO Quality Management System

ISO 14001: 2004: ISO Environment Management System

TS62941: Guideline for module design qualification and type approval

Positive power tolerance (0 ~ +5W) guaranteed

High module conversion efficiency (up to 20.3%)

Slower power degradation enabled by Low LID Mono PERC technology: first year <2%, 0.55% year 2-25

LR4-60HPB **345~370M**

Design (mm)

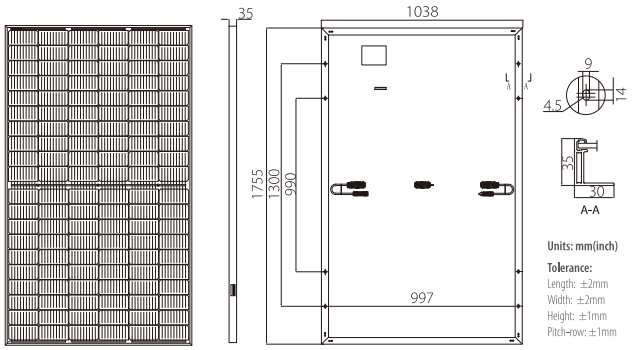

Mechanical Parameters

Cell Orientation: 120（6×20）
Junction Box: IP68, three diodes
Output Cable: 4mm², 1200mm in length
(for EU DG)
Connector: MC-MC4
Glass: Single glass
3.2mm coated tempered glass
Frame: Anodized aluminum alloy frame
Weight: 19.5kg
Dimension: 1755×1038×35mm
Packaging: 30pcs per pallet
180pcs per 20'GP
780pcs per 40'HC

Operating Parameters

Operational Temperature: -40℃~+85℃
Power Output Tolerance: 0~+5 W
Voc and Isc Tolerance: ±3%
Maximum System Voltage: DC1000V (IEC/UL)
Maximum Series Fuse Rating: 20A
Nominal Operating Cell Temperature: 45±2℃
Safety Class: Class Ⅱ
Fire Rating: UL type 1 or 2

Electrical Characteristics

Test uncertainty for Pmax: ±3%

Model Number	LR4-60HPB-345M		LR4-60HPB-350M		LR4-60HPB-355M		LR4-60HPB-360M		LR4-60HPB-365M		LR4-60HPB-370M	
Testing Condition	STC	NOCT	STC	NOCT	STC	NOCT	STC	NOCT	STC	NOCT	STC	NOCT
Maximum Power (Pmax/W)	345	257.6	350	261.4	355	265.1	360	268.8	365	272.6	370	276.3
Open Circuit Voltage (Voc/V)	40.2	37.7	40.4	37.9	40.6	38.1	40.8	38.2	41.0	38.4	41.2	38.6
Short Circuit Current (Isc/A)	11.06	8.95	11.16	9.02	11.25	9.09	11.33	9.16	11.41	9.23	11.50	9.30
Voltage at Maximum Power (Vmp/V)	34.2	31.8	34.4	32.0	34.6	32.2	34.8	32.4	35.0	32.6	35.2	32.8
Current at Maximum Power (Imp/A)	10.09	8.09	10.18	8.16	10.27	8.23	10.35	8.30	10.43	8.36	10.52	8.43
Module Efficiency(%)	18.9		19.2		19.5		19.8		20.0		20.3	

STC (Standard Testing Conditions): Irradiance 1000W/m², Cell Temperature 25℃, Spectra at AM1.5

NOCT (Nominal Operating Cell Temperature): Irradiance 800W/m², Ambient Temperature 20℃, Spectra at AM1.5, Wind at 1m/S

Temperature Ratings (STC)

Temperature Coefficient of Isc	+0.048%/℃
Temperature Coefficient of Voc	-0.270%/℃
Temperature Coefficient of Pmax	-0.350%/℃

Mechanical Loading

Front Side Maximum Static Loading	5400Pa
Rear Side Maximum Static Loading	2400Pa
Hailstone Test	25mm Hailstone at the speed of 23m/s

I-V Curve

Current-Voltage Curve (LR4-60HPB-360M)

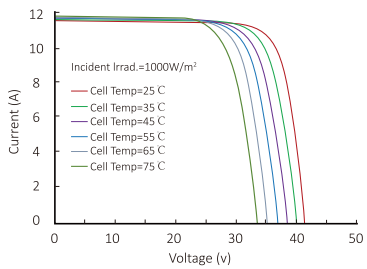

Power-Voltage Curve (LR4-60HPB-360M)

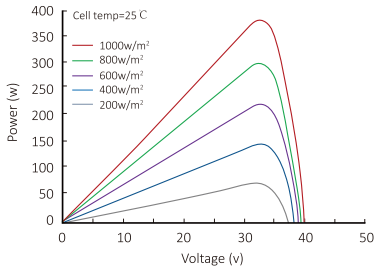

Current-Voltage Curve (LR4-60HPB-360M)

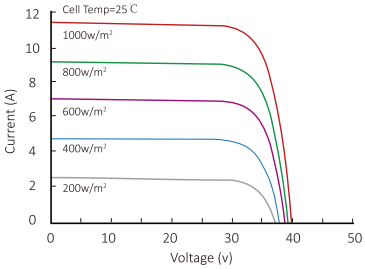

LONGi

Room 801, Tower 3, Lujiazui Financial Plaza, No.826 Century Avenue, Pudong Shanghai, 200120, China
Tel: +86-21-80162606 E-mail: module@longi-silicon.com Facebook: www.facebook.com/LONGi Solar

20200414V11 for EU DG only

C | AIS python script

Dora de Jong | AIS data | NL | 4 months

A.Importing package

In [12]:

```
# needed to read your environment variable
import os
# For opening local files
import pathlib

#geometry
import shapely.geometry
import numpy as np
import pyproj

# Test connection
# Make sure you have pip  install  azure-storage-blob==2.1.0 installed
# Do not install 12.1. this is not compatible yet with adlfs
# See https://github.com/dask/adlfs/issues/15
import azure.storage.blob

# this module loads dataframes in parallel
# requires pip install dask[complete] and fastparquet  and python-snappy
import dask.dataframe as dd
import pandas as pd
#import geopandas
#import movingpandas as mpd
import datetime

# this is  for plotting
import matplotlib.pyplot as plt
%matplotlib inline

# this is for environmental variables for secrets (needs python-dotenv)
# You can copy the  .env.example file and rename it to .env (one directory  up from the notebooks)
#
%load_ext dotenv
# Load environment variables from the .env file 1 directory up
%dotenv -v

# This should print 2.1.0
from distributed import Client
client = Client()
azure.storage.blob.__version__
client

# extra toe gevoeg door Dora
import openaistools
import scipy
```

B. Read sas token & Specify folder and file names

In [16]:
```
# read the environment variable from the  .env file
sas_token = os.environ['AZURE_BLOB_SAS_TOKEN']
sas_token

# Specify the foldername and the filename(s) using * if necessary
foldername = '201901040710_nederland'
#filenames1 = 'x00000_2019_output.parquet'  # 1 file
filenames1 = 'x0*_2019_output.parquet'     # Files: 0     -10.000
filenames2 = 'x1*_2019_output.parquet'     # Files: 10.000-20.000
filenames3 = 'x2*_2019_output.parquet'     # Files: 20.000-21.772

# This is the 2.1 version.  if the  BlockBlobService is missing, you probably installed a later version
service = azure.storage.blob.BlockBlobService(sas_token=sas_token, account_name='rwsais')
# As a test, show the  first blob
blob = next(iter(service.list_blobs('ais',  prefix='parquet/' + foldername)))
# this is one of subfiles that rijkswaterstaat provided
blob.name
```

C. Load data (ddf) & Convert to pandas dataframe (df) with the actual time

In [ ]:
```
# This loads some of the  data into memory (10  files)
pathname = 'abfs://ais/parquet/' + foldername + '/' + filenames1
pathname

ddf = dd.read_parquet(pathname, storage_options={"account_name": "rwsais", "sas_token": sas_token})
ddf

# Convert to pandas dataframe
df = ddf.compute()

# Generate a new index
df.reset_index(inplace=True)
df.rename(columns={"index": "oldindex"}, inplace=True)
df.rename(columns={"name": "shipname"}, inplace=True)

# Change the formats of timestamplast to actual date and time
df['newtimestamp'] = pd.to_datetime(df['timestamplast'], format="%Y-%m-%dT%H:%M:%S", utc=True, errors='coerce')
mask = df.newtimestamp.isnull()
df.loc[mask,'newtimestamp'] = pd.to_datetime(df[mask]['timestamplast'],unit='s', utc=True, errors='coerce')
df.head()
```

D. Processing the data

Remove duplicates

In [4]:
```
df.drop_duplicates(subset=['shipname', 'latitude', 'longitude'], keep='first', inplace=True)
```

Colum names

In [5]:
```
df= df[['shipname','vesseltypeERI' ,'newtimestamp' ,'longitude', 'latitude', 'width', 'length','heading','sog','imo']]
```

Remove small & big vessels

In [6]:
```
df = df[df.length>30]
df = df[df.length<200]
```

Select vessetypes

In [7]:
```
df = df[(df["vesseltypeERI"] == 8010) | (df["vesseltypeERI"] == 8030)  | (df["vesseltypeERI"] == 8070)  | (df["vesseltypeERI"] == 8090)  | (df["vesselt
```

Sort vessels by vesseltype, shipname and sort then by time

In [8]:
```
df=df.sort_values(by=['vesseltypeERI','shipname','newtimestamp'])
df.head()
```

Select timestap: one data set for every hour

In [9]:
```
#df['date'] = df['newtimestamp'].dt.strftime('%Y-%m-%d %H')
#df.drop_duplicates(subset=['imo','date'], keep='first', inplace=True)
#df= df[['date','shipname','vesseltypeERI' ,'Longitude', 'Latitude', 'width', 'Length','heading','sog']]



df['year'] = df['newtimestamp'].dt.strftime('%Y')
df['month'] = df['newtimestamp'].dt.strftime('%m')
df['day'] = df['newtimestamp'].dt.strftime('%d')
df['hour'] = df['newtimestamp'].dt.strftime('%H')

df.drop_duplicates(subset=['imo','year','month','day','hour'], keep='first', inplace=True)
df= df[['year','month','day','hour','shipname','vesseltypeERI' ,'longitude', 'latitude', 'width', 'length','heading','sog']]
```

D Characteristics of inland vessels

Table D.1: Characteristics of benchmark inland shipping vessels (Rijkswaterstaat, 2020)

CEMT-klasse	breedte (m)	lengte (m)	diepgang (m)		strijkhoogte (m)	laadverm. (ton)	motorverm. (kW)	boegschroef (kW)
			geladen	leeg				
I	5,05	38,5	2,5	1,2	4,25	365	175	100
II	6,6	50 - 55	2,6	1,4	5,25	535 - 615	240 - 300	130
III	8,2	67 - 85	2,7	1,5	5,35	910 - 1250	490 - 640	160 - 210
IV	9,5	80 - 105	3,0	1,6	5,55	1370 - 2040	750 - 1070	250
Va	11,4	110 - 135	3,5	1,8	6,40	2900 - 3735	1375 - 1750	435 - 705
VIa	17,0	135	4,0	2,0	8,75	6000	2400	1135

E | Perez circumsolar and horizon brightening coefficients

The complex empirical functions, as discussed in section 3.19, are calculated by the equations E.1 to E.6 (Perez et al., 1988). Table E.1 overviews the Perez coefficients that are used in the diffused irradiance model.

$$F_1 = \max\left[0, \left(f_{11} + f_{12}\Delta + \frac{\pi\theta_z}{180\check{r}} f_{13}\right)\right] \tag{E.1}$$

$$F_2 = f_{21} + f_{22}\Delta + \frac{\pi\theta_z}{180\check{r}} f_{23}\varepsilon = \frac{(DHI + DNI)/DHI + \kappa\theta_Z^3}{1 + \kappa\theta_Z^3} \tag{E.2}$$

$$\Delta = \frac{DHI \times AM_a}{E_a} \tag{E.3}$$

$$E_a = E_{\mathrm{sc}} \times \left(\frac{R_{av}}{R}\right)^2 \tag{E.4}$$

$$\left(\frac{R_{av}}{R}\right)^2 = (100011 + 3422.1\cos(b) + 128\sin(b) + 71.9\cos(2b) + 7.7\sin(2b))10^{-}5 \tag{E.5}$$

$$b = 2\pi\frac{DOY}{365} radians \tag{E.6}$$

With:
θ_z is the solar zenith angle
E_a is the extraterrestrial, the sun intensity at the top of the atmosphere
E_{sc} is a solar constant 1367 $[W/m^2]$
κ is a constant, 1.041
AM_a is the absolute air mass
ε is related to the the cloud cover[okta] bins in table E.1
DOY is the day of the year
R_{av} is the averaged distance to the sun from the earth
R is the distance to the sun from the earth at a specified time

Table E.1: Perez model coefficients

bin	f11	f12	f13	f21	f22	f23
1	-0.008	0.588	-0.062	-0.06	0.072	-0.022
2	0.13	0.683	-0.151	-0.019	0.066	-0.029
3	0.33	0.487	-0.221	0.055	-0.064	-0.026
4	0.568	0.187	-0.295	0.109	-0.152	-0.014
5	0.873	-0.392	-0.362	0.226	-0.462	0.001
6	1.132	-1.237	-0.412	0.288	-0.823	0.056
7	1.06	-1.6	-0.359	0.264	-1.127	0.131
8	0.678	-0.327	-0.25	0.156	-1.377	0.251

F | Sailing probability

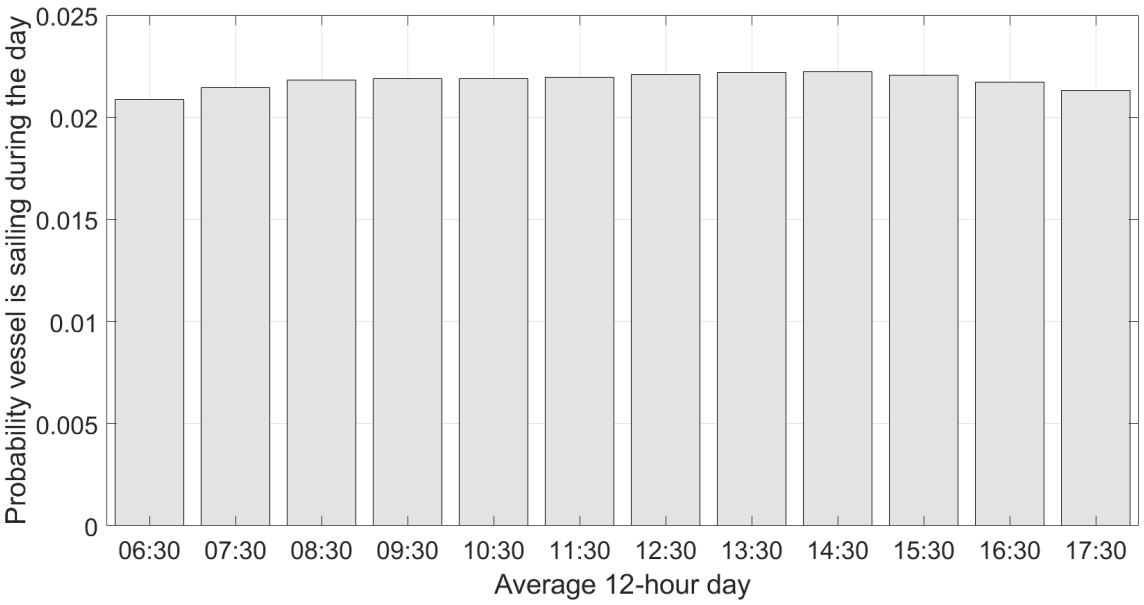

Figure F.1: Probability a vessel is sailing during an average 12-hour day

G | Sky view factor

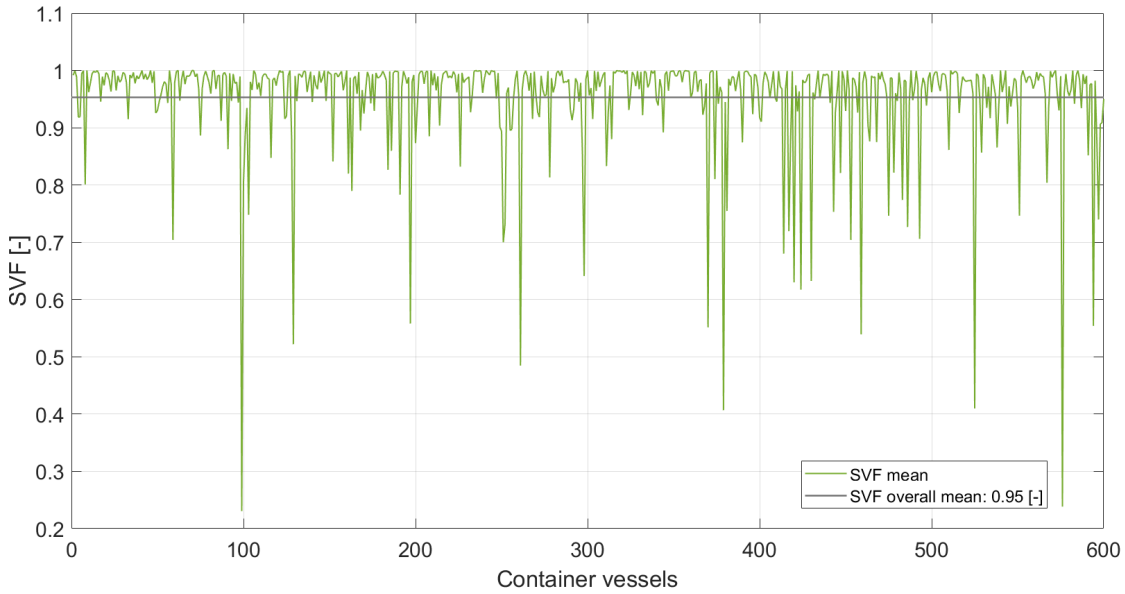

Figure G.1: SVF general cargo vessel to starboard side

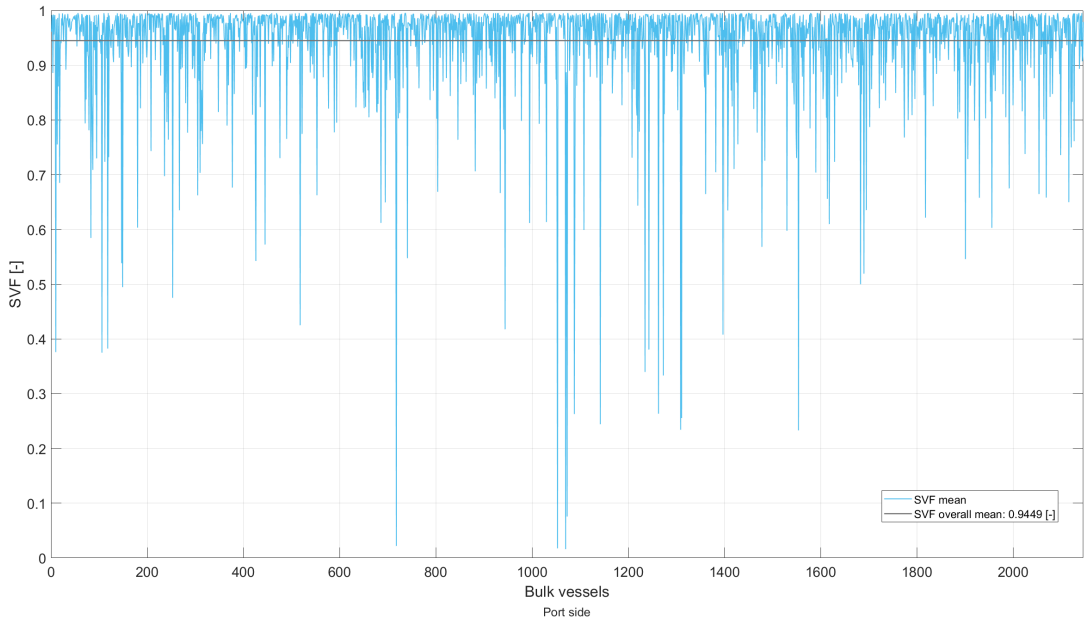

Figure G.2: Sky view factors container vessels

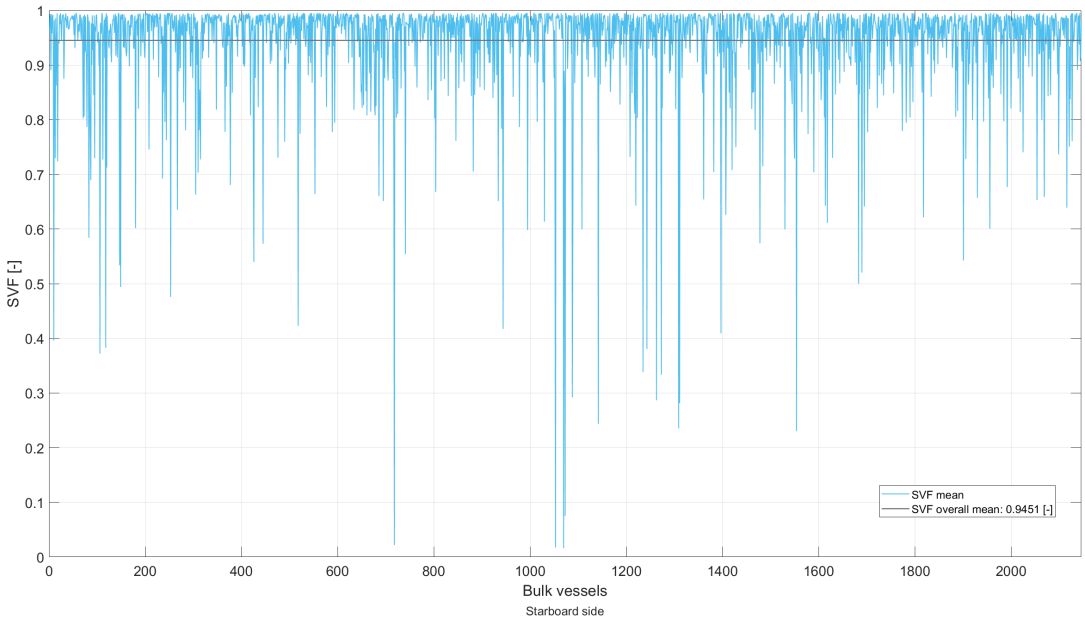

Figure G.3: Sky view factors bulk vessels, port side

H | Sky view factor distribution

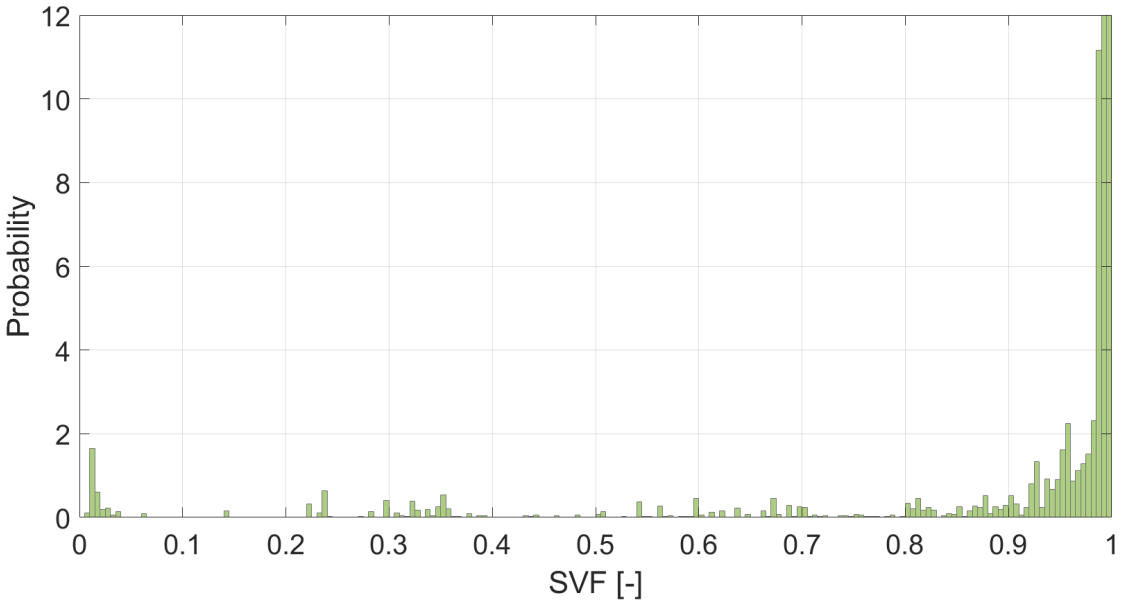

Figure H.1: SVF distribution for container vessels with bin width=0.005

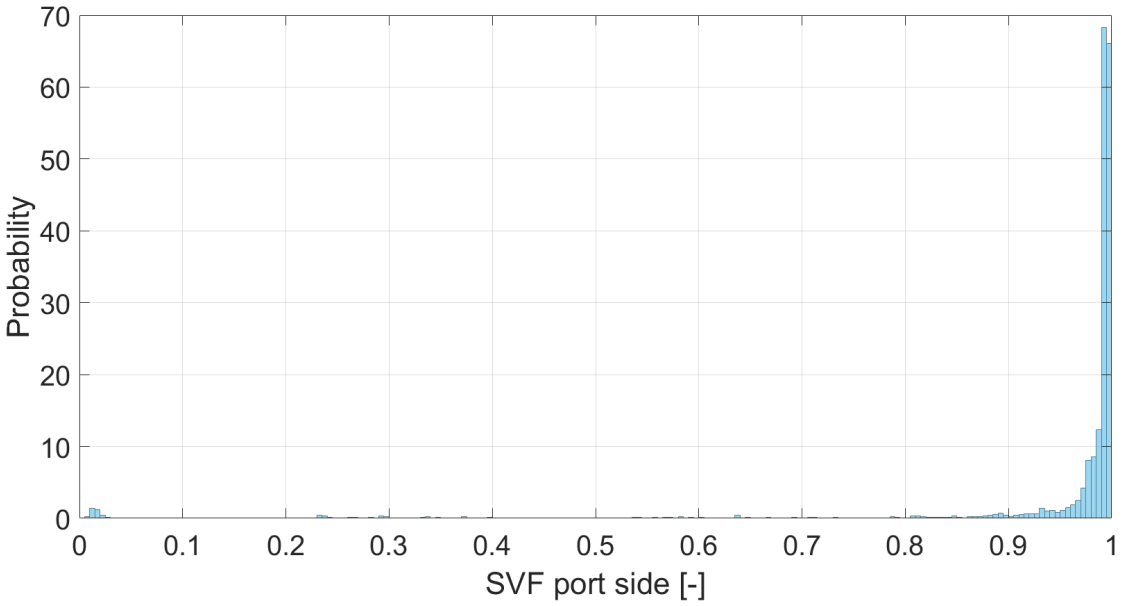

Figure H.2: SVF distribution for bulk vessels, port side, with bin width=0.005

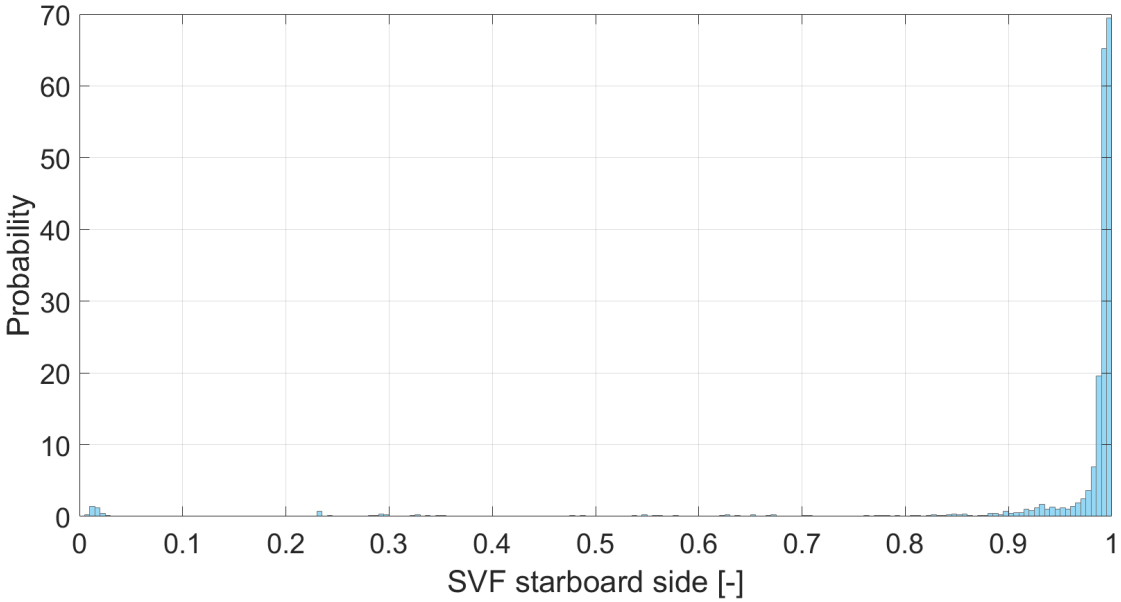

Figure H.3: SVF distribution for bulk vessels, starboard, with bin width=0.005

I | PV surface

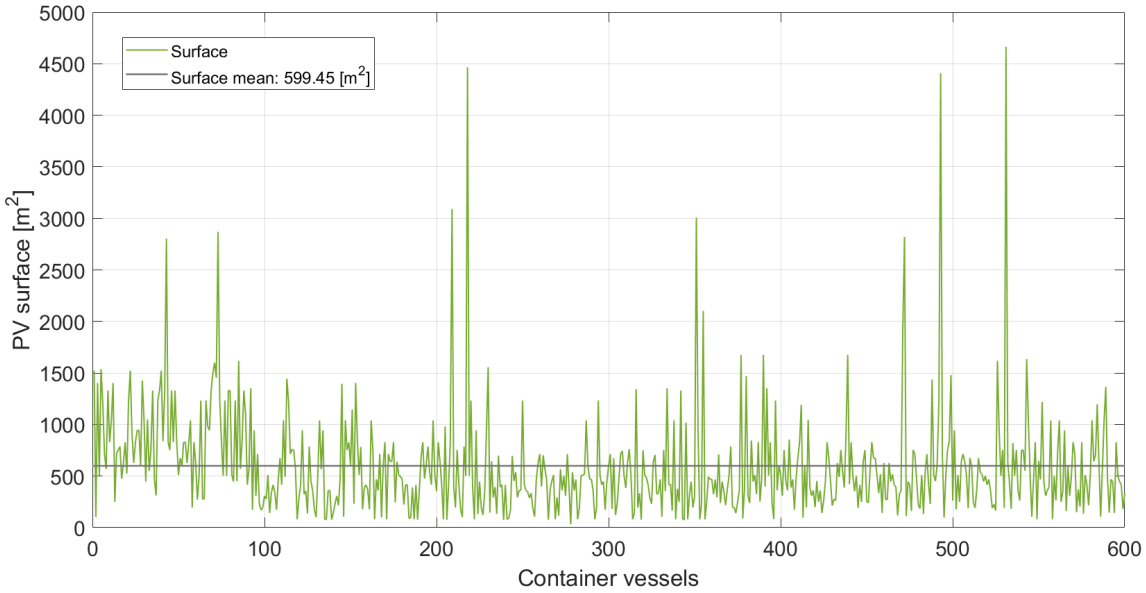

Figure I.1: Photovoltaic surface of the container vessels

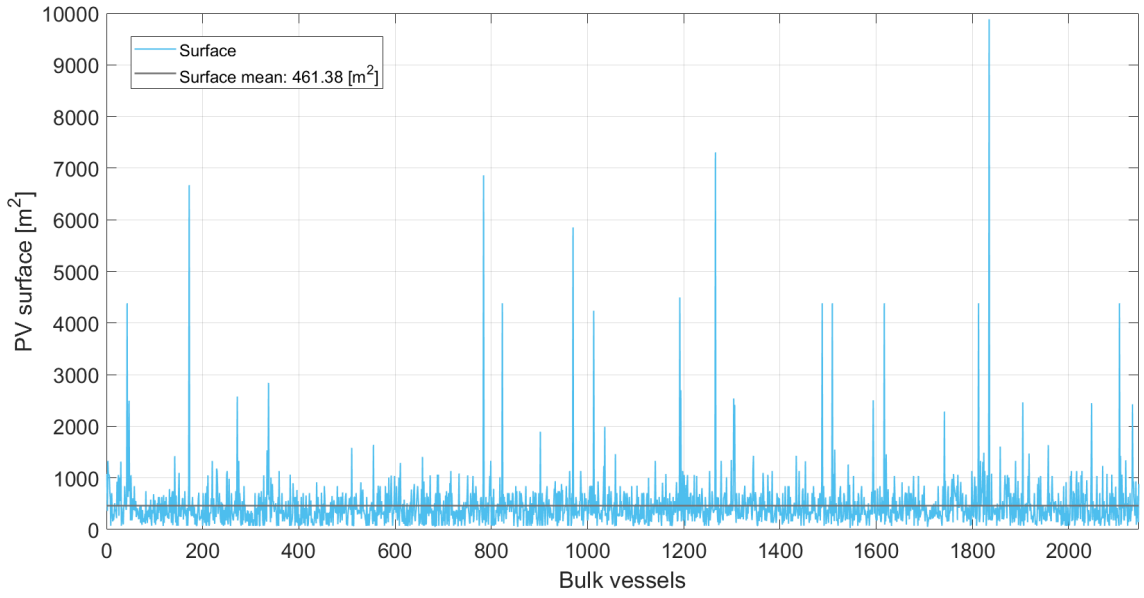

Figure I.2: Photovoltaic surface of the bulk vessels

J Surface utilisation

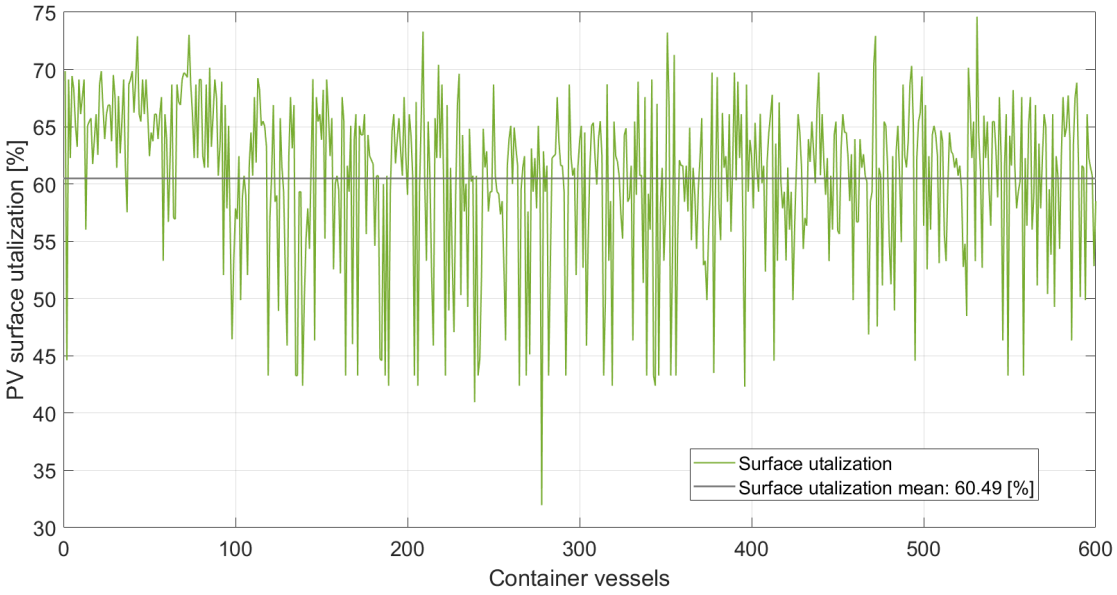

Figure J.1: Surface utilisation of the container vessels

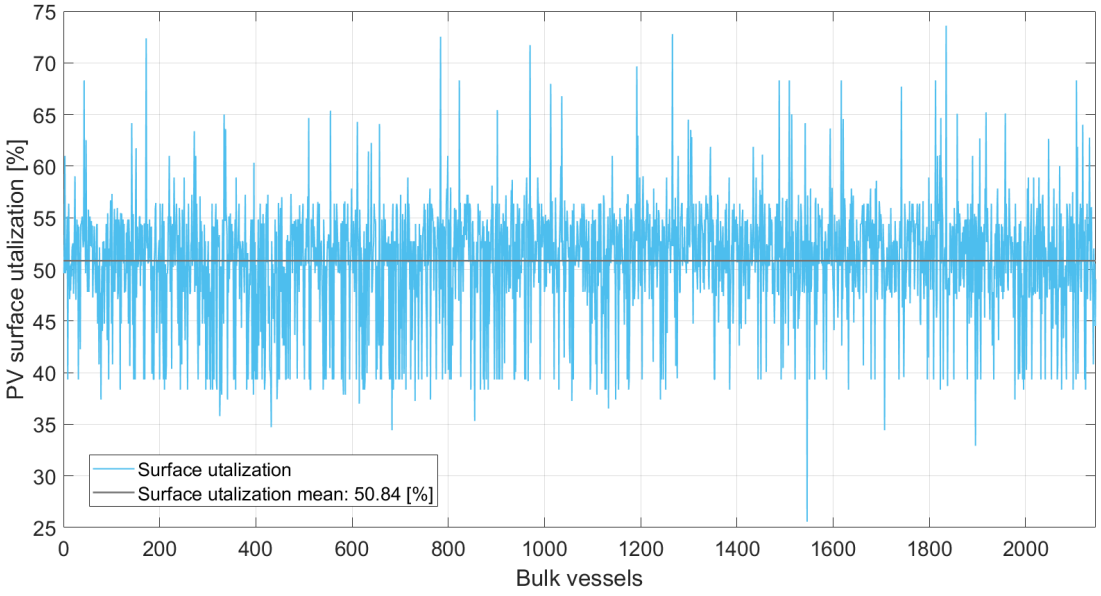

Figure J.2: Surface utilisation of the bulk vessels

K Installed PV power

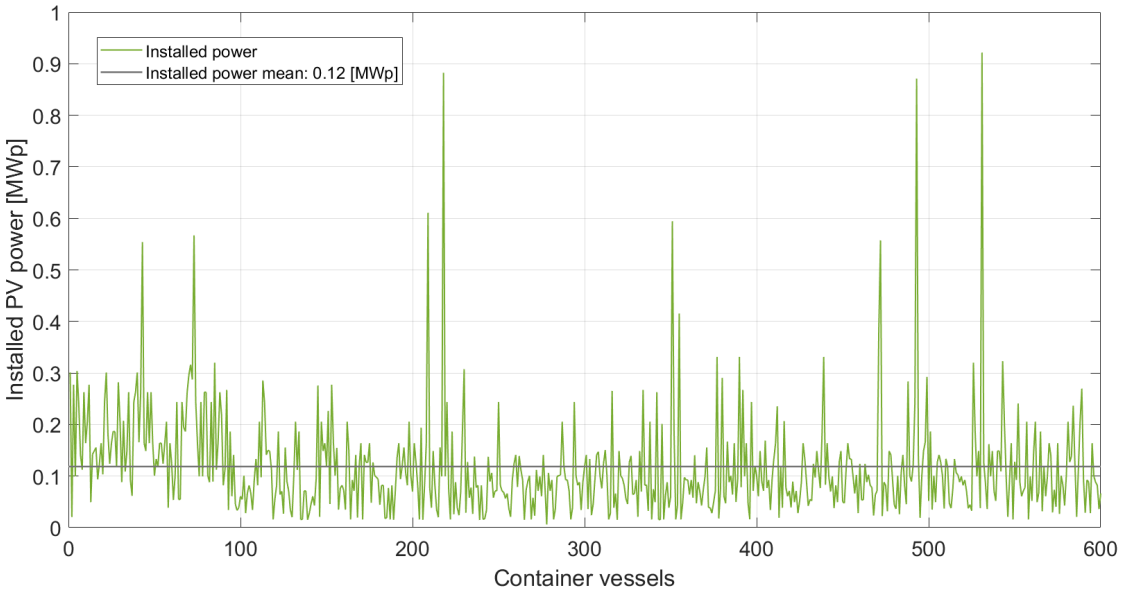

Figure K.1: Installed PV power of the container vessels

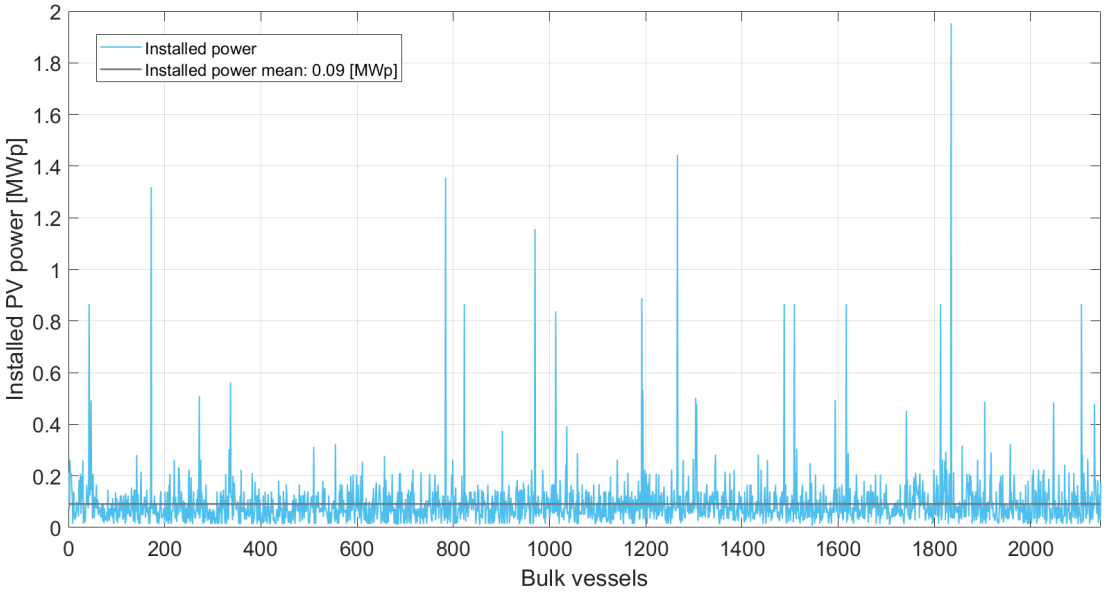

Figure K.2: Installed PV power of the bulk vessels

L | PV energy per unit area

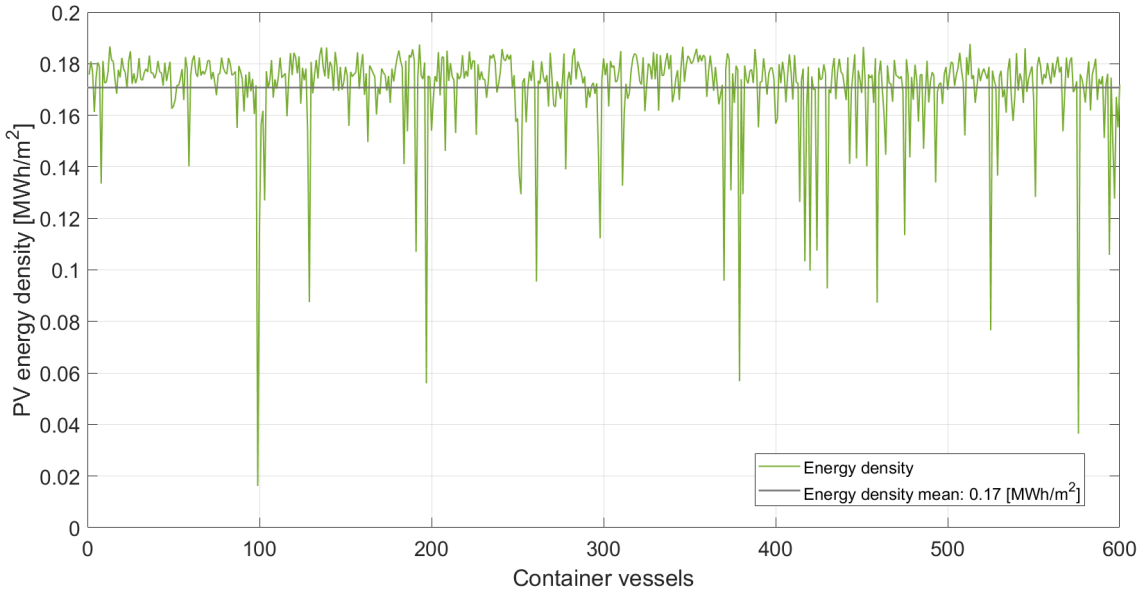

Figure L.1: Annual PV energy per unit area for container vessels

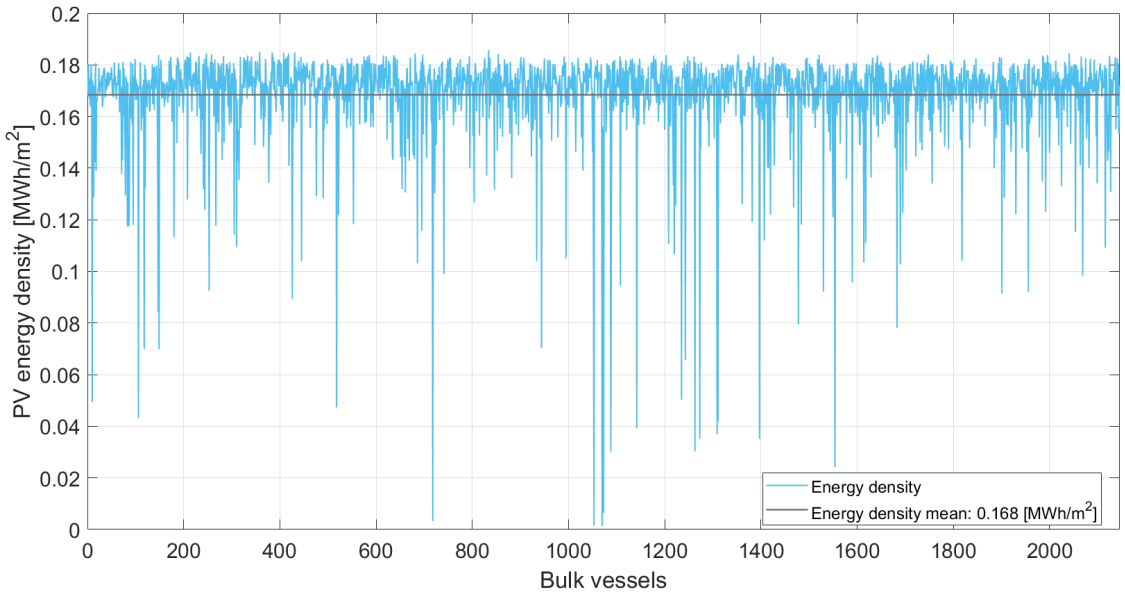

Figure L.2: Annual PV energy per unit area for bulk vessels

M Annual PV energy

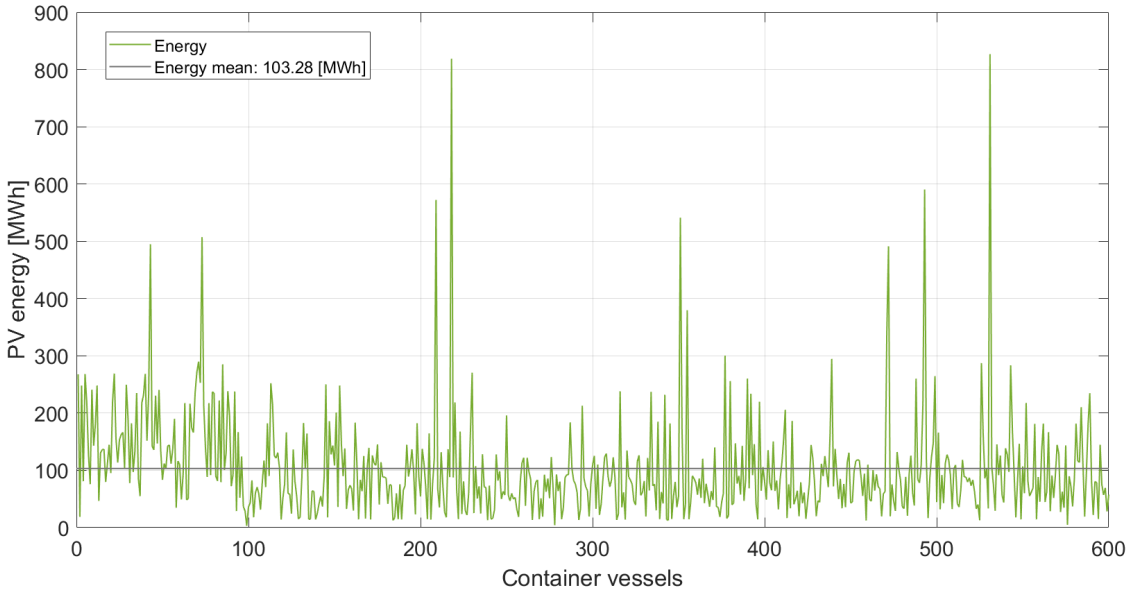

Figure M.1: Annual PV energy for container vessels

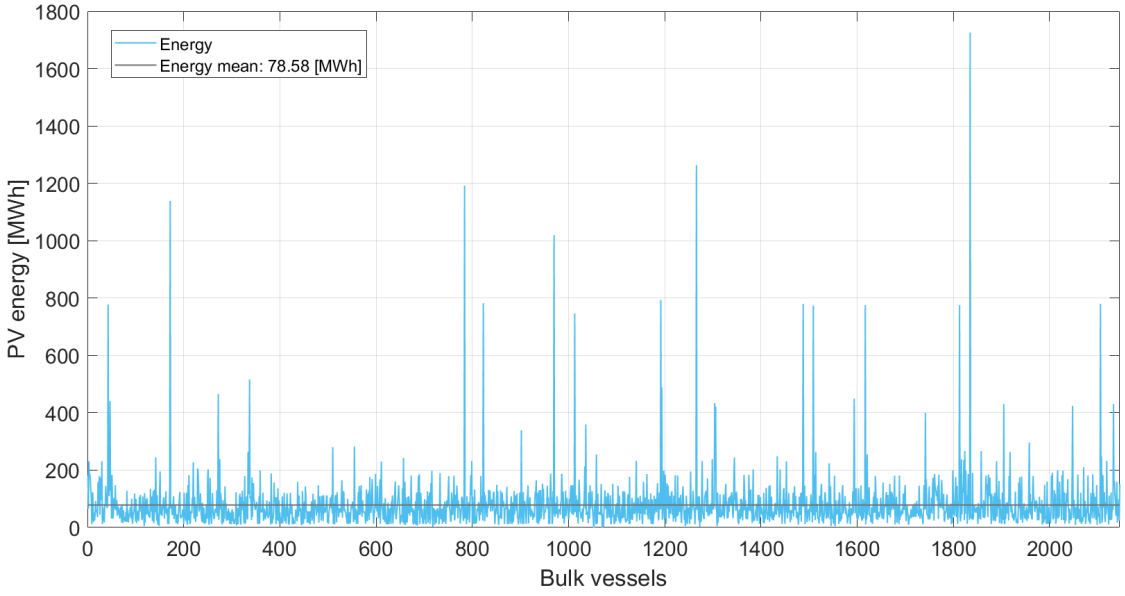

Figure M.2: Annual PV energy for bulk vessels

N | PV energy per installed power

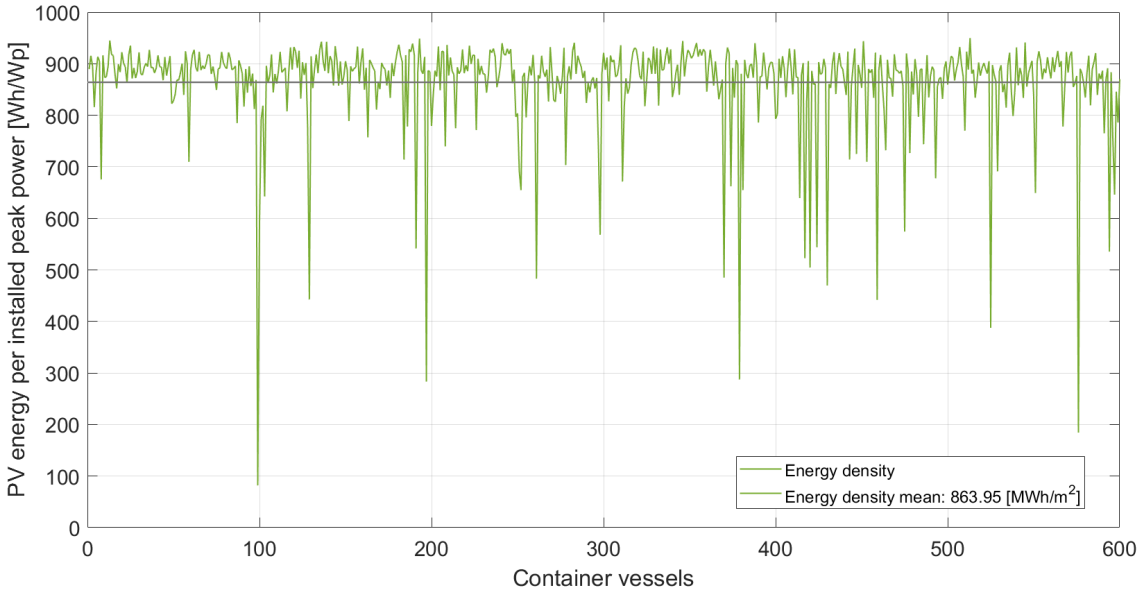

Figure N.1: Annual PV energy per installed power for container vessels

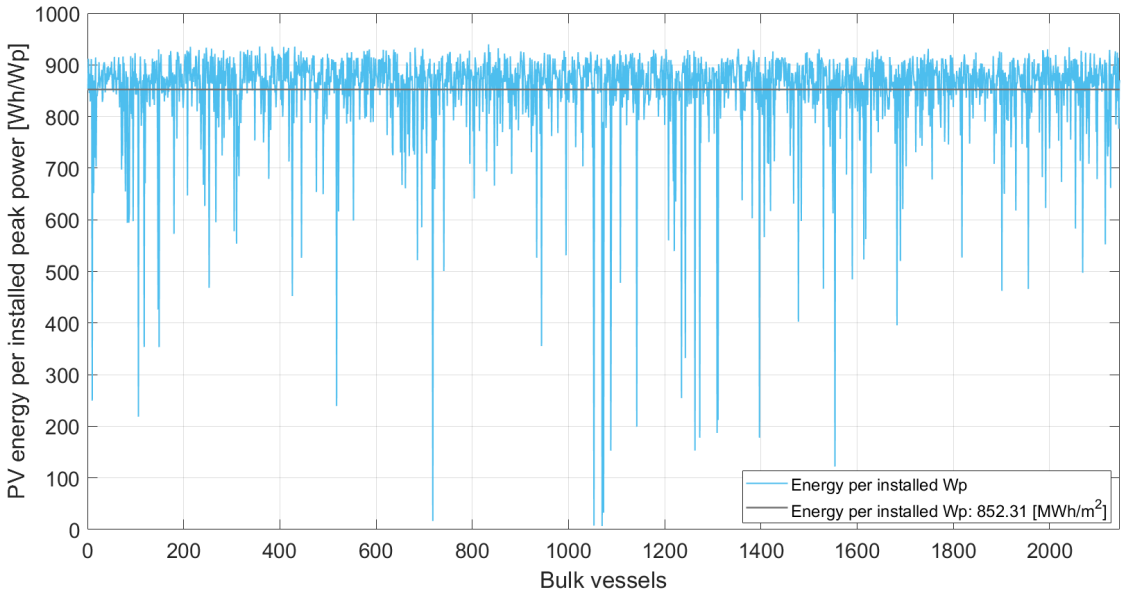

Figure N.2: Annual PV energy per installed power for bulk vessels

O | Traffic

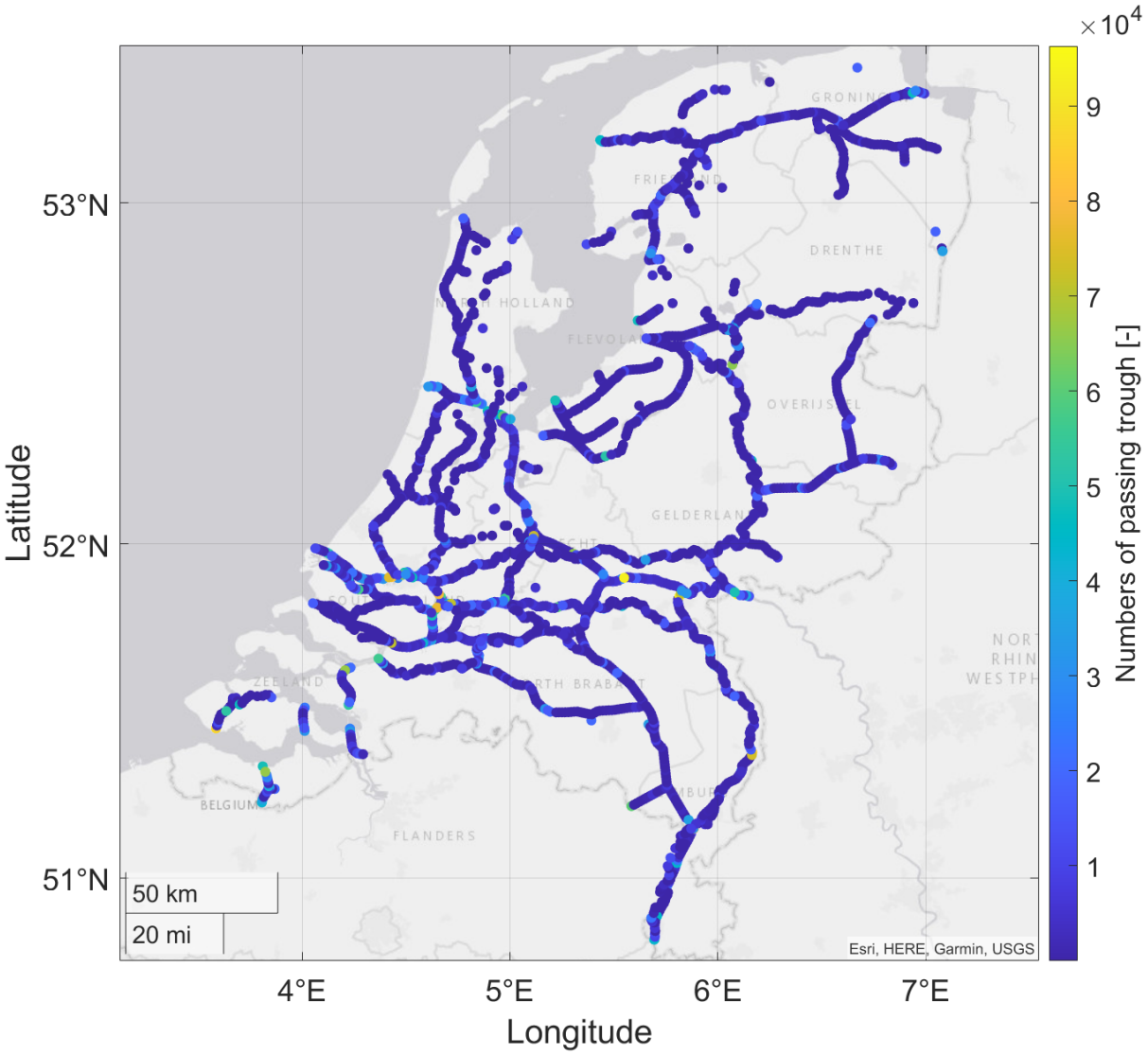

Figure O.1: General cargo traffic in the Netherlands

P Monthly energy distribution per unit area

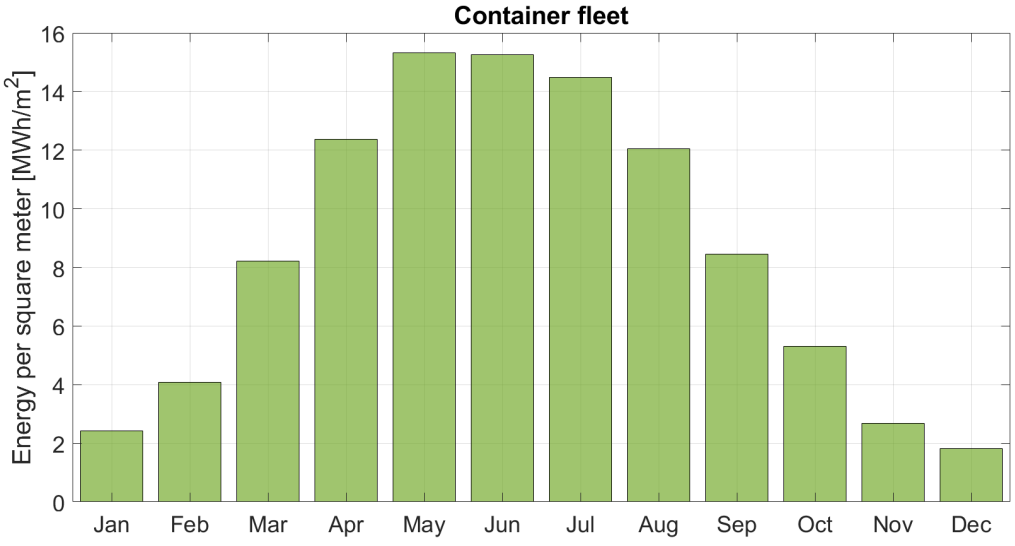

Figure P.1: Monthly energy distribution per unit area for container vessels

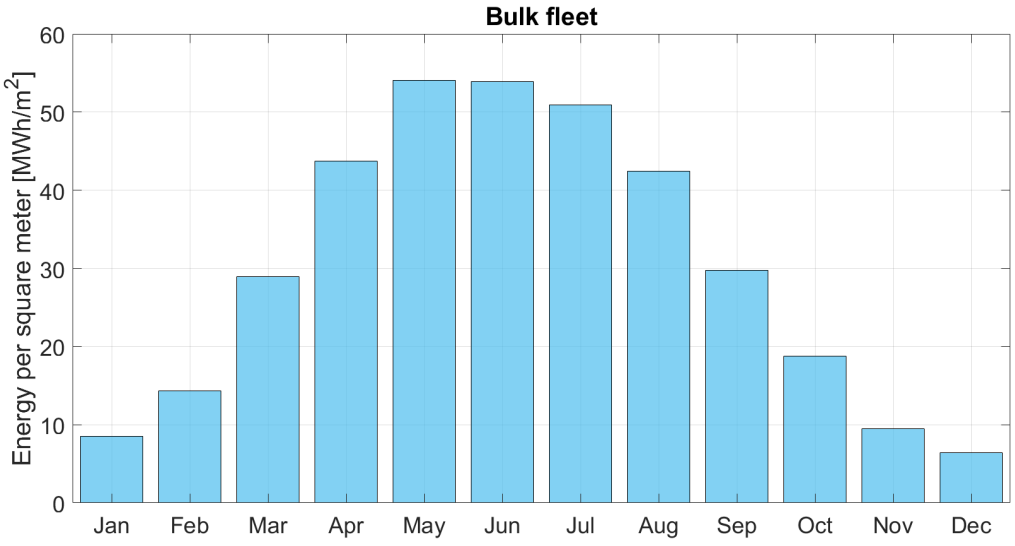

Figure P.2: Monthly energy distribution per unit area for bulk vessels

Q | Distribution tool with outliers

Figure Q.1 and Q.2 shows the distribution fitting tool for the annual PV energy per installed power when taking into account the outliers of the dataset, for container and bulk vessels respectively.

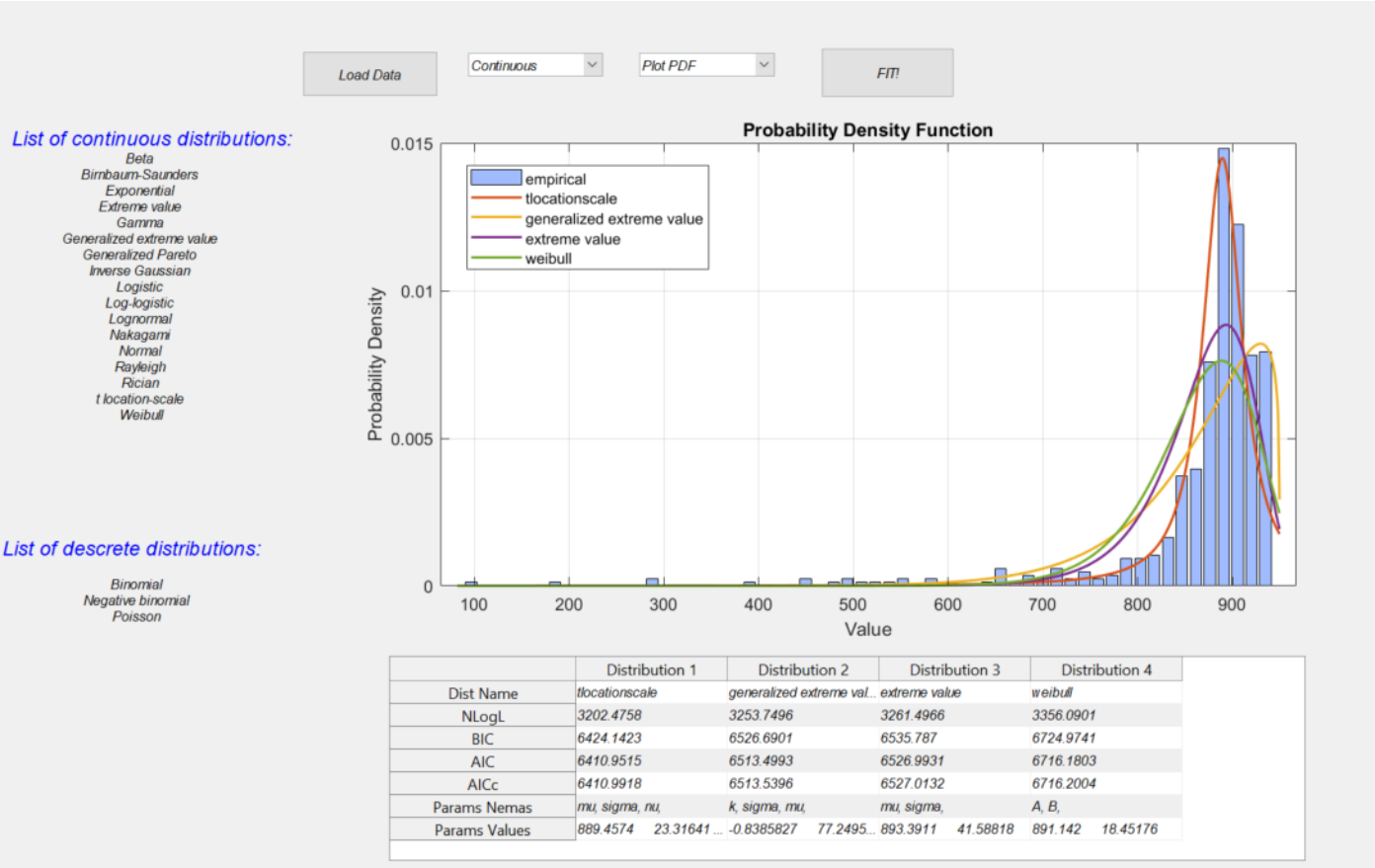

	Distribution 1	Distribution 2	Distribution 3	Distribution 4
Dist Name	tlocationscale	generalized extreme val...	extreme value	weibull
NLogL	3202.4758	3253.7496	3261.4966	3356.0901
BIC	6424.1423	6526.6901	6535.787	6724.9741
AIC	6410.9515	6513.4993	6526.9931	6716.1803
AICc	6410.9918	6513.5396	6527.0132	6716.2004
Params Nemas	mu, sigma, nu,	k, sigma, mu,	mu, sigma,	A, B,
Params Values	889.4574 23.31641 ...	-0.8385827 77.2495...	893.3911 41.58818	891.142 18.45176

Figure Q.1: Distribution fitting tool for the data set of the container vessels

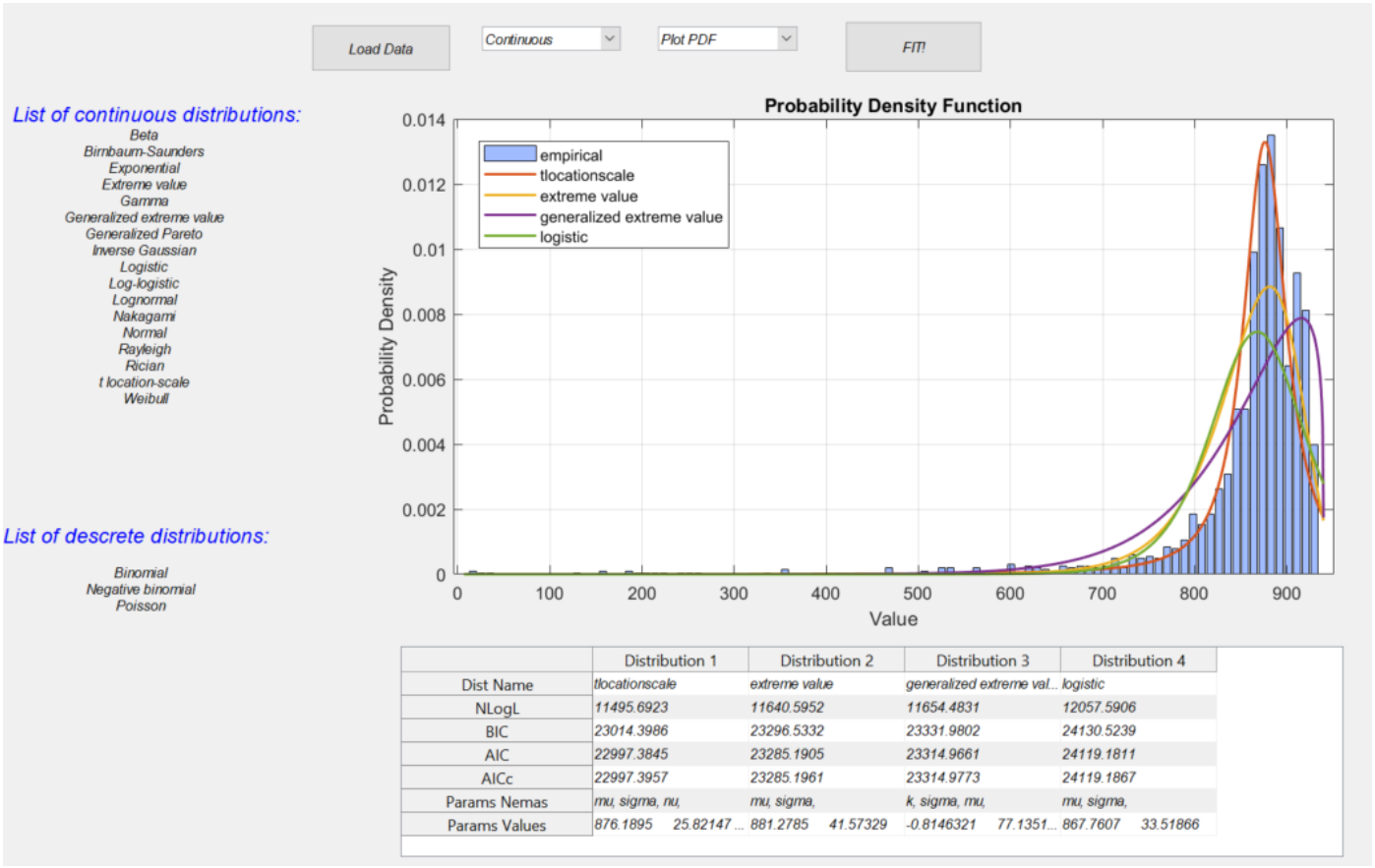

	Distribution 1	Distribution 2	Distribution 3	Distribution 4
Dist Name	tlocationscale	extreme value	generalized extreme val...	logistic
NLogL	11495.6923	11640.5952	11654.4831	12057.5906
BIC	23014.3986	23296.5332	23331.9802	24130.5239
AIC	22997.3845	23285.1905	23314.9661	24119.1811
AICc	22997.3957	23285.1961	23314.9773	24119.1867
Params Nemas	mu, sigma, nu,	mu, sigma,	k, sigma, mu,	mu, sigma,
Params Values	876.1895 25.82147 ...	881.2785 41.57329	-0.8146321 77.1351...	867.7607 33.51866

Figure Q.2: Distribution fitting tool for the data set of the bulk vessels

R | Distribution tool without outliers

Figure R.1 and R.2 shows the distribution fitting tool for the annual PV energy per installed power when the outliers of the dataset are removed, for container and bulk vessels respectively.

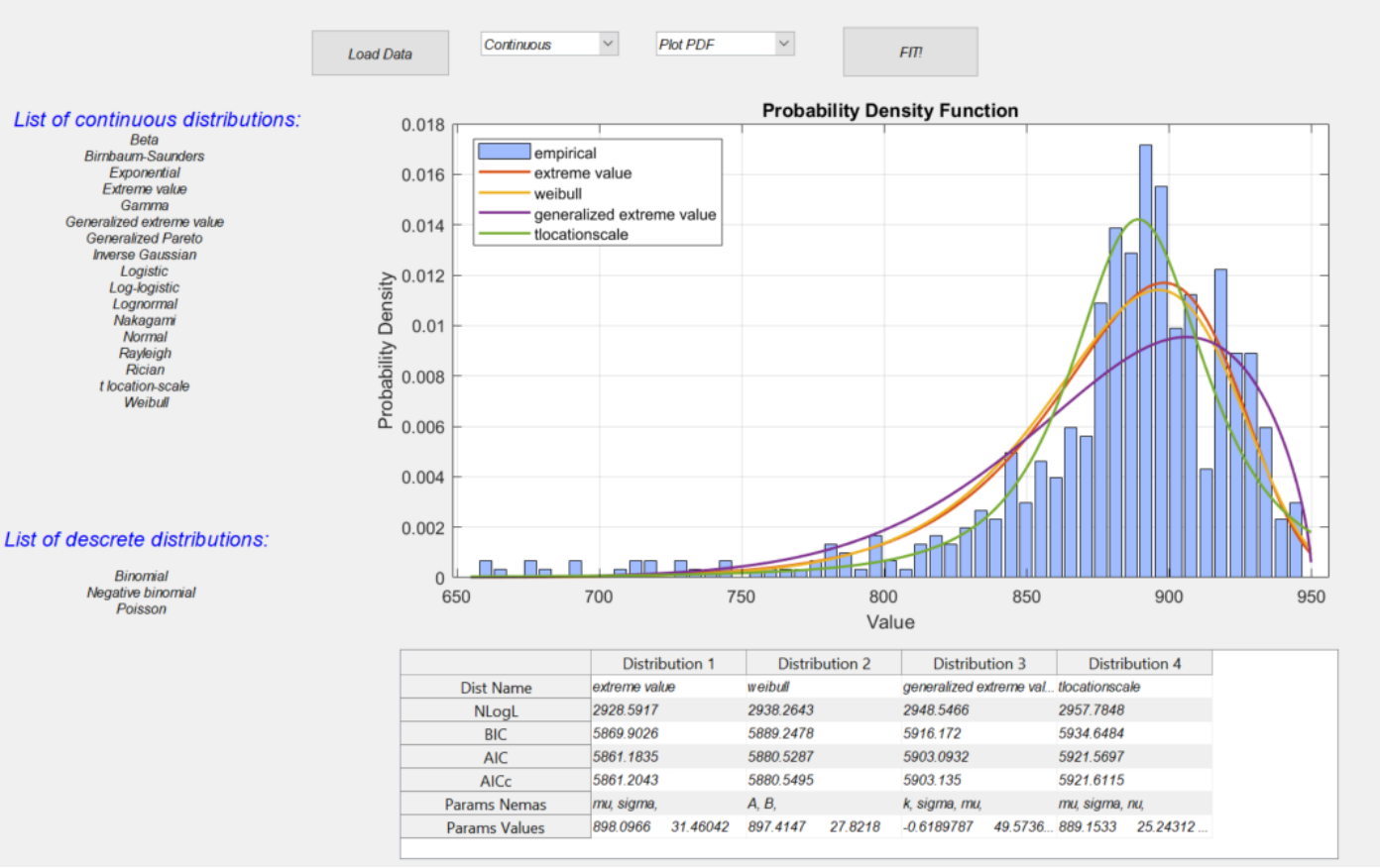

	Distribution 1	Distribution 2	Distribution 3	Distribution 4
Dist Name	extreme value	weibull	generalized extreme val...	tlocationscale
NLogL	2928.5917	2938.2643	2948.5466	2957.7848
BIC	5869.9026	5889.2478	5916.172	5934.6484
AIC	5861.1835	5880.5287	5903.0932	5921.5697
AICc	5861.2043	5880.5495	5903.135	5921.6115
Params Nemas	mu, sigma,	A, B,	k, sigma, mu,	mu, sigma, nu,
Params Values	898.0966 31.46042	897.4147 27.8218	-0.6189787 49.5736...	889.1533 25.24312 ...

Figure R.1: Distribution fitting tool for the data set of the container vessels

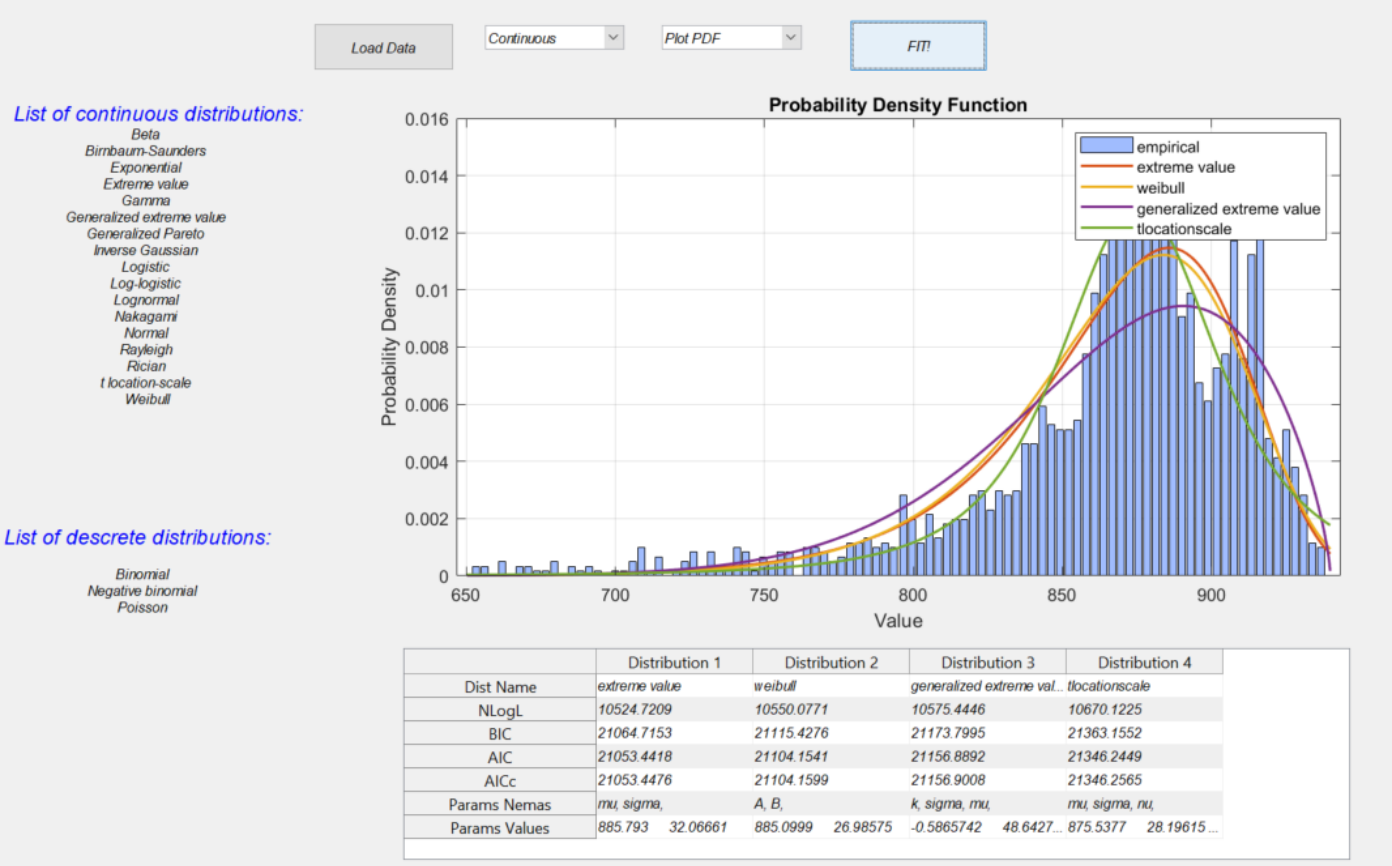

Figure R.2: Distribution fitting tool for the data set of the bulk vessels

S | PV panels weight ratio

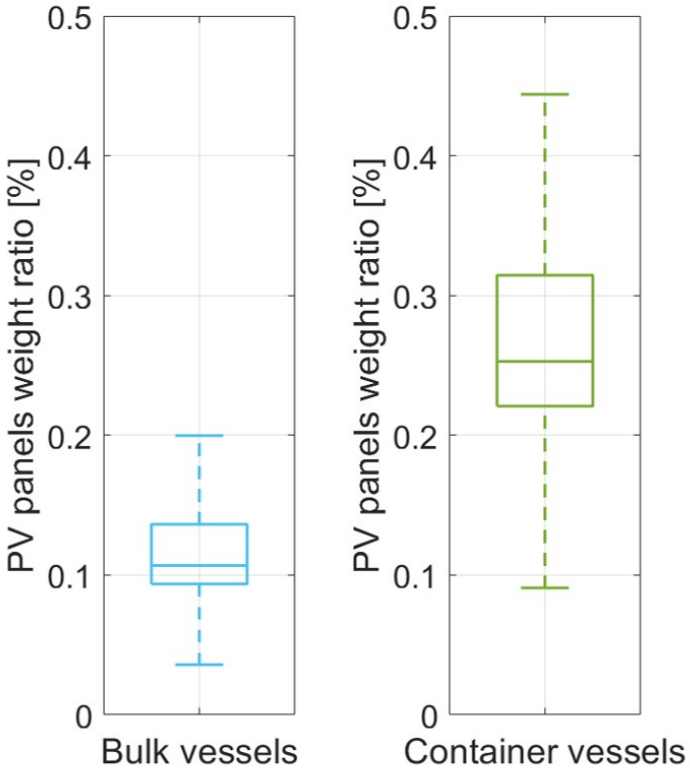

Figure S.1: Weight ratio between the installed PV panels and the vessel